SEQUENCE DEVELOPMENT AND DOLOMITIZATION OF A LATE JURASSIC GIANT OIL RESERVOIR, ARAB-D RESERVOIR, HAWIYAH (GHAWAR) and HARMALIYAH FIELDS, SAUDI ARABIA

Khalaf O. AlTemimi

Dissertation submitted to the faculty of the Virginia Polytechnic Institute and State University in partial fulfillment of the requirements for the degree of

DOCTOR OF PHILOSOPHY

In

GEOSCIENCES

J. Fred Read, Chair
Aus Al-Tawil
Robert J. Bodnar
Kenneth A. Eriksson

April 30th, 2012
Blacksburg VA

Keywords: Late Jurassic, Arab-D, Sequence Stratigraphy, Dolomitization

SEQUENCE DEVELOPMENT AND DOLOMITIZATION OF A LATE JURASSIC GIANT OIL RESERVOIR, ARAB-D RESERVOIR, HAWIYAH (GHAWAR) and HARMALIYAH FIELDS, SAUDI ARABIA

Khalaf O. AlTemimi

ABSTRACT

Thirty cores from the Late Jurassic uppermost Jubaila, Arab-D reservoir and Arab-D anhydrite in Hawiyah (Ghawar) and Harmaliyah fields, eastern Saudi Arabia were studied to document the detailed facies stacking and high resolution sequence stratigraphy. The Jubaila-Arab-D interval is a shallowing upward succession of two composite sequences, in which the Arab-D reservoir and overlying anhydrite have up to twelve higher frequency sequences.

Both fields are strikingly similar in terms of facies, parasequences, and vertical stacking of facies. The direction of the progrodaion is east and northeast and that is supported by northeast thickening of the Arab-D reservoir and by the stromatoporoid and *Cladocoropsis* facies progrodation. This suggests that the Arab-D reservoirs in both fields may represent part of a single carbonate ramp with subtle syndepositional highs. The scarcity of exposure surfaces with caliche in the Arab-D reflects the relatively high subsidence rate (~6 cm/k.y.) relative to the small sea level oscillations that formed the succession coupled with the long term shallowing trend up through the section.

Dolomites from the Arab-D reservoir zones 1 to 4, in both fields were studied to better understand their origin. The dolomites are dominantly fabric destructive medium to coarse grained types, and much less common fabric retentive finer grained dolomites in the uppermost

Arab-D reservoir. The $\delta^{13}C$ values are rock buffered while the $\delta^{18}O$ values have been greatly shifted toward negative values relative to unaltered early dolomite, and dolomite crystal rims generally have lighter $\delta^{18}O$ values than cores.

The dolomites were initiated at different times during shallowing phases on the Arab-D platform, with the bulk of the fabric destructive dolomites forming under near normal salinities, while the fabric preserving dolomites formed as a result of dolomitizing aragonitic sediments from more evaporated waters. With increasing burial and increasing temperature, the early dolomites re-equilibrated with the increasingly warm basinal brines resulting in replacement of cores, and dolomite cementation by rim overgrowth. Progressive plugging of higher dolomites earlier, caused some of these to retain slightly heavier $\delta^{18}O$ values and marine seawater Sr isotope values while those that remained permeable developed very light $\delta^{18}O$ values and more radiogenic Sr values, shifting them toward the field of late stage baroque dolomite.

DEDICATION

For my parents.

ACKNOWLEDGEMENTS

I would like to record my gratitude and appreciation to Dr. J. F. Read for his supervision, advice, guidance, and support through out the graduate program. I gratefully thank my mentor in Saudi Aramco Dr. A. Al-Tawil for all the support I got before and during the graduate program. Also, I would like to thank my other committee members; Dr. R. J. Bodnar, and Dr. K. A. Eriksson for their support and valuble discussions.

I wish to thank Saudi aramco, Exploration Organization, Reservoir Characterization Department, Southern Fields Characterization Division and Planning and Support Division for the support and for using Saudi Aramco data.

I would like to thank all the management and operation team in Core Lab Facilities in Saudi Aramco for providing the best services.

Many thank to the Jurassic Team in Saudi Aramco; A. Al-shamsi, A. Al-Mojel, S. Al-Awwad, M. Al-Thagafy, B. Ames, M. Al-Nezqah, R. Lindsay, R. Loucks, N. Al-Naji, W. Hughes, T. Thompson, D. Russel, L. B. Smith, C. Kerans, L. Pomar and many others.

I would also acknowledge J. Schiffbauer, R. Espoito, D. Moncada, L. Fedele, J. Hunter, and C. Loehn for the help and support provided during analyzing the project data.

Special thanks go to my collegues and friends; R. Al-Dukhayyil and F. Al-Khaldi for their emotional support and valuble disscusions in the carbonate lab. Also, I would like to thank my friend N. Al-Qahtani for his support all the time. And many thanks go to all my friends for their emotional support.

I would like to express my appreciations to my parents for their inseparable support and prayers. Also, I would like to thank my brothers and sisters for their emotional support. Last but not least, I would like to thank my wife and my daughter for their continous support.

TABLE OF CONTENTS

LIST OF FIGURES

LIST OF TABLES

CHAPTER 1

GENERAL INTRODUCTION

This dissertation is divided into two papers. The first part (Chapter 2) documents the detailed facies stacking and high resolution sequence stratigraphy in thirty cores through the Late Jurassic Arab D reservoir in Hawiyah (Ghawar) and Harmaliyah fields, eastern Saudi Arabia. These fields are major oil producers, and are the focus of efforts to develop more refined reservoir models. Outstanding problems associated with the study relate to:

- Defining a workable regionally mappable sequence stratigraphic framework tied to lithology and wireline logs, and defined on lithological criteria rather than just wireline logs
- Whether the present day structures formed individual carbonate platforms or whether they were part of a single platform.
- Lack of facies maps associated with time slices, which limits analysis of regional trends
- Defining the directions of progradation in the succession – were they toward the pre-existing intrashelf basin to the west, or to the south into a shallow southern depocenter, or to the east and north east, along the regional paleoslope defined by isopach maps.
- Defining controls on the development of the layering of flow units and baffles within the reservoir and how does this relate to global eustatic curves or evidence of Milankovitch forcing from elsewhere.

In order to address this problem, detailed lithologic logs were made of 30 cores tied to wireline logs. Cross sections were constructed and various scales of sequences and component parasequences were defined. Based on the data, a sea level curve was constructed and compared with local and global curves to assess evidence for eustasy. Also, evidence for Milankovitch forcing in deeper water facies elsewhere was used to better understand the development of the parasequence scale units on the platform. Subsidence rates calculated for the interval were relatively high compared to the rest of the Mesozoic-Cenozoic succession, and these appear to have had a significant effect on the development of facies and suppression of the formation of emergence surfaces at parasequence and sequence boundaries. From the cross sections and facies maps, progradation directions were obtained, and comparison the stratigraphy of the two fields was made to assess whether the structures were part of a single platform or local platforms.

The second part (Chapter 3) documents the dolomites within the Arab D reservoir and their origins. Previous work on the dolomites (Cantrell et al. 2001, 2004; Swarts et al., 2005) has developed an outline of the petrography of the dolomites from the various reservoir zones, and proposed several genetic models of dolomitization that might have affected the succession. What was lacking in the previous work was documentation of the original composition of the late Jurassic dolomites prior to their being reset by burial. In addition, the lack of zonation (either defined by cathodoluminescence or back scattered electron imaging) of the dolomites also hampered previous analysis and interpretation.

This dolomite study, besides using bulk sample analysis (for stable isotopes and Sr isotopes) focussed on micro-analysis of discrete crystals within selected dolomite samples from the different reservoir zones to better define any chemical and oxygen isotopic variation from

core to rim. It then used data from Croatian near surface dolomites and limestones that had been little altered by burial to develop an idea of the orginal compositions of the dolomites. The geochemical major and trace element and isotope data was then used to develop a paragenetic model for the development of the different types of dolomites from the seafloor to burial to present reservoir depths.

Notable results include the recognition that the dolomites intially formed from marine waters that had relatively elevated oxygen isotope compositions, due to evaporation of the shallow platform waters, and that the burial waters likely had very heavy oxygen isotope compositions compatible with having formed from evaporitic brines coupled with carbonate rock-water interactions at depth. The Sr isotope data proved important in documenting the role of Kimmeridgian seawater in dolomitization versus hydrothermal brines moving up-section, as well as leading to a model in which the widepread Arab D reservoir facies acted as a Kimmeridgian seawater reservoir that continued to supply fluids into the structure.

REFERENCES

Cantrell, D. L., P. K. Swart, R. C. Handford, C.G. Kendall, and H. Westphal 2001. Geology and production significance of dolomite, Arab-D reservoir, Ghawar field, Saudi Arabia. GeoArabia, v. 6, no. 1, p. 45-60.

Cantrell, D. L., P. K. Swart, and R. M. Hagerty, 2004. Genesis and characterization of dolomite, Arab-D reservoir, Ghawar field, Saudi Arabia. GeoArabia, v. 9, no. 2, p. 11-36.

Swart, P. K., D. L. Cantrell, H. Westphal, C. R. Handford, and C. G. Kendall, 2005. Origin of dolomite in the Arab-D reservoir from the Ghawar field, Saudi Arabia: Evidence from petrographic and geochemical constraints: Journal of Sedimentary Research, v. 75, p. 480 – 495.

CHAPTER 2

SEQUENCE DEVELOPMENT OF A LATE JURASSIC GIANT OIL RESERVOIR, ARAB-D RESERVOIR, HAWIYAH (GHAWAR) AND HARMALIYAH FIELDS, SAUDI ARABIA

ABSTRACT

Thirty cores from the Late Jurassic uppermost Jubaila, Arab-D reservoir and Arab-D anhydrite in Hawiyah (Ghawar) and Harmaliyah fields, eastern Saudi Arabia were studied to document the detailed facies stacking and high resolution sequence stratigraphy. The Jubaila-Arab-D interval is a shallowing upward succession of two composite sequences, in which the Arab-D reservoir and overlying Arab-D anhydrite have up to twelve higher frequency sequences. Facies in ascending order include: deeper, hardground-capped lime mudstone, wackestone and intraclastic rudstone; fine packstone forebank apron, and extensive stromatoporoid banks; *Cladocoropsis* peloid packstone/ grainstone/floatstone; fine algal packstone/wackestone; peloid packstone/grainstone, nearshore ooid/mollusk grainstone/packstone, rare peritidal laminites, and anhydrite.

The upper part of the lower sequence (Upper Juabaila-Lower Arab-D), is dominated by deeper water mudstones and intraclastic rudstones shallowing up into intraclstic carbonates at the sequence boundary, The upper sequence (Arab-D reservoir) contains thin deeper water mudstones and intraclastic units (in the east) overlain by parasequences dominated successively by stromatoporoid carbonate parasequences (within the transgressive tract), overlain by *Cladocoropsis* and algal wackestone carbonates, and then lime grainstone (making up the highstand tract). These record initial deepening followed by increasingly high-energy (within fairweather wave base) culminating in hypersalinity and restriction. The upper sequence boundary appears to lie on top of the Arab-D reservoir carbonates. Thus the Arab-D anhydrite appears to be a lowstand tract.

Between the two fields, the facies, parasequences, and vertical stacking of facies are very similar. Regional isopach maps show a gradual northeast thickening trend, which is supported by

the direction of progradation based on the distribution of stromatoporoid facies and *Cladocoropsis* facies both of which appear earlier in the west, and climb to the east. In addition, the ooid grainstone facies thin to the east and the two lowest evaporites in the Arab-D anhydrite become thinner and pinch out toward the east, whereas the Arab-D anhydrite overall thickens westward. This suggests that the Arab-D reservoirs of these two fields may represent part of a single carbonate ramp, at least in their upper part, although the present structures were subtle syndepositional highs.

The scarcity of exposure surfaces with caliche in the Arab-D reflects the relatively high subsidence rate (~6 cm/k.y.) relative to the small sea level oscillations that formed the succession coupled with the long term shallowing trend up through the section.

INTRODUCTION

The Kimmeridgian to early Tithonian (Late Jurassic) Arab Formation carbonates and evaporites of Ghawar field form several of the reservoir units and seals of the world's largest oil field (Al-Husseini, 1997). The Late Jurassic carbonates, which were deposited on the Arabian Platform at low southern latitudes, have been studied by Powers et al. (1962, 1968), Mitchell et al. (1988), Meyer and Price (1993), Handford et al. (2002), and Lindsay et al. (2006) in terms of facies, porosity distribution, super-permeability zones, and high resolution sequence stratigraphy. This project focuses on the sequence development of the Arab-D carbonates and evaporites of Hawiyah field, part of Ghawar, and the smaller Harmaliyah field east of Ghawar utilizing close spaced cored wells (Fig. 2.1). It is part of a larger Saudi Aramco Oil Company project to determine the high resolution sequence stratigraphy of the Jurassic of Arabia to provide a framework for a new generation of reservoir models.

The Mesozoic was considered to have been a greenhouse climate (Fischer, 1964) but more recently it has been suggested to have been cooler in the Early Jurassic and warmer in the Late Jurassic (Royer et al., 2004), with full greenhouse conditions established by the latest Jurassic Tithonian (Husinec and Read, 2007). The Kimmeridgian Arab-D succession should preserve a record of sea-level changes that document whether the Kimmeridgian climate already had warmed into global greenhouse, whether there were small ice caps driving transitional eustasy (in the sense of Read, 1998), and how these influenced the sequence development and reservoir layering.

Milankovitch climate forcing has been well documented by spectral analysis on time series from Kimmeridgian deep water sections of Europe (Weedon et al., 2004; Boulila et al. 2008). The cored wells through the Arab-D carbonates and evaporites, provide an opportunity to determine how this, together with tectonics, climate, sedimentary processes and the calcareous biota, influenced the accumulating succession that developed into the major reservoir of the world's largest oil field.

The role of the Arabian Basin (west and south of Ghawar) has long been controversial in its influence on progradation directions within the Arab-D of Ghawar (Ziegler, 2001; Lindsay et al., 2006). It is not clear whether the Arabian Basin in the Kimmeridgian was a bathymetric basin, or merely the site of increased subsidence and sediment thickening. Detailed facies based, sequence stratigraphic cross sections extending from Ghawar to Harmaliyah, hold the key to asssessing progradation direction in the region, in that they should show climbing of facies in the highstands in the direction of progradation in the absence of major ice-driven forced regressions. If the Arabian Basin was a bathymetric low then it should have strongly influenced progradation off Ghawar.

The close spacing of cored wells provides a test of continuity of the various scales of parasequences, high frequency sequences (HFSs) and sequences, and their effects on porosity layering in the reservoir. Lack of tidal flat facies or emergence features (erosion surfaces, breccias, paleosols) throughout much of the Arab-D reservoir interval is striking, in contrast to typical greenhouse platforms. Also, the facies of the lower Arab-D have been controversial in the past, as they have been interpreted to be very shallow water muds, deep ramp muds and storm beds (Handford et al., 2002; Lindsay et al., 2006), and as deep water turbidite facies (Meyer et al. 1993). The study provides an opportunity to assess what magnitudes of sea level changes are compatible with the development of the parasequences, within the various depositional settings.

Calcite peloids in the Arab-D facies are an abundant component of the reservoir facies. We evaluate whether the Kimmeridgian was a calcite vs. aragonite sea (Stanley and Hardie, 1998), and determine how this might have affected diagenesis and reservoir properties (Cantrell et al., 2001; Mitchell et al., 1988) . In addition the Late Jurassic was a time of maximum microbial calcification for the Phanerozoic (Riding, 2000, 2006; Riding and Liang, 2005) which was important in peloid formation and thus may have influenced the diagenetic response of the sediment pile.

The modern day structures such as Ghawar and Harmaliyah, which localize the Saudi Arabian oil fields, developed over a long time, at least back to the Permian (Abu-Ali, 2005). The study allows the influence of subtle topography over the Ghawar and Harmaliyah structures during Arab-D deposition to be assessed (Fig. 2.2).

REGIONAL AND STRATIGRAPHIC SETTING

Regional Structural Setting

The regional structural setting of the study area is shown in Figure 2.3. The tectonic evolution of the Arabian plate is summarized in detail in Ziegler (2001) and Sharland et al. (2001). During the Late Devonian to the Early Jurassic, back-arc rifting occurred on the northern part of the Arabian plate associated with SW-directed subduction of the Palaeo-Tethys beneath the former passive margin of Gondwana. The northern margin of Gondwana at this time was the site of an Andean type arc (now in part of present day Iran). Most of the Gondwanan plates were emergent and sites of non-deposition. The end of this phase is marked by the Hercynian (Carboniferous) unconformity (the pre-Unayzah unconformity of Saudi Arabia). During this time there was a 90° clockwise rotation (Sharland et al., 2001). During the Late Carboniferous to the Mid-Permian, rifting within the northwest trending Zagros Rift separated the Arabian plate from the Sanandaj-Sirjan, northwest Iran and central Iran terranes. This rifting culminated in opening of the Neo-Tethys Ocean and a new passive margin.

The sediments of the Late Permian passive margin of northeastern Gondwana overlie the pre-Khuff unconformity. The Arabian Plate sloped toward the east-northeaest, and the Permian-Triassic Khuff Formation was deposited on this surface as a succession of low latitude, shallow marine and evaporitic facies (Ziegler, 2001).

In the Early Jurassic, a rift formed on the northern Arabian Plate during opening of the Mediterranean Sea. During the Late Jurassic, India separated from the Afro-Arabian Plate, and there was rifting in southern Yemen (Sharland et al., 2001). During the Early to Late Middle Jurassic, three intrashelf basins developed on the Arabian Plate (Fig. 2.3). These include the Gotnia Basin (at the northern end of the present day Arabian Gulf), which was separated from

the Arabian Basin immediately to the south by the Rimthan Arch. The Qatar Arch separated the Arabian Basin from the Rub Al-Khali or Southern Arabian Basin (Fig. 2.3). What effect the Arabian Basin had on Jubaila-Arab-D deposition and progradation directions has been contentious, some reconstructions showing a sand-shoal over Ghawar marginal to the basin with progradation into the basin to the southwest as well as to the north (summarized in Figure 2.5 of Lindsay et al., 2006).

The Gotnia Basin provided access of Neo-Tethyan waters onto the Arabian Plate. Oceanic waters also entered the Arabian Platform from the northeast across a broad shallow shelf (extending into present day Iran), and from the east via a deep re-entrant in the margin in Oman, as well as via a narrow strait between northern Ghawar and the Rimthan Arch (Fig. 2.3). Widespread Jurassic carbonates culminating in later Jurassic carbonate and evaporites developed on the Arabian plate. Erosion of the Western Arabian Craton supplied eastern Arabia with terrigenous and shallow marine sands (Ziegler, 2001).

Passive margin carbonates (along with nearshore siliciclastic facies) continued to be deposited on the Arabian Plate until the Late Cretaceous. At this time, compression of the Arabian Plate and Neo-Tethys formed an active margin on the northern and northeastern margins of the plate. Onset of collision was marked by emplacement of the obducted Oman ophiolites. With continued collision, the Arabian Plate and Eurasia collided to form the Zagros fold-thrust belt. This collision closed the Neo-Tethys Ocean and formed the Cenozoic foreland basin (Sharland et al., 2001). Today, the Arabian plate (Fig. 2.3) is bordered by the Zagros fold thrust belt to the northeast and the Indian Ocean/ transform margin to the southeast. The Red Sea rift borders the plate to the southwest and the Dead Sea transform fault to the northwest (Sharland et al., 2001).

Ghawar and Harmaliyah (Figs. 2.1 and 2.2) are elongate domes that exhibit 4-way closure, and localize the present day oil and gas fields. Ghawar is underlain by NS trending basement faults, which were reactivated periodically. They appear to have had a long history of active growth having been initiated at least by the Permian, and have continued to grow throughout the Mesozoic and Cenozoic, with most of their growth in the Late Cretaceous. This was due to compressive-transpressive stresses related to closing of Neo-Tethys (Beydoun 1991; Nicholson 2000, 2002). Throughout much of its history the surface expression of the Ghawar structure seems to have been one of low relief that subtly influenced deposition.

Paleogeographic and Climatic Setting

During the Late Jurassic, the Arabian Platform of northeastern Gondwana straddled the equator extending perhaps to 10-15 °S of the equator (Scotese, 2003; Fig. 2.4). Even though Arabia was close to the equator, the effect of the Intertropical Convergence Zone (ITCZ) drew moisture away from Arabia and made the tropical belt, including Arabia, hot and dry (Sellwood et al., 2000). The thick anhydrites (the Arab-D, C, B and Hith anhydrites) in the Late Jurassic Arab-Hith succession (Fig. 2.5) are evidence of the restriction of the shelf and the hot and arid paleoclimate during lowered sea level phases (Fig. 2.6). The Late Jurassic platform contained several intrashelf basins separated by intraplatform highs (Handford et al., 2002; Fig. 2.3). Hawiyah field within Ghawar, along with Harmiliyah to the east, were separated from the Rimthan Arch to the north by a shallow depression north of Ghawar, and were some 400 kilometers inboard from the platform margin bordering Neo-Tethys to the northeast (Fig. 2.4).

Stratigraphic Framework

Sharland et al. (2001) divided the Arabian Plate succession into eleven tectonostratigraphic megasequences; the Arab Formation is part of megasequence AP7. During

megasequence AP7 deposition, most of Arabian Plate was dominated by the Jurassic platform, with its carbonate ramp and intra-shelf basin sediments. Megasequence AP7 has at its base the late Toarcian unconformity, related to the major rifting in the northern part of the Arabian plate. During the Bajocian to Bathonian (Middle Jurassic), the Dhruma Formation was deposited in an open-marine environment. The carbonate-prone Upper Dhruma and Tuwaiq Mountain carbonates were deposited during the Mid- to late Jurassic Callovian to Oxfordian. These were succeeded by the Late Jurassic (Kimmeridgian) Hanifa Formation, which contains a major source rock. A major sea level rise initiated deposition of the Kimmeridgian Jubaila Formation unconformably on the Hanifa Formation. This was followed by deposition of the Kimmeridgian Arab Formation and early Tithonian Hith Anhydrite (Ayres et al., 1982; Sharland et al., 2001; Ziegler, 2001; Handford et al., 2002) (Fig. 2.5). The end of AP7 is marked by the early Tithonian unconformity associated with the spreading of India from Oman and a major relative fall of sea level (Sharland et al., 2001).

Age controls of Arab Formation

Age constraints on the Jurassic Kimmeridigian units (Fig. 2.5) are summarized in Hughes (2004). A mid-Oxfordian age for the lowermost Hanifa Formation is based on *Euaspidoceras* cf. catena perarimatum. The early Kimmeridgian age of the upper part of the Hanifa Formation is based on regional correlations with the maximum flooding surface J60 of Sharland et al. (2001) and Haq and Al-Qatahni (2005). The Early Kimmeridgian age for the Jubaila Formation is constrained by the ammonite *Perisphinctes jubailensis* in the lower part, and nautiloids. The overlying Arab-D reservoir interval lacks ammonites or coccoliths, and its Kimmeridgian age is based on its benthic foram assemblage.

The ages of the Jubaila-Arab units also are based on ties to regional flooding surfaces. However, correlation within the Hanifa-Jubaila-Arab Formation across the Arabian Plate on the basis of flooding surfaces is not consistent. There appears to be some misidentification of the maximum flooding surfaces, or conversely, the lithostratigraphic boundaries. For example, flooding surface J60 has been placed within the Hanifa Formation as in Qatif (Sharland et al., 2001). The J70 flood generally has been picked just above the Hanifa Formation within Jubaila Formation (Sharland et al., 2001). The top of the Arab-D Anhydrite is constrained by the overlying Arab-C carbonates, which is coincident with the J80 flood; these generally have been assigned a mid-Kimmeridgian age, with the overlying Arab-B (J90 flood) and Arab-A carbonates (J100 flood) being assigned successively younger Kimmeridgian ages. The Hith anhydrite is generally placed in the early Tithonian (Haq and Al-Qahtani, 2005; Sharland et al., 2001). For this paper we follow the consensus opinion with J70 (154 Ma) in the Jubaila Formation, J80 (152.5 Ma) in the Arab-C carbonates, J90 (151.5 Ma) in the Arab-B carbonates, and J100 (150.75 Ma) in the Arab-A carbonates (Fig. 2.5). The Hith Anhydrite is placed in the Late Jurassic within Tithonian stage.

METHODS

Thirty slabbed cores of Arab-D reservoir from Hawiyah field, Ghawar and nearby Harmaliyah field, Saudi Arabia, were logged at the Saudi Aramco Core Laboratory Facilities in Dhahran, Saudi Arabia. The cores were tied to the wireline logs using the cross over of density and porosity logs marking dolomite intervals, and tying anhydrite layers to the density log. Cores were logged using a binocular microscope, noting stylolites and fractures, porosity percent and pore type (Choquette and Pray, 1970) mineralogy (calcite, dolomite, anhydrite), sedimentary structures, extended Dunham classification (Dunham, 1962; Embry and Klovan, 1971), grain

size, fossil types, cement and other diagenetic fabrics such as leached components. Dolomite crystal size was divided into petrophysical classes - fine (< 20 microns), medium (20 to 100 microns) and coarse (> 100 microns; Lucia, 1995). Data were plotted on in-house Saudi Aramco core description sheets at 10 feet per inch. Facies then were defined by grain type and Dunham textures and color coded using the standard scheme defined by the Aramco Jurassic working group. Parasequences were picked on the basis of flooding surfaces, except in the deeper water mud-dominated units where they were picked at bases of grainy facies (commonly on hardgrounds). Sequences on the core logs were picked on the basis of upward deepening to upward shallowing trends in stacks of parasequences.

North to south and east to west cross sections were constructed from the logged wells using a top datum at the top of the PADS (post-Arab-D stringer) which is a regional thin carbonate about 30 to 40 ft. above the base of the Arab-D anhydrite. Given the cyclic nature of the successions and the general scarcity of obvious emergence/ erosional features, sequence boundaries were picked on top of the shallowest water facies; maximum flooding surfaces were picked at the turnaround between high accommodation facies and low accommodation facies (cf. Handford and Loucks, 1993). The various log suites (especially gamma ray and porosity) were used to constrain correlations between wells. Density and porosity data were subsequently removed from the core logs and cross sections subsequently, at the request of Saudi Aramco Oil Company. Two sets of facies maps of selected sequences were made using 1. maximum flooding facies and 2. facies immediately beneath the upper sequence boundaries.

FACIES AND DEPOSITIONAL ENVIRONMENTS

The Arab-D facies and depositional environments in Ghawar have been discussed by Powers et al. (1962, 1968), Mitchell et al. (1988), Meyer and Price (1993), Handford et al.

(2002), and Lindsay et al. (2006). However, there is relatively little detailed information on the Harmaliyah-Hawiyah study area. In addition, most of the previous studies tended to lump the facies based largely on grain type, rather than a combination of grain type and depositional texture as used in this paper (Dunham, 1962), the latter being closely tied to porosity classes (Lucia, 1995). The facies are shown on the depositional model (Fig. 2.7) and slabs of cores illustrating the basic facies types shown in Figure 2.8; the description of the facies and interpreted settings are summarized in Table 2.1. The vertical distribution of the facies is shown in a selected core (Fig. 2.9) and the regional distribution of facies is shown on the cross sections (Figs. 2.10A, B, C and D), and on the facies maps (Fig. 2.11).

Anhydrite

These facies (described in Table 2.1) occur in the upper Arab-D member, in a 40 m thick unit, with interbedded microbial laminated dolomite layers and lenses. They are white, massive-nodular or bedded-nodular unfossiliferous anhydrite (Fig. 2.8A).

The anhydrites were deposited in supratidal sabkhas (Warren and Kendall, 1985; Warren, 2006) based on abundant nodular, displacive (and replacive?) fabrics, and association with microbial laminites (Mitchell et al., 1988), although the pure anhydrite units, some of which show relict upright growth fabrics, and layering, are likely to be subaqueous gypsum salina deposits (Charlotte Schrieber, pers. comm. 2012). Lack of marine fossils or trace fossils indicates highly saline marine waters in the gypsum-anhydrite fields.

Microbial Laminite

These facies (Table 2.1) occur in the upper Arab-D carbonate and the D-Anhydrite, in units from 0.6 m to 0.8 m thick. They are brown oil-stained, planar, wavy, and crinkly microbially laminated units, and dominantly of limestone. They consist of fine pellet layers

alternating with fine mud laminae. Some laminites are partially to completely altered to fine structure-preserving dolomite.

These laminites resemble those in the modern Arabian Gulf tidal flats, and formed in low energy tidal flats, indicated by abundant planar, wavy and crinkly microbial lamination, and abundant fine mud-size carbonate (Evans et al., 1975). Dolomitization was probably associated with frequent infiltration and reflux of hypersaline brines derived from tidal flooding of intertidal areas, or from storm-recharge of supratidal flats (Patterson and Kinsman, 1982; McKenzie 1981; McKenzie et al., 1980; Cantrell et al., 2004; Swart et al., 2005). However, there are significant dolomites in the Arab-D that are not associated with laminites and may be related to deep reflux Cantrell et al 2004; Swart et al 2005).

Ooid grainstone to packstone

These units (Table 2.1) occur in the upper Arab-D, in units from 0.2 m to 1 m thick. They are light to medium brown oil-stained, locally cross-bedded or with low angle horizontal lamination. They consist of fine to medium sand-size, well-rounded, well-sorted concentric to faintly radial ooids (Cantrell, 2006), micrite-coated grains, peloids and forams, with lesser small mollusks and gastropods; minor lime mud occurs in the packstones (Fig. 2.8B). The oolitic carbonates have high, interparticle porosity, with some moldic and micro-porosity.

High energy, shallow subtidal, wave- and current-reworked settings highly supersaturated with respect to calcium carbonate (mainly aragonite; Cantrell, 2006), are indicated by mud-free fabrics, high energy sedimentary structures, and the abundant oolitically coated grains (Mitchell et al., 1988). Beach environments are indicated by low angle horizontal laminition in oolites, whereas cross-bedded units formed on high energy subtidal sand flats and oolitic channels. The

restricted biota and common close association with anhydrites suggest hypersaline environments adjacent to evaporitic flats and salinas.

Gastropod ooid grainstone

These facies (Table 2.1) form 0.3- 1 m thick units in the upper Arab-D, beneath anhydrite facies. They are light gray to white, locally cross-bedded to massive, and consist of fine sand- to gravel-size ooids and micrite-coated grains, peloids, forams, whole and fragmented small gastropods and small clams, with minor lime mud in packstones (Fig. 2.8C). They are commonly replaced by fabric-preserving fine dolomite with abundant moldic porosity in former aragonite shells and ooid nuclei.

These facies were formed in hypersaline ponds/ lagoons, indicated by close association with anhydrite units, restricted assemblages dominated by small gastropods, and abundant ooids and coated grains. Cross-bedded grainstones formed on high energy sandflats and in shallow channels (Handford et al., 2002), whereas massive packstones formed in low energy pond/lagoon settings.

Peloid, skeletal-fragment grainstone-packstone

These facies (Table 2.1) occur in the upper Arab-D, in units from 0.3 m to 1.2 m thick. They are light brown to brown oil-stained, horizontal laminated, cross laminated or massive units, composed of fine sand- to granule-size peloids, mollusks, miliolid forams, and rare *Cladocoropsis*; packstones contain minor lime mud (Fig. 2.8D). These facies have one of the highest interparticle porosity in Arab-D.

These peloid skeletal-fragment facies were deposited on high energy wave- and tide-reworked shallow subtidal sandflats, indicated by winnowed fabrics, abraded and rounded grains, horizontal- and cross lamination; massive units formed by bioturbation on inactive sandflats

(Handford et al., 2002). Very shallow, moderately restricted waters are suggested by the scarcity of *Cladocoropsis* and lack of open marine forams (Hughes, 2004) The abundant peloids probably formed from micritization of sand- and granule-size skeletal fragments by microbial boring and recrystallization on the seafloor, coupled with microbial induced precipitation of micrite on grains (Bathurst 1976; Reid and Macintyre, 1998; Riding, 2000; Riding and Liang, 2005)

Algal wackestone to packstone

These units (Table 2.1) occur in the upper Arab-D in units from 0.2- 1.2 m. They are light to medium brown-stained units, with common to abundant subhorizontal to short vertical burrows (< 1cm diameter), and are dominantly limestone consisting of silt- to very coarse sand-size peloids, calcareous algae (encrusting *Thaumatoporella* and the stick-like Clypeina), forams, and rare *Cladocoropsis* with common to abundant lime mud (Fig. 2.8E). Some units have been partly to completely altered to fine and medium dolomite. These facies have low porosity.

The calcified algae formed locally dense meadows on the shallow seafloor in water depths certainly less than 20 m and probably less than 10 m by comparison with the modern Arabian Gulf; (Purser, 1973), Waters were moderately restricted indicated by scarcity of stromatoporoids. Relatively low energy, lagoon settings are suggested by abundant lime mud, although the abundant encrusting habit of Thaumatoporella is suggestive of an epiphytic habit on soft baffles. Moderate to intense bioturbation by infaunal shrimps and others formed the burrowed to massive fabrics.

Peloid-Cladocoropsis grainstone to wackestone

These facies (Table 2.1; Fig. 2.8F) occur in the upper and middle Arab-D, in units ranging from 0.3 m to 2.1 m that are brown stained. Grainstones locally are cross-bedded or horizontally laminated, and are composed of mud- to granule-size peloids, coated grains, stick-

like stromatoporoids (*Cladocoropsis*), calcified algae (*Clypeina* and *Thaumatoporella*), various types of forams, and bivalves, and rare to abundant lime mud (in packstone and wackestone). These units may be partially to totally dolomitized with leached *Cladocoropsis*. They have moderate to low interparticle and intraskeletal porosity.

Cladocoropsis grainstones formed in moderate energy, shallow subtidal settings indicated by medium/very coarse grain sizes, mud-poor fabrics, and cross-bedding and mechanical lamination. *Cladocoropsis* also inhabited lower energy lagoonal settings to form muddy packstone and wackestone. The relatively open-marine biota and regional facies distribution indicates *Cladocoropsis* formed in settings with only limited restriction behind domal-stromatoporoid banks (Lindsay et al., 2006).

Stromatoporoid packstone to wackestone

These facies (Table 2.1; Fig. 2.8G) occur in units from 0.3 m to 3 m thick in the middle Arab-D. They are brown-stained, massive dominantly limestone units of packstone, wackestone and floatstone, that consist of mud- to pebble-size peloids, coated grains, encrusting- and domal stromatoporoids, thin leached platy corals, various forams, *Cladocoropsis*, and rare large gastropods with variable amounts of lime mud. Some units are partially to completely dolomitized. Intraskeletal- and some interparticle porosity occurs in the limestones, and intercrystalline porosity is common in dolomites.

The stromatoporoid carbonates formed mid-ramp, low relief banks in shallow near-normal marine waters, indicated by the relatively diverse biotic assemblages, regional stratigraphic setting beneath and in front of *Cladocoropsis* facies and above and updip from deep ramp muddy carbonates with storm-beds. Stromatoporoids likely had microbial photosymbionts (Leinfelder et al., 2005), supporting water depths less than 15 m. Mud-poor stromatoporoid

facies were deposited in moderate to low energy settings near and just below fair- weather wave-base. Mud-rich stromatoporoid facies may have formed in relatively low energy settings below fair-weather wave-base (Handford et al., 2002). They also could have formed in shallower, moderate energy settings beneath soft organic baffles (macroalgae) or aragonitic algae; the stromoporoids attached to either soft-bodied organisms or aragonitic algae (indicated by presence of tubular molds), while others encrusted large gastropods. The dominantly massive fabrics resulted from intense bioturbation. The stromatoporoids were rolled during storms thus few are in place (Lindsay et al. 2006). With shallowing, stromatoporoids cohabited with *Cladocoropsis* indicating more back-bank or lagoonal settings (Leinfelder et al., 2005). The stromatoporoid assemblages of the Arab-D are semi-restricted, when compared to shelf edge Jurassic assemblages; additionally tropical assemblages of this age show low diversity, perhaps related to high tropical water temperatures (Leinfelder et al., 2005).

Fine grained pelletal-skeletal packstone and lesser grainstone

These facies (Table 2.1; Fig. 2.8H) occur in the middle Arab-D, in units from a few centimeters to 2 m thick. They are brown-stained, massive and less commonly laminated units, some of which overlie coarse rudstone beds. They consist of silt- to very fine-sand size pellets, lime mud and scattered gravel-sized mollusks, brachiopods, and echinoderms (which have rim cements). Most are relatively tight, but some dolomitized units may have intercrystal porosity.

These fine pelletal skeletal facies formed a downslope apron in front of stromatoporoid banks, and were resedimented to form caps to storm beds on the deep ramp. This is indicated by their stratigraphic position below the stromatoporoid interval in the Arab-D and above deep ramp wackestone/mudstone and resedimented rudstone. Fine sediment was transported from the shallow ramp during storms or extreme tides and admixed with sparse skeletal debris from the

resident assemblage. Intense bioturbation created the massive units. Laminated units above rudstones/floatstone formed during waning phases of storms, and were subsequently overlain by lime mud settling from suspension. The common echinoderms in the pelletal facies indicate normal marine salinities. Water depths likely were greater than 10 m but generally above storm wave-base, based on the fine grain size, association with resedimented beds, and relative lack of *in situ* photic organisms.

Intraclast rudstone to floatstone

These facies (Table 2.1; Fig. 2.8I) occur in the middle and lower Arab-D, in units from a few centimeters to over 1 m and commonly rest on firmgrounds or hardgrounds above wackestone or mudstone. They are gray, and consist of fine to pebble-size, poorly sorted, locally upward fining intraclasts (some with micritized rims), peloids, coated grains, very rare ooids, along with whole and fragmented mollusks, thin brachiopods, rare reworked encrusting stromatoporoids and some interstitial lime mud. They have low to high interparticle porosity.

Meyer and Price (1993) interpreted these facies as turbidites shed into deeper water. However the relatively low gradients on the shelf (less than 0.1 degrees even on the ramp slope north of Ghawar) and the shallow basinal water depths, suggest that storm deposition was the dominant process (perhaps influenced by Milankovitch-driven base-level change), indicated by the crude upward-fining units, very poor sorting, coarse grain-size and presence of high-energy rudstone in predominantly muddy successions. The common erosive bases to the rudstones, or basal contacts with hardgrounds/firmgrounds, indicate strong erosive currents that caused sediment bypassing, followed by deposition of gravelly sands, followed by laminated pellet grainstone during waning energy; these became capped by wackestone or mudstone during low energy background sedimentation. *Cladocoropsis*, calcareous algae and ooids are very rare in

these facies, indicating that storms only eroded and transported bank and fore-bank sediments (including microbially coated grains small domal and encrusting stromatoporoids from within the photic zone) and rarely tapped back-bank *Cladocoropsis* meadows or lagoonal facies (Lindsay et al., 2006).

Peloid skeletal wackestone

These facies (Table 2.1; Fig. 2.8J) occur in the lower Arab-D, in units from a few centimeters to 1 m thick, that are commonly capped by hardground surfaces. They are light to dark gray, locally burrowed, contain rare horizontal and wavy laminae, and consist of fine to medium-size peloids and coated grains, sponge spicules, rare *Lenticulina* forams, and whole and fragmented mollusks and brachiopods. Partially dolomitized units have dolomite concentrated in burrows, but others are completely dolomitized. They generally are tight.

These wackestones formed on the low energy deep ramp, slightly above to below storm wave base, in the moderately oxygenated mixed layer (above the thermocline) (cf. Lindsay et al., 2006). Relatively normal marine waters are indicated by common brachiopods and bivalves, some echinoderms, sponge spicules, and *Lenticulina* forams (Hughes, 2004). Peloids and coated grains in these muddy facies probably were transported from updip and deposited as peloidal layers during high energy events, that became subsequently admixed by burrowers with the muddy background sediment, to produce massive and burrowed fabrics.

Lime mudstone

Lime mudstone (Table 2.1; Fig. 2.8K) occurs in the lower Arab-D in units from a few centimeters to over 2 m. They are light to dark gray, massive to locally laminated, with vertical and horizontal burrows and commonly are capped by firmground or hardground surfaces. They consist dominantly of lime mud, along with silt- to medium sand-size peloids, sponge spicules,

and rare mollusk and brachiopod fragments. Some are partially to completely dolomitized, and typically are tight.

Based on their association with deep ramp wackestone and resedimented rudstones, these lime mudstones were deposited below storm wave base (> 15 m water depth). The dark gray mudstones were deposited below the mixed layer in a weakly stratified basin with low oxygen conditions, but the lack of regular/even layering argues against full anoxia (cf. Wilson, 1974). The lighter gray mudstones were deposited under more oxygenated conditions, either shallower water depths or following breakdown of the thermocline. The laminated muds were formed from rapid suspension-settling from tidal flows or storm waves/ currents (Handford et al., 2002). The fine mud that makes up the bulk of the lime mudstones, besides having a component winnowed from shallow water settings and resulting from skeletal breakdown, disintegration of weakly calcified organisms and physico-chemical precipitation, could also be from whitings precipitated within the surface waters of the intrashelf basin.

Hardgrounds

Hardgrounds (Table 2.I; Fig. 2.8L) are common in the Arab-D especially associated with deeper ramp lime mudstones and wackestones, beneath resedimented grainstones containing clasts of hardground sediment. The hardgrounds in the cores are wavy to highly irregular, corroded surfaces. The more mature hardgrounds are blackened with finely disseminated pyrite, are high corroded and embayed, and some are sites of subsequent stylolitization, with pyritic black shale partings. The overlying grainstones extend down into the underlying sediments via *Thallassinoides* burrows (Pemberton 2005).

Pemberton (2005) suggests that the *Thallasinoides* burrows in the lime mudstones were generated during ravinement, using burrowed ravinement surfaces in bases of mesotidal channels

cutting siliciclastic tidal flats as analogs; however such structures are not restricted to tidal flat settings, but can extend offshore at bases of tidal channels to depths of 10 m or so (S. George Pemberton, personal communication, 2009). However, the deeper water settings of the lime mudstones argue against a tidal flat setting. The burrowing occurred during base level fall, and increased oxygenation of the bottom, when crustaceans were able to form open deep burrow systems in the firm sediment. Gentle bottom currents would have been necessary to provide Ca and carbonate ions for sea floor lithification to form the hardgrounds, perhaps beneath microbial "soups" on the sea floor; few if any were subaerially exposed during formation (cf. Dickson et al., 2008). Burrows were backfilled, and hardgrounds were overlain by resedimented grainstone/rudstone as deepening was initiated, allowing storage of grainy sediment above what were previously bypass surfaces.

SEQUENCE STRATIGRAPHY

The sequence stratigraphic framework is shown on the selected column (Fig. 2.9) and the cross sections (Fig. 2.10A, B, C and D), which illustrate the detailed facies distributions, the bounding surfaces, and the systems tracts. Arab-D high frequency sequences (HFSs) were labeled AD-1 to AD-9, with higher frequency sequences labeled as AD-5.1, 5.2 (Saudi Aramco Jurassic Reservoir Team). The numbering does not necessarily imply hierarchical order of the sequences (e.g. 3rd order or 4th order); some sequences such as sequence 4 probably are a similar scale as sequence 5.1 for example. By convention, the sequence boundary is the basal boundary of a depositional sequence, and is labelled accordingly (Mitchum et al., 1977; Van Waggoner et al., 1988). However, the field geologist picks on the wireline logs are sequence tops and are labeled accordingly.

The characteristics of the Arab-D sequences in the study area are summarized in Table 2.2 and the bounding surfaces and systems tracts are briefly described below. Within these highly cyclic successions, on this aggraded platform interior the maximum flooding surfaces were placed at the change from relatively open marine, thicker parasequences to relatively restricted, thinner parasequences because this marks the change from high accommodation in the transgressive system tract (TST) to lower accommodation in the highstand system tract (HST) (Handford and Loucks, 1993; Montanez and Osleger, 1993). Regional facies maps of selected high frequency sequences from the two fields were constructed to show lateral facies trends, using the maximum flooding surfaces, and the uppermost facies for the HST maps for sequences AD-3.1, 5.1, 5.3, and 6 (Fig. 2.11).

Parasequences

The basic types of parasequences, the basic building blocks of the sequences, are illustrated in Figure 2.12. They typically range from 1 to 3 m, although parasequences low and high in the Arab-D are generally thin whereas those in the middle of the Arab-D are relatively thick. Distinctive types of parasequences typify specific intervals within the Arab-D reservoir, and are briefly summarized below. They are discussed in order of relative water depth on the depositional profile.

Intraclast rudstone-lime mudstone parasequences: these parasequences (Fig. 2.12 A, B) occur in the lower Arab-D reservoir. They are characterized by 1. hardground overlain by a fining upward (deepening upward) succession of 2. intraclastic rudstone/floatstone, grading up into 3. lime wackestone or fine pellet packstone/grainstone, then 4. lime mudstone which may be capped by a hardground, terminating the parasequence, or overlain by a coarsening (shallowing) upward unit of 5. lime wackestone or fine pellet packstone to hardground.

Stromatoporoid-parasequences: these (Fig. 2.12 C) consist of upward shallowing units of 1. fine skeletal packstone/wackestone (may be absent) overlain by 2. domal and encrusting stromatoporoid packstone/wackestone overlain by 3. *Cladocoropsis*-peloid grainstone/wackestone, up into 4. algal wackestone/packstone (sharp or gradational top).

Cladocoropsis-parasequences: These (Fig. 2.12 D) consist of upward shallowing of 1. *Cladocoropsis*-peloid grainstone/wackestone overlain by 2. algal wackestone/packstone to 3. peloid grainstone (sharp or gradation top).

Oolitic parasequences: These (Fig. 2.12 E) typically consist of a shallowing upward succession of 1. basal peloid grainstone (locally with ripups) overlain by 2. gastropod grainstone/packstone (may be absent), passing up into 3. ooid grainstone and then 4. massive or microbially laminated carbonate mudstone (locally with anhydrite nodules) that has a sharp top or may be capped by 5. anhydrite.

Third Order Sequences

The Jubaila-Arab-D succession is considered to be a 3rd order composite sequence containing two subsequences. The subsequences in turn are composed of several high frequency sequences (Lindsay et al., 2006). The study interval (Fig. 2.5) comprising the Arab-D carbonate and overlying anhydrite includes the top of the lower subsequence, the complete upper subsequence, and ensuing lowstand. The TST of the lower subsequence consists of the deeper ramp, lower Jubaila Formation. The HST of the lower subsequence consists of the upper Jubaila-lower Arab-D reservoir that form an upward shallowing succession of deep ramp carbonates with increasing storm beds, and units of coated-grain grainstone upsection that include Arab-D HFSs AD-1 to AD-3.2.

The base the upper subsequence is the sequence boundary at the base of HFS AD-4. The TST of the upper subsequence consists of stromatoporoid-rich HFSs AD-4 and 5.1. The HST of the upper subsequence consists of HFSs AD-5.2 to 6 characterized by progressive upward shallowing units from *Cladocoropsis* units, to algal wackestone and capped by ooid and peloid-grainstone dominated units at the top of AD-6.

The top of AD-6 is the 3rd order sequence boundary, which generally marks the change from Arab-D carbonates below to Arab-D anhydrites above. This correlates with breccias and infiltrated terra rossa noted on this surface elsewhere in Ghawar (Lindsay et al., 2006) and Abqaiq to the north of Ghawar (Read pers. comm 2012). A postulated 3rd order lowstand systems tract (LST) includes the overlying Arab-D anhydrite, consisting of HFSs AD-7 to 9. The top of the postulated 3rd order LST is placed on the top anhydrite, beneath the Arab-C carbonates.

High Frequency Sequence Boundaries (SBs)

Sequence boundaries (SB's) in the Arab-D succession (Table 2.2) are difficult to pick due to the scarcity of obvious exposure surfaces. The SBs were placed at the turnaround between shallowing successions beneath the boundary and deepening above the boundary.

Sequence boundaries AD-1, 2, 3.1 and 3.2: The basal boundary of sequence AD-1 was not cored. Basal boundaries of sequences AD-2, 3.1 and 3.2 are placed on resedimented intraclastic carbonates facies that commonly overlie hardgrounds developed on muddy units (e.g. wells 2, 4; Fig. 2.10A). The sequence boundaries were placed at the gradational contact between resedimented units and the overlying finer grained facies, although a case could be made for placing them at the sharp contacts beneath resedimented units.

Sequence boundaries AD-4, 5.1, 5.2 and 5.3: The sequence boundary of AD-4 is on thin oolitic or resedimented grainy carbonate locally underlain by hardgrounds. The sequence boundary for

AD-5.1 is placed on thin lagoonal wackestone/mudstone, and locally on grainy, peloidal facies. The sequence boundaries for AD-5.2 and AD-5.3 are placed on peloid- or *Cladocoropsis*-bearing grainy carbonates, or lagoonal muddy carbonates. Most contacts are conformable and gradational into the overlying facies.

Sequence boundaries AD-6 and 7: Sequence boundary 6 commonly is a gradational contact on algal wackestone facies, and rarely on thin oolitic or peloidal grainstone. They commonly are overlain by *Cladocoropsis*- or *Cladocoropsis*- stromatoporiod -bearing grainy carbonates. Sequence boundary 7 commonly is a hardground on oolitic and peloidal grainstone packstone (e.g. wells 4, 10; Fig. 2.10), locally overlain by one or more intraclastic units (wells 2,14; Fig. 2.10).

Sequence boundaries AD-8 and 9: Sequence boundaries 8 and 9 are placed on regional anhydrite units above thin carbonates. Both sequence boundaries are sharp contacts between carbonates and the underlying anhydrite (Fig. 2.10). The top boundary of sequence 9 is placed at the contact between the anhydrite and overlying Arab-C carbonate.

High Frequency Low Stand Systems Tracts (LSTs)

These generally are not recognized in the study area, given its platform interior setting. However in the lower sequences which include slightly deeper water facies, LSTs may be represented by grainy resedimented units below sequence boundaries 2 and 3.1 which were included in the late HST of the underlying sequence.

High Frequency Transgressive Systems Tracts (TSTs) and Maximum Flooding Surfaces (MFSs)

Transgressive system tracts of HFSs are bounded below by the sequence boundary and above by the maximum flooding surface on relatively open marine facies. The characteristic of the TSTs are summarized in Table 2.2.

TSTs, Sequences AD-1, 2, 3.1 and 3.2: Parasequences within the TSTs (and HSTs) of these deeper water sequences typically fine- and deepen upward (Fig. 2.10). The TST and MFS of sequence AD-1 was not cored. The TSTs of AD-2, 3.1 and 3.2 consist of a set of parasequences of intraclastic floatstone/rudstone-lime mudstone, (wells 2, 4; Fig. 2.10). The MFSs for sequences 2, 3.1 and 3.2 typically were placed near the base of deeper water lime mudstone that is locally dolomitized. Facies mapping of the flooding facies of HFS 3.1 indicates that deeper water lime muds completely covered both Hawiyah and Harmaliyah (Fig. 2.11A), and that this was the situation also for sequences AD-1 through 3.2.

TST, Sequence AD- 4: The TST of sequence AD-4 consists of a deepening-upward parasequence set composed of a fining -upward unit of partially to completely dolomitized muddy carbonates, and locally resedimented grainy units. The MFS of AD-4 was placed above the upward deepening portion of the lower parasequence, in dolomitized fine grained carbonate.

TSTs, Sequences AD-5.1, 5.2, 5.3 and 6: The TST of AD-5.1 commonly consists of stromatoporoid carbonates which are developed throughout the two fields (Fig. 2.10). The MFS was arbitrarily placed within the lowest parasequence within or near the top of the regional stromatoporoid unit that covers most of Hawiyah and Harmaliyah (Figs. 2.10 and 2.11C).

The TST of AD-5.2 in Harmaliyah is dominated by stromatoporoid carbonates, which also occur locally in the TST of sequence 5.3, whereas to the west in Hawiyah the TSTs are

dominated by *Cladocoropsis* carbonates and algal wackestones, which also occur in the TST of sequence 6. The base of the stromatoporoid facies climb stratigraphically from west to east (Figs. 2.10C, D). The MFSs for these sequences were arbitrarily placed within or on *Cladocoropsis* units in the lower parasequence. Facies maps of AD-5.3 and 6 show that these *Cladocoropsis* facies cover almost all of Hawiyah and much of Harmaliyah, passing into stromatoporoid facies to the south (Figs. 2.11E and G).

TST, Sequence AD-7: The TST of sequence AD-7 consists of a parasequence set of muddy and commonly oolitic carbonates that cover both fields. The MFS was placed at the turnaround between carbonate and overlying evaporite.

TSTs, Sequence 8 and 9: The TSTs of AD-8 and AD-9 consists of the basal thin carbonate units that can be traced over both fields, and the MFSs for these sequences were placed at the tops of the carbonate units and beneath the overlying highstand anhydrites.

High Frequency High Stand Systems Tracts (HSTs)

The highstand system tracts of the HFSs extend from the maximum flooding surface to the overlying high frequency sequence boundary. Their characteristics are summarized in Table 2.2.

HST, Sequence AD-1: Most of the AD-1 HST was not cored, but where there was core, the HST was mud-dominated with thin resedimented beds.

HSTs, Sequences AD-2, 3.1 and 3.2: These HSTs consist of coarsening-upward parasequence of intraclastic rudstone-lime mudstone each of which deepens and fines upward. The facies map shows that intraclastic carbonates cover much of Hawiyah field, fining into pelletal carbonates over Harmaliyah to the east (Fig. 2.11B). The upper portion of the sequence AD-3.2 HST has skeletal, pelletal wackestone/ packstone facies in the parasequences.

HST, Sequence AD-4: The HST of sequence AD-4 consists of 2 to 5 parasequences dominated by muddy to grainy stromatoporoid carbonates, with deeper water muddy carbonates at the base of the basal parasequence locally. The stromatoporoid carbonates, pass into deeper water lime mudstone/intraclast rudstone parasequences in Harmaliyah. Algal wackestone/mudstone commonly caps the stromatoporoid carbonates.

HSTs, AD-5.1, 5.2 and 5.3: The HSTs form the bulk of these sequences and consist of shallowing up parasequences of stromatoporoid- to *Cladocoropsis*- to algal carbonate units. They are locally capped by sheets of peloid grainstone. Facies maps of the late highstand facies show that lagoonal muddy carbonates blanket both fields (Figs. 2.11D, F), with local development of stromatoporoids in Harmaliyah during AD-5.1.

HST, Sequence AD-6: The HST of this sequence consists of multiple shallowing up parasequences of *Cladocoropsis* grading up into algal wackestone/mudstone and capped by peloid- and ooid grainstone. Facies maps show grainstones blanketing much of Hawiyah, becoming oolitic in the south, while on Harmaliyah, the grainstones are located at the north and south ends of the field bordering a central mud area (Fig. 2.11H).

Sequences AD-7, 8 and 9: The HSTs of these sequences are composed mainly of blankets of anhydrite. Thin carbonate stringers occur at bases of rare component anhydrite parasequences.

DISCUSSION

Tectonics

Subsidence Rates

Passive margin subsidence rates based on geohistory curves of Abu-Ali (2005) were relatively low for much of early Jurassic (0.4 cm/k.y.) but were higher starting in mid-Jurassic

(1.25 cm/k.y.), peaking in the latest Jurassic (2 cm/k.y.) and then slowing into the Cretaceous (Fig. 2.13). Estimated-long term accumulation rates during deposition of the Jubaila-Arab-Hith succession (Late Jurassic Kimmeridgian-Tithonian) based on the 330 m thickness (Sharland et al., 2001) divided by the likely age range of 5.25 m.y., were relatively high, ~6 cm/k.y. These high rates still lie within the range of most passive margins (few centimeters to 15 cm/k.y.; Steckler and Watts, 1982; Bott, 1992; Schlager 1989; Read, 1989). These accumulation rates are reasonable estimates of total subsidence rates (driving subsidence plus water- and sediment-loading subsidence) over the time interval studied, although it may include a component of long term sea level change, which was relatively small for this time interval (Haq and Al-Qahtani, 2005).

These Late Jurassic subsidence rates are the highest of any time for the Arabian passive margin (Abu-Ali, 2005), and could, in part, be due to loading by dense anhydrite units. However, this subsidence pulse is also evident on the Adriatic platform, Croatia which lacks evaporites (Husinec and Read, 2007) suggesting it is a widespread feature within Neo-Tethys. In general the passive margin subsidence resulted from cooling and subsidence of Neo-Tethyan lithosphere, and the increased subsidence pulse in the Late Jurassic could relate to renewed extension, rifting and crustal thinning (evident in the eastern Mediterranean and Yemen) followed by cooling (Sharland et al., 2001).

Abu-Ali (2005) shows that Ghawar (containing Hawiyah field) and Harmaliyah were subtle positive structures for much of the Mesozoic, based on regional isopachs of the Triassic to Early Cretaceous. However, the rate of differential relief formation would have been low (300 m of differential thickness divided by 100 m.y. duration equals 3 m/ m.y.) and easily levelled by deposition. The similarity of the successions in Hawiyah and Harmliyah (Figs. 2.10A to D),

suggests that topography at the HFS scale was subdued, which is compatible with the slow differential growth of the structures.

Regional isopachs of the Arab-D reservoir (L.B. Smith, personal communication, 2010), show that differential subsidence increased from south to north over Ghawar and Harmaliyah, suggesting progradation into the shallow basin between Ghawar to the south and the Rimthan Arch to the north. However, within Hawiyah and Harmaliyah, there was subtle warping. This is indicated by subtle thickness changes within the Arab-D reservoir that are evident when hung from the top of the post-Arab-D stringer (PADS). This subtle variation likely reflects movement on basement structures (Al-Husseini, 1997; Murris, 1980; Sharland et al., 2001).

Climate, Polar Ice and Milankovitch Driven Eustasy

Pangea, Monsoons, Aridity

The landmass of the supercontinent Pangea, which had undergone rifting in the Late Triassic-Early Jurassic, had a strong influence on rainfall distribution. This resulted in widespread deserts throughout the tropics, which included Arabia on the northeastern margin of Gondwana (Fig. 2.6). This aridity was associated with the megamonsoons which reached their maximum strength during the Triassic while Pangea was fully assembled (Parrish, 1993). Even after the start of Pangean break up, large areas of the Pangean landmass in the northern and southern hemisphere still influenced the monsoonal circulation. During northern summer, low pressure zones formed in the interior of the continents. This led to a shift in wind direction from the equatorial zone to the interior of the northern landmasses. During southern summer, wind directions shifted to the south. Thus the tropical westerlies and the shift of wind direction into the interior of the land masses and away from the equator formed arid climates in the equatorial zone covering northeastern Africa and Arabia during the late Jurassic. Computer general circulation

climate models (Sellwood et al., 2000) support this qualitative model, with very low surface soil moisture for most of the year over Arabia and environs, thus making the Arabian plate very arid (Sellwood et al., 2000).

Paleotemperature and Polar Ice

Frakes et al. (1992) and Scotese et al. (1999) considered the mid Jurassic to Early Cretaceous as a "cool" climate mode, but far more moderate than the previous glacial modes. However, Royer et al. (2004) using oxygen isotope paleotemperatures corrected for CO2, and oceanic Ca ion concentration and pH, showed a major mid-Jurassic cooling of global climate, which starts to warm into the later Jurassic (Royer et al. 2004; their Fig.2. 4).

Price (1999) recognized the Late Jurassic as one of the periods that have evidence of cold or sub-freezing polar climate. Ice-rafted debris and glendonite nodules are indicative of the cold climate in the northern hemisphere and in central Australia (Scotese et al., 1999). Although Price (1999) shows a disappearance of glendonites into the Kimmeridgian, there is a marked increase in occurrences of dropstones and tillites. Sellwood et al. (2000) used two general circulation models (GCMs) to simulate the climate during the Late Jurassic period. Both models indicate large seasonal variation in temperature. The temperature variation caused heavy snow in the high latitudes of most of Gondwana (southern hemisphere) during winter and melting of most of the snow during summer, although the models do suggest that there could have been some ice buildup at the poles. Thus Gondwana may have developed a dynamic ice cap. The northern hemisphere behaved similarly, but with a smaller area and less snow depth. Faunal and floral data and oxygen isotope data indicating glacial meltwaters, and phases of lowered sea levels, are other indicators of the existence of cold climate and perhaps some polar ice in the Late Jurassic (Price, 1999).

Milankovitch Orbital Forcing in the Kimmeridgian

Deep water sections of the Kimmeridgian in Britain and France have been used to evaluate the significance of Milankovitch orbital forcing of climate, productivity and sea level using spectral analysis of time-series derived from a variety of proxies (Weedon et al. 2004; Boulila et al., 2008). There is a well developed obliquity signal and a lesser precessional signal in the deeper water facies for the Kimmeridge Clay of southern England (Weedon et al. 2004). However, magnetic susceptibility on deeper water sediments in France shows a full spectrum of frequencies from precession, obliquity, to short- (95-128 k.y.) and long-term eccentricity (405 k.y.); the precession and long-term eccentricity being the most pronounced (Boulila et al., 2008). In addition, there may be long term obliquity forcing associated with nodes in the solar insolation curves at 1.2 m.y. (cf. Boulila et al 2008; discussed later).

Eustasy

Correlation of 3rd Order Sequences and Fischer Plots

Global and inter-regional biostratigraphic correlation is not of sufficiently high resolution to accurately correlate 3rd order and higher accommodation cycles given the time span of species versus the duration of third order sequences (cf. Miall, 1991). Given the lack of Carbon isotope chemostratigraphic markers and absence of paleomagnetic data for the Arab-D, the lack of high resolution correlation is a major problem, and is further hindered by the relatively restricted biotic assemblages on the Arabian platform interior (Hughes, 2004). Accepting an early Kimmeridgian age for the Hanifa, suggests that the Jubalia through Arab-D extends into the mid-Kimmeridgian (Fig. 2.5; Sharland et al., 2001; Haq and Al-Qahtani, 2005).

Selected coastal onlap curves for Arabia, Europe, as well as the Saudi Aramco/Mobil curve are shown in Figure 2.14, based on data from Snedden and Liu (2010), McGuire et al.

(1993), Haq and Al-Qahtani (2005). The duration of the Kimmeridgian probably is between 3.4 to 4.8 m.y. (Fig. 2.14; Weedon et al. 1999; Gradstein et al. 2004) but the absolute ages on Figure 2.14 should be used with caution as the ages bounding the Kimmeridgian typically are +/- 3 to 4 m.y. (Gradstein et al., 2004, International Stratigraphic Chart). Initially the calculated curves of Matthews and Frohlich (2002) based on orbital forcing were included on Figure 2.14, but were finally not used because of major problems between the absolute ages used versus the timing of regional flooding events.

Because of the poor biostratigraphic constraints, the sea level cycles within the Kimmeridgian have been correlated based on the relative ages and number of the sea level cycles. The third-order coastal onlap curves show a sea level cycle in the Early Kimmeridgian within the upper Hanifa Formation.

The two major cycles in the Jubaila to Arab-D reservoir interval are evident on the Haq and Al-Qahtani (2005) and Sneddon and Lui (2010) curves. The Jubaila MFS appears to correspond to the J70 MFS (Haq and Al-Qahtani, 2005). The sequence boundary between the two sea-level cycles within the Jubaila-Arab-D interval falls roughly at the base of the Arab-D member (top SB-3.2, this paper). However, the Markello et al., (2008) CATT curve (not shown on Figure 2.14) only shows one event in the Jubaila-Arab-D interval. The Arab-C, B and A cycles can be correlated with the upper 3 coastal onlap cycles on the curves, although their relative timing is poorly constrained (Fig. 2.14). Thus in terms of numbers of sea level cycles, the various curves are in general agreement, and suggest a 3rd order global eustatic control on the Kimmeridgian units. However, better age control is needed to constrain the curves in time.

Fischer plots roughly track accommodation change on cyclic carbonate platforms (Fischer, 1964; Goldhammer, 1987; Read and Goldhammer, 1988; Sadler et al., 1993) by

plotting cumulative departure from average cycle thickness, vs. cycle (i.e. parasequence) number. An earlier Fischer plot of the Arab-D succession from Shedgum field (Ghawar) was done by Lindsay et al. (2006). Two Fischer plots were constructed for two wells in the study area to evaluate their use on the Arab-D interval (Figs. 2.14, 2.15). The lower part of the Fischer plot captures the sea level fall portion of the uppermost Jubaila-basal Arab-D sea level cycle. This relative sea-level drop starts from sequence AD-1, the lower and deeper part of the reservoir to sequence AD-3.2, below stromatoporoid facies. The second accommodation cycle on the Fischer plot starts with flooding within and below stromatoporoid facies and ends with gradual sea-level drop prior to deposition of the Arab-D anhydrite. A major problem with the Fischer plot is that it is plotting parasequences formed in two very different settings. The lower part of the plot spans deeper subtidal cycles (whose tops are controlled by wave abrasion depth and which may contain random storm beds) while the upper part of the plot spans shallow subtidal and peritidal cycles which are controlled by the position of sea level. However, that the plots are crudely tracking accommodation is indicated by the rough synchronicity of the two accommodation cycles on the Fischer plots with the two coastal onlap cycles shown on the coastal onlap chart (Fig. 2.14).

Duration of 3rd Order Sequences, High Frequency Sequences and Parasequences

The Kimmeridgian could have a duration of 5 m.y. (Gradstein et al., 2004) to 7.5 m.y. (based on cycles stratigraphy,; Weedon et al., 2004), suggesting a duration of 6 +/- 1.25 m.y. Given the approximately 5 to 7.5 m.y. for the Kimmeridgian, then the average duration of the six sea level cycles within the Hanifa, Jubaila, Arab-D, C, B and A interval, suggests that these cycles are approximately 1 to 1.2 m.y. average duration, and are thus 3rd order. It is possible that these ~1 m.y. cycles relate to long term obliquity forcing, which has nodes spaced at 1.2 m.y. (Boulila et al., 2008). Such obliquity nodes are associated with cooling and periods of ice sheet

buildup in the Cenozoic, because they are characterized by cool summers. This effect is even manifested in the relatively warm Eocene greenhouse (Boulila et al., 2008). If the ~1 m.y. sequences are associated with the 1.2 m.y. obliquity cycle then it suggests that the Late Jurassic was not truly ice free.

Magnitude of the 3rd order sea level changes measured from Haq and Al-Qahtani (2005) are ~30 to 40 m. Sea-level changes of this magnitude may occur during cooling phases within overall greenhouse climates, similar to the Early-Middle Devonian example studied by Elrick et al. (2009) using oxygen isotopes of conodont apatite. They also add further support to the idea that the ~1 m.y. sea level changes are driven by ice-sheet waxing and waning.

The sea level cycles which generated the high frequency sequences within the Arab-D documented in this study, correspond to smaller scale cycles of accommodation not shown on Figure 2.14. Given the estimated 1.3 to 1.5 m.y. duration of the cored interval (Fig. 2.14), which has 12 HFSs, would imply that the HFSs average ~100 to 125 k.y. This suggests that the HFSs are 4th order, short term eccentricity driven cycles, which also are evident in the deeper water sections of France (Boulila et al., 2008). These 4th order high frequency cycles are captured to a limited extent by the Fischer plots (Fig. 2.15). Some of the HFSs occur as a rise and fall on the plots, where they have thicker followed by thinner parasequences. However, this pattern is complicated by missing beats that result in merging of cycles, by autocycles that are local, and by differing short term changes in accumulation rates between sections. Thus the Fischer plots map out the longer term 3rd order trends but are less successful in capturing every high frequency sequence.

Parasequences making up the HFSs in the Arab-D succession likely are orbital precessional cycles (~20 k.y.), given that there are over 60 cycles within the roughly 1.3 to 1.5

m.y. interval, and that there are roughly 4 to 6 cycles in many of the ~100 to 125 k.y. HFS, although in some there are double this number. This is compatible with the strong precessional signal evident in the magnetic susceptibility signal from deeper water sections in France (Boulila et al., 2008) perhaps coupled with autocyclic processes or storm deposition.

In summary, it seems likely that the 3rd order and higher frequency sequences were driven by global eustasy, but it is not possible to document synchroneity between the 3rd order cycles inter-regionally given the poor time control. It could also be argued that these events are not truly synchronous but accommodation related to sea level was modified by variation in subsidence, resulting in slight offsetting of relative sea-level events (Miall, 1991). The estimated duration of the high frequency cycles within the short term eccentricity band also is suggestive of a eustatic origin for these cycles, as is the evidence for precessional cyclicity for the parasequences.

Effect of Subsidence Rate on Relative Sea Level Change

The relatively rapid subsidence rates of the Late Jurassic would tend to suppress effects of eustatic sea level falls. Given the roughly 1.2 m.y. duration, third order sea level cycles with sea level magnitudes of ~30 to 40 m (Haq and Al-Qahtani, 2005) and assuming symmetrical rise and fall, would give 30 to 40 m divided by 600 k.y. (for a 1.2 m.y. obliquity cycle) resulting in ~6 cm/k.y. fall rates. This roughly matches the calculated subsidence rates. Thus at the 3rd order scale, subsidence would offset 3rd order sea level fall, tending to suppress emergence of tops of sequences.

At the HFS scale, assuming the regional cycles are indeed 100 k.y. cycles, assuming sea level falls of about 10 m occuring over 85 k.y. would give 12 cm/ k.y. sea level fall for an asymmetrical rise and fall. This would slightly exceed the 6 cm/k.y. subsidence rate. However

assuming 5 m sea level change (perhaps more reasonable given the scarcity of emergence features) would result in a sea level fall rate that would roughly match subsidence resulting in little relative sea level fall. This would tend to limit erosion and exposure of HFS tops during the fall.

At the parasequence scale, assuming that these are indeed precessional cycles, then if 10 m sea level cycles were involved (a high value), the fall rate would be 10 m divided by 17 k.y. or 60 cm/k.y. fall rate (or 30 cm/k.y. fall rate for 5 m sea level falls). These clearly are several times the subsidence rate and would expose the shallow platform during precessional falls. Tackling this another way, for 17 k.y. of sea level fall to match the 6 cm/k.y. subsidence so that emergence of cycles was limited, would be able to accommodate a sea level change of only 1 m or less. The fact that individual parasequences rarely can be traced across the platform (although the bundles are regionally traceable), and there is little evidence of significant exposure at tops of most parasequences, suggests that precessional sea level changes were small.

Conversely, for flooding, 10 m sea level rise over 15 k.y. for the 100 k.y. cycles would give rise rates of at least 66 cm/k.y. and 33 cm/k.y. for 5m rises; water loading would increase this by over 40%. These rise rates likely were in excess of sedimentation rate, given the platform interior setting of the study area far from the global ocean. For the parasequences, 1 m sea level rise over 3 k.y. would amount to over 30 cm/k.y., which also would outstrip most sedimentation rates given the interior platform setting, thus allowing deepening to occur.

Late Jurassic Calcite Seas and Microbiology

Stanley and Hardie (1998) show that for the Late Jurassic the Mg/Ca ratios of the global ocean were low (below 2) and the dominant carbonate mineralogy was calcite, as opposed to aragonite or high-Mg calcite which characterizes modern tropical platforms. This dominantly

calcite mineralogy for much of the Arab-D carbonates would limit grain dissolution within limestone units. However, where units were dolomitized calcite grains could be leached, due to the relative solubilities of calcite and dolomite in subsurface bines. Aragonitic ooids (Cantrell, 2006) could form on interiors of calcite-sea platforms where high salinities and high carbonate supersaturation occurred, such as just below the Arab-D anhydrite.

Riding (2000), and Riding and Liang (2005) suggest that the Late Jurassic was one of the peaks in microbial calcification for the Mesozoic. The abundant microbial calcifiers were an important source of peloidal and cryptocrystalline calcite for the sediments, and probably encrusted hard substrates including upright calcified algae and stromatoporoids, as well as grains on the seafloor (to form coated grains), and in shallow water, lithified hardground substrates. Continued accretion on coated grains formed oncoids, which would have required intermittent storm- or tide-reworking to generate the coatings.

All stages of micritization of skeletal grains are seen in thin sections of the Arab-D carbonates from incipient alteration of surfaces to complete alteration of skeletons and intraskeletal voids (as in *Cladocoropsis* and whole and fragmented clam shells). The low Mg/Ca ratios of the Late Jurassic seas suggests that any grain alteration probably also formed calcite as the stable phase on the sea floor. This alteration resulted from activities of boring microbes (Bathurst, 1970) and by recrystallization on the sea floor (Reid and Macintyre, 1998). The dominantly calcite mineralogy of the peloidal sediments in the Arab-D made them resistant to leaching (except during late dolomitization). Also, the micritic composition of the peloids inhibited growth of calcite cement because of the polycrystalline substrates. Thus most of the peloid reservoir rocks have primary porosity.

Microporosity is a common feature of the Arab-D carbonates, occurring in many types of grains. Microporosity has been suggested to develop as a result of fine grained calcite recrystallizing to small blocky calcite rhombs while fine, metastable particles are dissolved. This can occur in both the meteoric and burial environments (Perkins, 1993; Choquette and James, 1990), although the arid climate and scarcity of meteoric indicators favor a burial origin of the Arab-D microporosity.

Controls on Depositional Sequences

Development of 3rd Order Sequence Boundaries

To facilitate discussion, the sequence boundaries on Figure 2.14 were labelled K0 to K5, as in Snedden and Liu (2010). The large scale sequence boundary at the base of the lower subsequence (Jubaila Formation) appears to correlate with K1 sea level fall on the Haq and Al-Qahtani (2005) and McGuire et al. (1993), and possibly the slightly younger K1 sequence boundary of Snedden and Liu (2010). The sequence boundary at the base of the Arab-D member (base AD-4; Fig. 2.10) appears to correlate with the K2 sequence boundary of Haq and Al-Qahtani (2005), Snedden and Liu (2010), and McGuire et al. (1993; Fig. 2.14).

The sequence boundary on top of the upper subsequence (upper Arab-D) was placed on top of the thick anhydrite (top of our sequence AD-8) two-thirds the way up in the D Anhydrite by Al-Husseini and Matthews (2008). Alternatively, if the upper sequence boundary is at the base of our sequence AD-7, roughly at the turnaround from carbonate to anhydrite (Fig. 2.10), located on the falling limb of the sea level curve that formed the upper subsequence (Fig. 2.16), then this would make the anhydrite a low stand deposit. This latter sequence boundary pick correlates well with the K3 sequence boundary of Haq and Al-Qahtani (2005) and Snedden and Liu (2010) (Fig. 2.14). This is supported by Lindsay et al (2006), who note breccias filled with

terra rosa at the boundary between the Arab-D carbonate and the Arab-D anhydrite, which would be equivalent to the base of AD-7. A major sequence boundary on AD-6 is compatible with the development of initial low stand carbonates at the base of AD-7 north of Ghawar in Abqaiq field (J. F. Read, personal communication, 2012), as well as emergence and karstic features reported in cores from Ghawar at this level (Robert Lindsay, personal Communication, 2008). The sequence boundary of the upper subsequence on top of the Arab-D carbonates (top of AD-6), is compatible with maximum 3rd order fall rates immediately following the late highstand. These 3rd order fall rates would have been roughly matched by 6 cm/k.y. subsidence rates resulting in zero accommodation. This suggests that emergence horizons in the upper part of the Arab-D carbonates were triggered by the combination of very low accommodation and the superimposed 100 k.y. sea level falls (Fig. 2.16).

Formation of TSTs of 3rd order sequences

The 3rd order TST of the Jubaila subsequence is below the Arab-D study interval but probably is associated with the J70 flood of Sharland et al. (2001). The TST of the Arab-D 3rd order sequence is represented by the stromatoporoid facies (HFSs 4, 5.1 and 5.2) that mark deepening above the shallow water coated grain grainstone cap to HFS 3. The interval from this sequence boundary to the turnaround between higher accommodation, domal stromatoporoid facies and the overlying lower accommodation *Cladocoropsis* units may mark the 3rd order TST of the Arab-D subsequence (Fig. 2.16).

Origin of the 3rd order highstands

The bulk of the highstand of the Jubaila subsequence is below the study interval, but the uppermost part includes the shallowing into the lower Arab-D carbonates marked by increase in

resedimented debris, which correlates with the gradual sea level fall culminating in the K2 (base AD-4) sequence boundary (Fig. 2.14).

The 3rd order highstand of the upper subsequence (within the upper Arab-D), shows shallowing from the stromatoporoid facies through progressively shallower parasequences culminating in ooid- and lesser evaporitic sediments of the late HST (Fig. 2.16). The transition from the carbonates to the oolitic carbonates and thin capping anhydrites marks gradually increasing salinities and increasing restriction due to shallowing over the regional sills.

The D anhydrite as a 3rd order lowstand system tract

A low stand systems tract near the base of the Arab-D (base of the upper subsequence; Fig. 2.14) is not evident in the study area, although widespread shallowing from deep ramp facies is marked by widespread, multiple coated-grain grainstones.

With regard to the LST at the top of the Arab-D, if the top sequence boundary is on the thick anhydrite in the upper two thirds of the D anhydrite (discussed previously), it would then follow that the uppermost anhydrite would be the third order low stand tract prior to deposition of the Arab-C carbonate. However, if the top sequence boundary of the Arab-D is at the base of AD-7 (at the turnaround from Arab-D carbonates to evaporites), then the full succession of the D-anhydrites would be 3rd order lowstand evaporites, which seems simpler, and more likely (Fig. 2.16). Deposition of lowstand evaporites on the platform interior would be would be aided during lowstand by minimum rates of sea level change (typical of lowstands), coupled with the high subsidence rate augmented by the loading effect of dense anhydrite units. This rapid subsidence would provide the needed accommodation for evaporite deposition, while 3rd order eustatic sea level was relatively static but sea level was in a low position on the Arabian Platform. Note that in areas of lower subsidence than Ghawar (on the regional arches) sea level

would fall faster than subsidence thus creating barriers that restricted inflow of seawater into the basin, allowing evaporite deposition.

Controls on High Frequency Sequences

Development of High Frequency Sequence (HFS) Boundaries

The boundaries at the bases of HFSs are beyond the resolution of the global sea level cycle charts. However, the well documented eccentricity and precessional forcing observed in deeper water sections elsewhere, likely was the driver of the high frequency (~100 k.y.) sea level falls that formed the sequence boundaries of the 4th order sequences.

The sequence boundaries of HFSs 2, 3.1 and 3.2 in the lower Arab-D, which are dominated by muddy deep ramp facies, are located above slightly thickened intraclast rudstone caps. These boundaries mark deepening above the underlying resedimented storm beds deposited during upward-shallowing, sediment upbuilding and base-level fall that promoted intermittent deposition of coarse storm debris (Handford et al., 2002; Lindsay et al., 2006). As such the HFS boundaries on the storm beds, mark transgressive deepening in deep-ramp settings. Hardgrounds that commonly underlie the major resedimented grainstones could mark marine condensed intervals or regressive surfaces of marine erosion (Fig. 2.17). It is not clear whether the magnitude of sea level change was higher during deposition of the upper Jubaila-lower Arab-D than later. If so, this could have been associated with cooling associated with the K2 sea level fall (Fig.2.14). Such sea level changes (and perhaps more stormy conditions) would have lowered storm wave base, promoting deposition of resedimented storm debris over areas that were previously sites of lime mud deposition (Fig. 2.17A; Brett et al., 2003).

HFS boundaries within the domal/encrusting stromatoporoid bank-dominated sequences (HFSs 4, 5.1, regionally and 5.2 in Hawiyah) and the overlying *Cladocoropsis* units (AD-5.2 in

Hawiyah, and 5.3 regionally) typically are developed on slightly shallower grainy or thin, muddy lagoonal facies capping HFSs. The rarity of hardened erosive contacts veneered by rip-ups indicates that substrates remained soft prior to flooding and colonization by stromatoporoid assemblages. This could be due to lack of fresh-water diagenesis due to arid climate. It could also be due to limited duration of emergence because the ramp was not yet aggraded to sea level (Fig. 2.17B) and continued subsidence suppressed relative sea level fall associated with the small sea-level fluctuations within the 100 k.y. band.

HFS boundaries within the oolitic and evaporitic sequences AD-6 and 7 commonly are marked by hardened erosional surfaces with rip-ups, indicating substrates beneath HFS boundaries became cemented by micritic and fibrous marine cementation in the shallow subtidal and interitidal zone or during extended emergence. The platform would have shallowed to the highstand of sea level, resulting in longer periods of emergence (Fig. 2.17C). These cemented surfaces provided clasts for transgressive lags veneering the surfaces.

Sequence boundaries within the evaporite-dominated successions occur on the evaporites, beneath the thin carbonate units, indicating that flooding associated with eustatic sea level rise was relatively rapid over the anhydrite surface, moving the waters from anhydrite precipitation (> 90 psu) prior to emergence, into carbonate precipitation fields (considerably below 90 psu). This could only be accomplished regionally by deepening over the sill on the Rimthan Arch and the broad sill east of Ghawar localized over the Qatar Arch (Fig. 2.3).

Thus in summary, the high frequency sequence boundaries changed from hardground surfaces beneath resedimentated grainstones in deep ramp settings, to minor erosional contacts on soft to firm substrates in middle ramp settings, to increasingly indurated, marine-cemented surfaces overlain by reworked intraclast veneers as shallowing continued into shallow inner ramp

settings. At the same time, salinities increased and carbonate supersaturation increased culminating in evaporite deposition.

Development of Transgressive Systems Tracts and Maximum Flooding Surfaces of HFSs

The transgressive systems tracts of the HFSs resulted from short term sea level rise associated with orbital eccentricity forcing of sea level. Superimposed precessional sea-level changes, coupled with local autocyclic effects generated the one or two parasequences within the TSTs of the high frequency sequences. The maximum flooding facies within the HFSs, become progressively shallower from one HFS to the next due to the overall 3rd order shallowing.

TSTs of deeper ramp HFSs 1 to 3.2 which are characterized by parasequences of basal hardgrounds to resedimented grainstone to lime mudstone that progressively deepen upsection, reflects sedimentation lagging relative sea level rise. This was due to rapid, short term sea level rise outpacing sedimentation. The low sedimentation rates could have been associated with regional deepening over the Arabian platform which pushed the carbonate factory further updip (westward) decreasing sedimentation in more distal areas (over Ghawar). These deepening events culminated in regional lime mudstone deposition and hardground development over Ghawar, which developed during maximum flooding (Fig. 2.11A). The deepening events were interrupted by short intervals of shallowing driven by precessional sea level falls, and/or storm deposition of resedimented grainstone (Fig. 2.17A).

The TST and maximum flooding facies of HFS 5.1 is dominated by stromatoporoid parasequences in both fields, while stromatoporoid parasequences are only widespread in Harmaliyah in HFS 5.2 and developed only locally in Harmaliyah in HFS 5.3 (Fig. 2.11E). The stromatoporoid facies mark flooding perhaps to 10 m water depths (17B; Leinfelder et al., 2005). This allowed colonization of shallow, well-lit substrates by nodular and encrusting

stromatoporoids under relatively normal salinities, suggesting that the marginal sills of the Arabian platform were flooded to depths of 10 m or more, allowing relatively open marine conditions over the platform interior. The distribution of the stromatoporoid parasequences supports the idea of eastward progradation and more open conditions to the east.

The TSTs of HFSs 5.3 and 6 which are dominated by *Cladocoropsis* parasequences (Fig. 2.11E, G), probably formed in shallower water depths (Fig. 2.17B; Leinfelder et al., 2005) and more restricted, perhaps metahaline salinities of less than 50 psu. TSTS of HFSs 7 to 9, which are oolitic with restricted peloidal and gastropod grain-rich facies (and evaporite highstands), attest to the platform being highly aggraded, such that short term sea level rises only flooded the platform to shallow depths (Fig. 2.17C). This resulted in elevated salinities and high calcium carbonate supersaturation.

Origin of the High Frequency, Highstand Systems Tracts

Shallowing of high frequency sequences was most likely due to sea level fall driven by orbital eccentricity, coupled with variable amounts of upbuilding by sedimentation. Superimposed precessional (and perhaps obliquity forcing) coupled with local autocyclic processes, generated the component parasequences. The parasequences within the highstand systems tracts which tend to consist of increasingly shallower water facies upward in the HSTs, reflect sedimentation greater than accommodation as sea levels fall. The highstand facies of the HFSs, which also become progressively shallower from one HFS to the next upsection, was due to the superimposed long term, 3rd order decrease in accommodation.

The HSTs of deeper ramp HFSs 1 to 3.2, which are dominated by upward shallowing from lime mudstone up into resedimented grainy facies, mark gradual sea level falls associated with a small amount of sediment upbuilding. Lowering of base-level and consequently storm

wave-base resulted in increasing export of fine- and coarse-grained sediment into formerly deeper water areas to generate the upward-coarsening deep ramp, highstand successions (Fig. 2.17A; Handford et al., 2002; Lindsay et al., 2006). However, the common deepening-upward motif of some individual parasequences within the HST (and TSTs) probably resulted from storm-induced, erosional truncation of the upward-shallowing phase during precessional base-level lowering (Fig. 2.17A).

Stromatoporoid facies make up the HST of HFS 4, above transgressive deeper water mudstones. The clear progradation to the east in the cross section (Fig. 2.10D) was controlled by increased accommodation to the east, so that eastern areas remained deep ramp settings for longer than those in the west, which became sites of stromatoporoid carbonate deposition. The *Cladocoropsis*-algal carbonate HSTs of sequence 5.2 and 5.3, were generated following decrease in accommodation, which resulted in formation of *Cladocoropsis* meadows followed by deposition of low energy lagoonal muds (commonly in swales) over transgressive stromatopoid facies. These more restricted facies mark regional shallowing perhaps coupled with slightly increased salinities, and (for the muds) a marked decrease in energy due to widespread shallow-water conditions limiting wave generation.

The HST of HFS 6 which is dominated by deposition of ooid and peloid grainstone over transgressive *Cladocoropsis*-dominated facies, mark decreased accommodation with sea level fall (Figs. 2.16, 2.17). This caused shallowing into fair-weather wave-base, generation of mobile substrates with few organisms, supersaturation with respect to carbonate phases, and precipitation of ooids.

The HSTs of HFSs 7 to 9 of the Arab-D anhydrite resulted from regional shallowing by upbuilding of the platform, coupled with long term 3rd order accommodation decrease, along

with superimposed 100 k.y. sea level falls, culminating in very shallow depths over the regional Arabian sills (Figs. 2.3, 2.16, 2.17). This restricted inflow of marine waters to replenish those lost to evaporation, pushed the waters from hypersaline values (associated with the TST carbonates of the Arab-D anhydrite) into saline brines in the calcium sulfate precipitation field as highstand sea-levels slowed and then fell. This resulted in widespread anhydrite deposition during 100 k.y. highstands (and lowstands). Note however, that at the 3rd order scale the anhydrites appear to be lowstand deposits (Fig. 2.16).

Comparison of Hawiyah and Harmaliyah Fields: Implications for Progradation Directions

Comparison of the stratigraphic successions of Hawiyah and Harmaliyah fields provides insight into whether the facies of these two fields were dominantly influenced by development on highs associated with growth of the present-day structures, or whether they were part of a single platform, on which very subtle structure influenced deposition.

Both fields have similar thicknesses, although there is a slight thickening of the Arab-D section toward the east into Harmaliyah. This is compatible with the overall northeast thickening of the Arab-D based on wireline logs (Taury Smith, pers. comm 2008). In addition, both fields have very similar sequence stratigraphy, down to the makeup of most of the parasquences (Fig. 2.10).

The transition from deep ramp facies up into stromatoporoid facies is grossly synchronous in both fields, occurring in AD-3.2. However, the base of the stromatoporoid facies climbs slightly to the east, over deeper water facies (Fig. 2.10 D). Also, the stromatoporoids persist longer to the east in Harmaliyah (into AD-5.2) compared to the west in Hawiyah, where they only extend up into AD-5.1. This indicateds progradation to the east (or northeast) which is compatible with the regional northeast paleoslope of a single platform indicated by regional

isopach maps based on log picks (L. B. Smith, personal communication., 2012). The lack of any evidence of progradation to the west, argues against a bathymetric basin (Arabian Basin) in close proximity to Ghawar controlling progradation direction, or even existing during Arab-D reservoir deposition (Fig. 2.3). This suggests that the Hanifa intrashelf basin (Murris, 1980; Ziegler, 2001), although it may have influenced Jubaila deposition, likely had filled by Arab-D reservoir deposition. The east (or northeast) progradation also is compatible with progradation directions evident in northern Ghawar and Abqaiq.

However, the facies maps (Figs. 2.11D, E and G), suggest that at times, more open marine facies developed of the northern and southern edges of Harmaliyah field, perhaps reflecting subtle structural control that locally modified the northeast regional paleoslope. Also, the widespread deposition of ooid grainstones appears to be relatively synchronous in both fields, occurring within sequence AD-6 and marking onset of hypersalinity. Finally, widespread onset of evaporite deposition occurs at the same time in AD-7 in both fields, although there is localized deposition of anhydrite at the top of AD-6 in central Hawiyah, suggesting local highly restricted conditions developed to the west, again compatible with the regional northeast paleoslope. Some thin carbonate tongues in the anhydrites also appear to be best developed in the east, pinching out westward, again supporting more open conditions to the east (and northeast).

Thus the sequence stratigraphy is strongly suggestive of a single platform extending across Ghawar and into Harmaliyah at least by the time of Arab-D deposition. It seems likely that during the late Jurassic, the present day structures had subtle topography on their crests, which had a local influence on the facies distribution. Given the approximately 20% difference in Jurassic thickness on and off the structures in the study area (Fig. 2.2B), would imply that during Arab-D deposition, the highs might have been subsiding at 6 cm/k.y. while the sags were

subsiding at just over 7 cm/k.y. This would hardly be enough to generate distinctive facies differentiation over the structures. However, to test this, cored stratigraphic test wells need to be drilled in the sags between the structures.

CONCLUSIONS

Overall facies and thickness trends across Harmaliyah and Hawiyah fields suggest slight thickening to the east and north-east, accompanied by slightly more open marine conditions in these directions. The strikingly similar sequence stratigraphic and facies development between the two fields suggests that they were part of a single platform at least during Arab-D deposition. However the facies trends were locally complicated by subtle topography developed over these structures.

Subsidence rates of ~6 cm/k.y. coupled with eustatically induced, incipient drowning of the Jubaila platform, provided substantial accommodation for subsequent Arab-D deposition. This generally acted to suppress the effects of sea-level fall, thus limiting the development of emergence surfaces. The 3rd order composite sequence within the Jubaila-Arab-D interval, with its two subsequences (each ~ 1 m.y. duration) may relate to Milankovitch long term obliquity forcing which has nodes at 1.2 m.y. The estimated durations of the 12 high frequency sequences mapped between the two fields likely relate to short term (100 k.y.) orbital eccentricity. The component meter scale parasquences could relate to precessional and sub-precessional forcing and autocyclic processes, given the well documented Milankovitch forcing evident in deeper water sections elsewhere and the average parasequence duraions. This external forcing of sea level resulted in slicing of the reservoir into hierarchical bundles of reservoir- and baffle units.

Juxtaposition of high-energy storm-beds onto deep ramp muds within the Arab-D, likely reflect significant base level changes associated with high frequency sea level changes. This is suggestive of cool- or transitional mode global climates with some buildup of Gondwana ice sheets during times of cool summers. However, it is likely that the bulk of the Arab-D carbonates and evaporites, which generally lack significant emergence features, were deposited under greenhouse conditions, with only periodic buildup of small continental ice sheets.

The overall transition from deep ramp mud-storm bed units, through stromatoporoid and *Cladocoropsis* facies to peloid- and ooid grainstone to evaporite facies, reflect long term shallowing, with increasingly shallow water depths over the Arabian sills north and east of the study area, which was critical in controlling facies and carbonate versus evaporite deposition. Grainy reservoir units within the Arab-D formed within a window where water depths had become shallow enough for the sediments to be winnowed by waves and tidal currents, but sill depths were deep enough for the platform waters to remain in the carbonate precipitation field.

The thick Arab-D anhydrite is suggested to have formed during third-order lowstand. At this time, lowered sea levels restricted marine inflow across the sills of the Arabian Platform. Evaporite deposition at this time of relatively static sea level was favored by high rates of subsidence coupled with loading by dense anhydrite.

The dominant calcite mineralogy of the Arab-D grainy facies (excluding the probable updip originally aragonitic ooids) is compatible with low Mg/Ca ratios in the Late Jurassic. The widespread development of coated grains and peloids reflects a well documented peak in microbial calcification at the end of the Jurassic. The arid climate, dominant calcite mineralogies and cryptocrystalline composition of many of the grains may have favored preservation of primary porosity by inhibiting near-surface cementation.

FIGURES

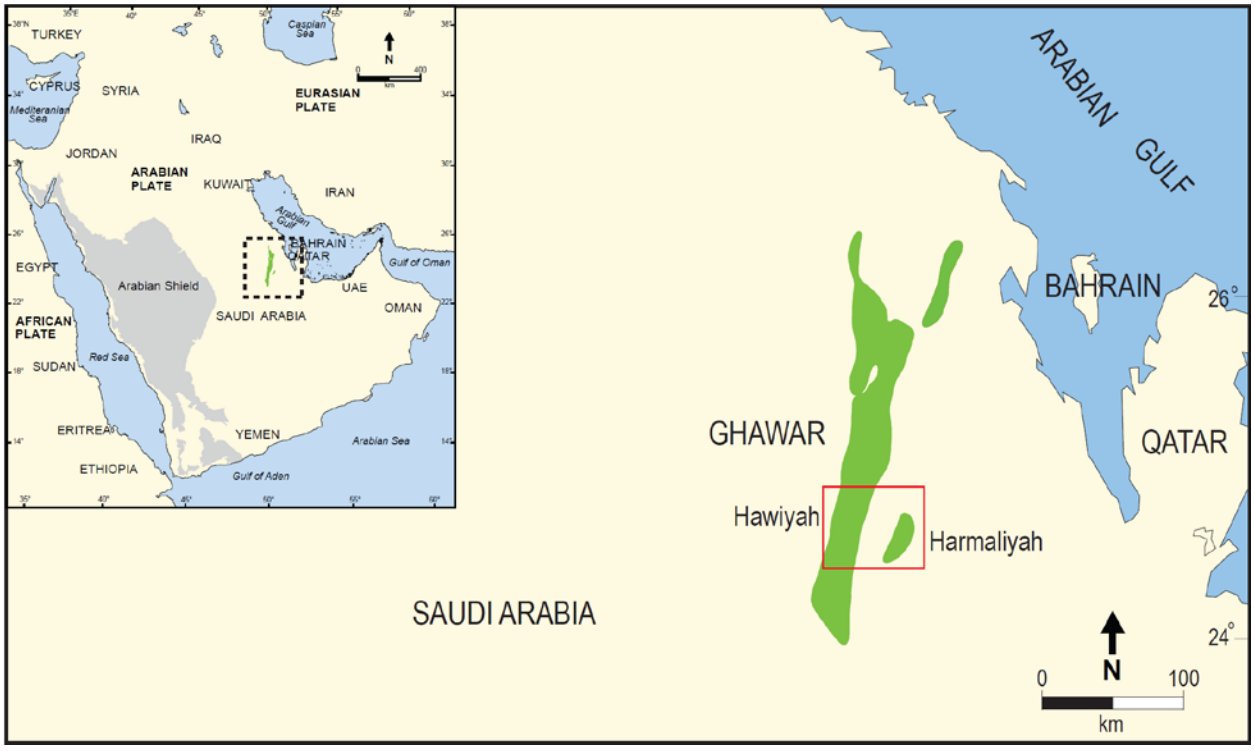

Figure 2. 1: Location map showing study area (red box) comprising Hawiyah field (Ghawar) and Harmaliyah field, Eastern Province, Saudi Arabia. Inset map shows location of study area (dashed rectangle) within the Middle East region.

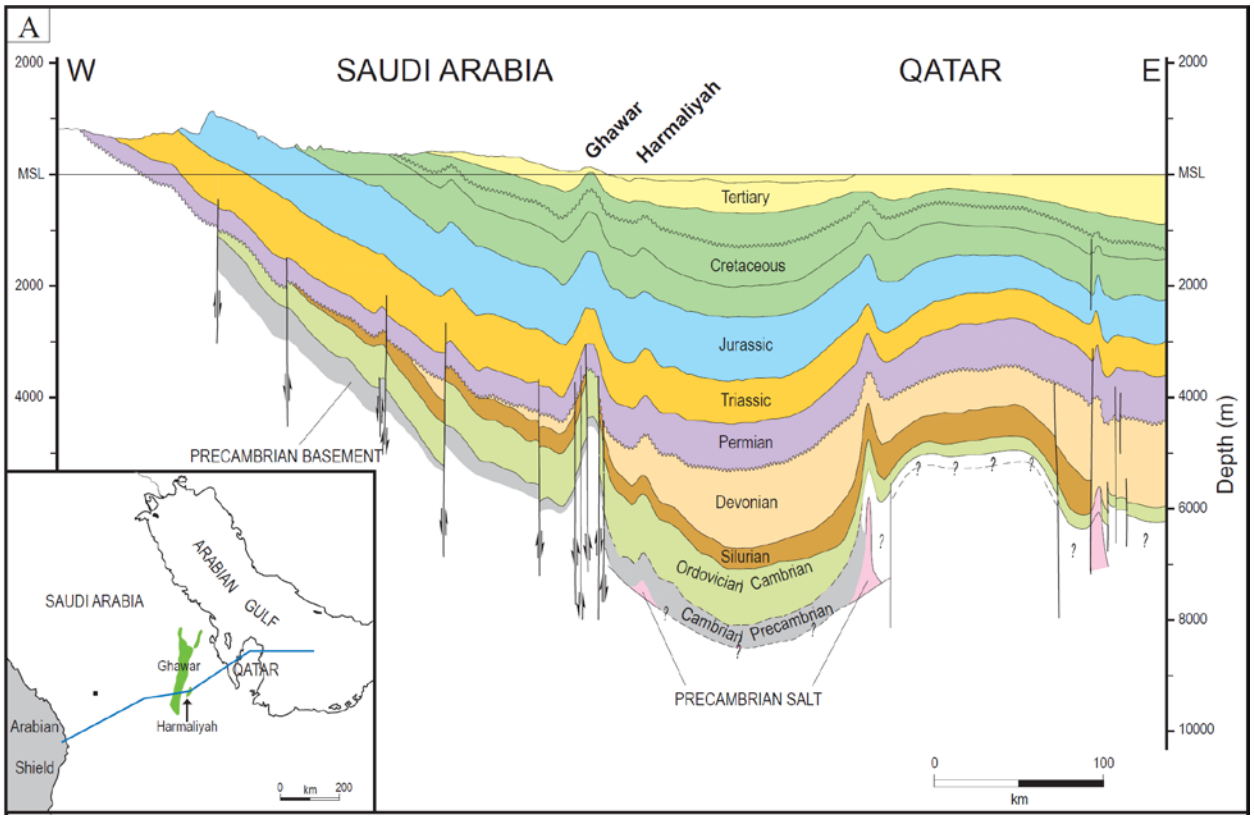

Figure 2.2A: East-west structural and stratigraphic cross-section across Arabian Plate passing through the study area (modified from Konert et al., 2001 and Abu-Ali, 2005). B. Restored cross-section of the Jurassic interval, datumed on top of the Jurassic. Section thickens into the Arabian Basin, and thins slightly over Ghawar and Harmaliyah fields, thickening off structure. The Jurassic then thins eastward over an outer shelf high.

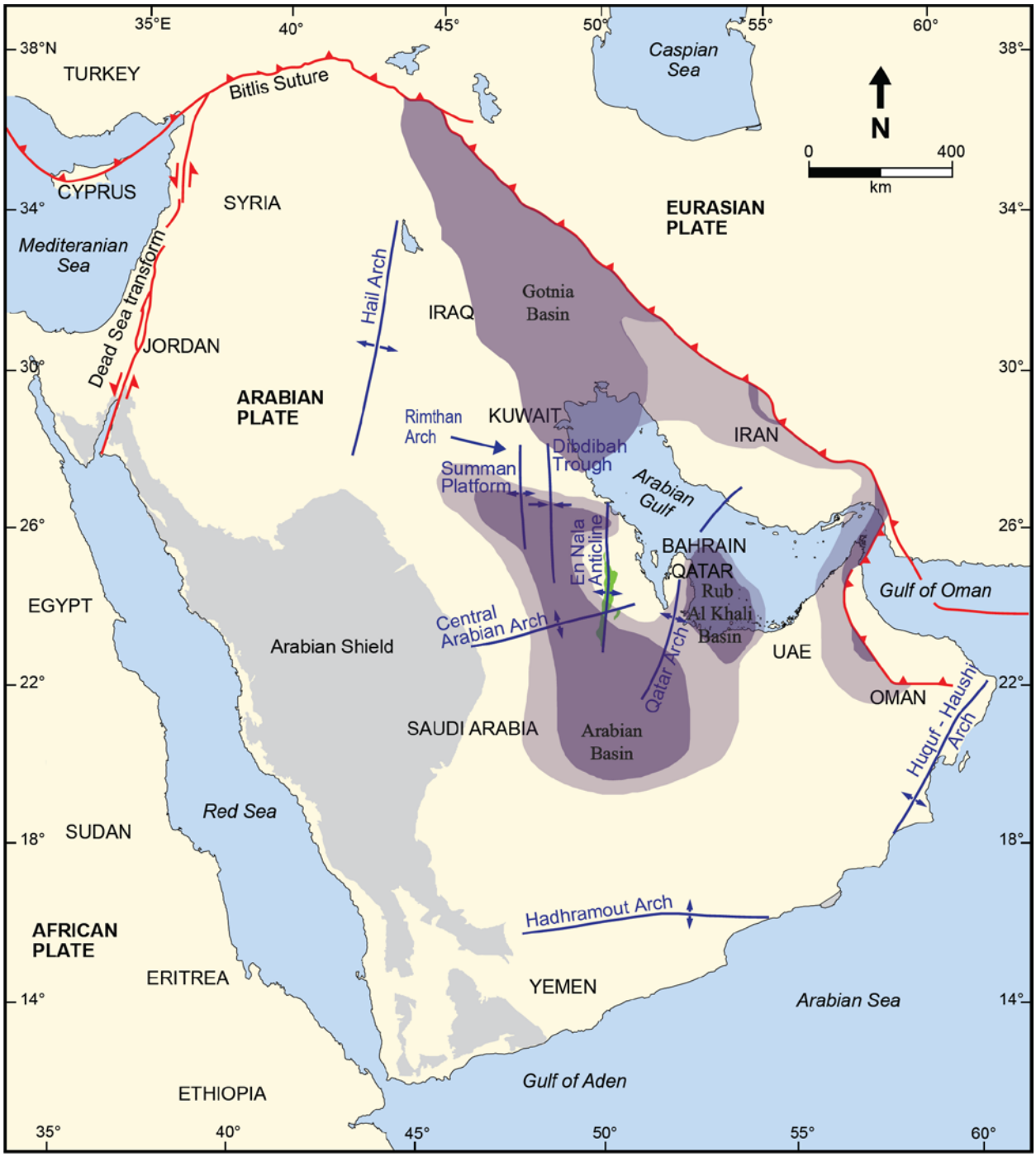

Figure 2.3: Major structures and sedimentary basins within Arabian Plate (modified after Konert et al., 2001; Ziegler, 2001; Lindsay et al., 2006; and Faqirah et al., 2009). The study area of Hawiyah (Ghawar) and Harmaliyah fields (green) are in the vicinity of the En Nala Anticline and just east of the Arabian Basin.

.

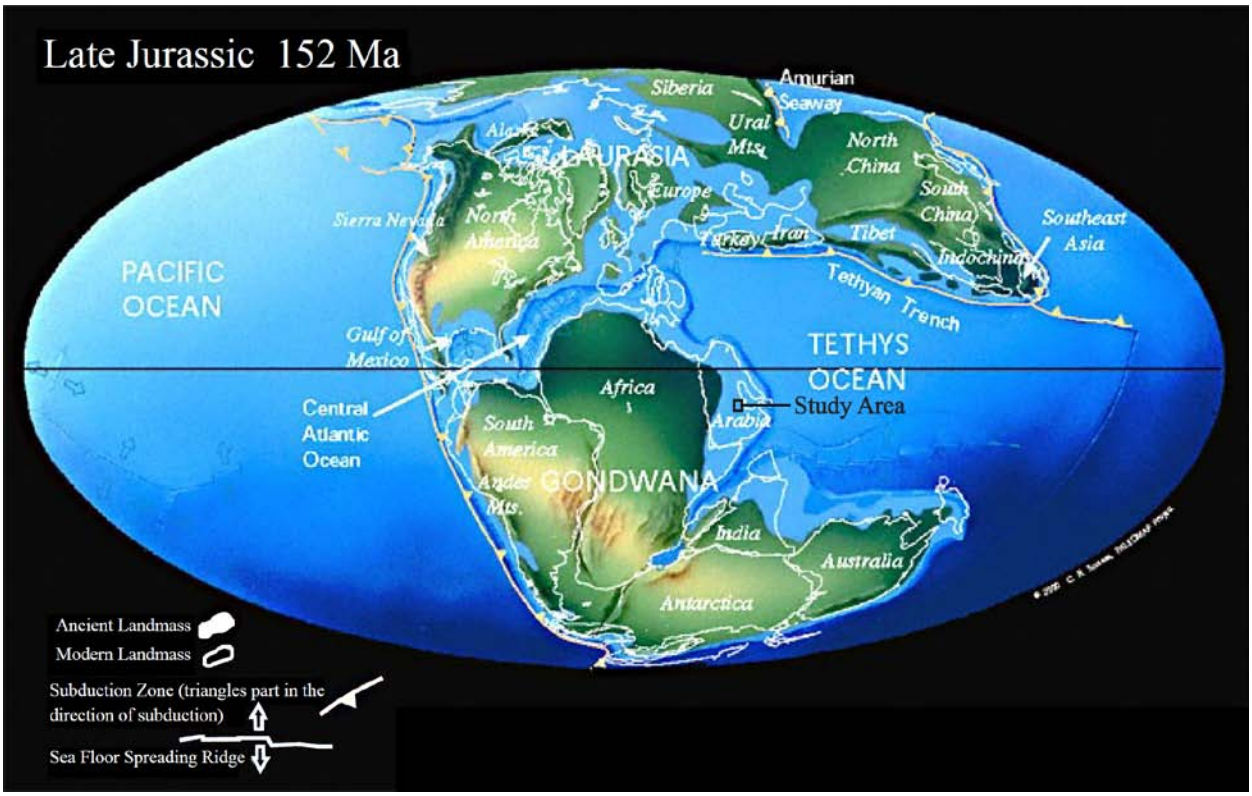

Figure 2. 4: Late Jurassic paleogeographic map, modified from Scotese (2003), with the study area outlined by the black rectangle.

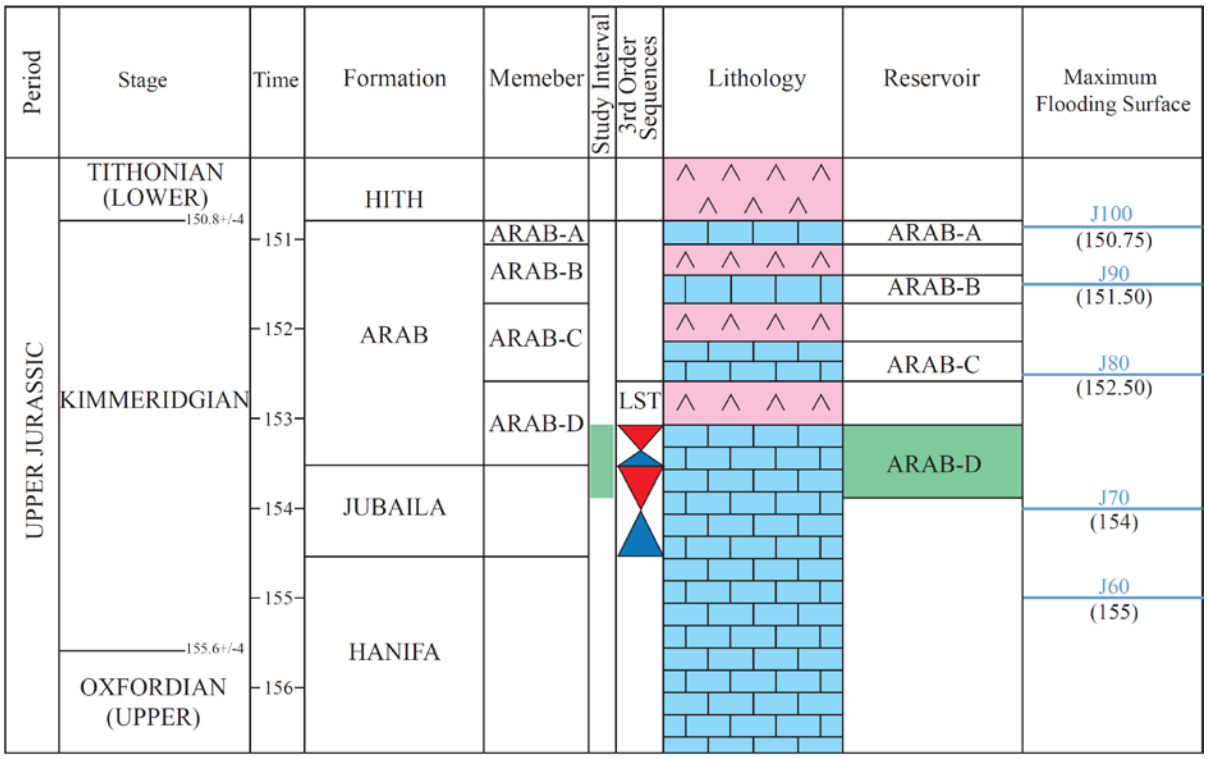

Figure 2.5: Chronostratigraphic chart showing age relations of the Late Jurassic units, and the Arab-D reservoir study interval. The blue triangle represents the 3rd order TSTs and the red triangle represents the 3rd order HSTs. Kimmeridgian is 5 m.y long (Gradstein et al., 2004) to 7.5 m.y. long (based on cyclostratigraphy; Weedon et al., 2004). Time scale from Gradstein et al. (2004).

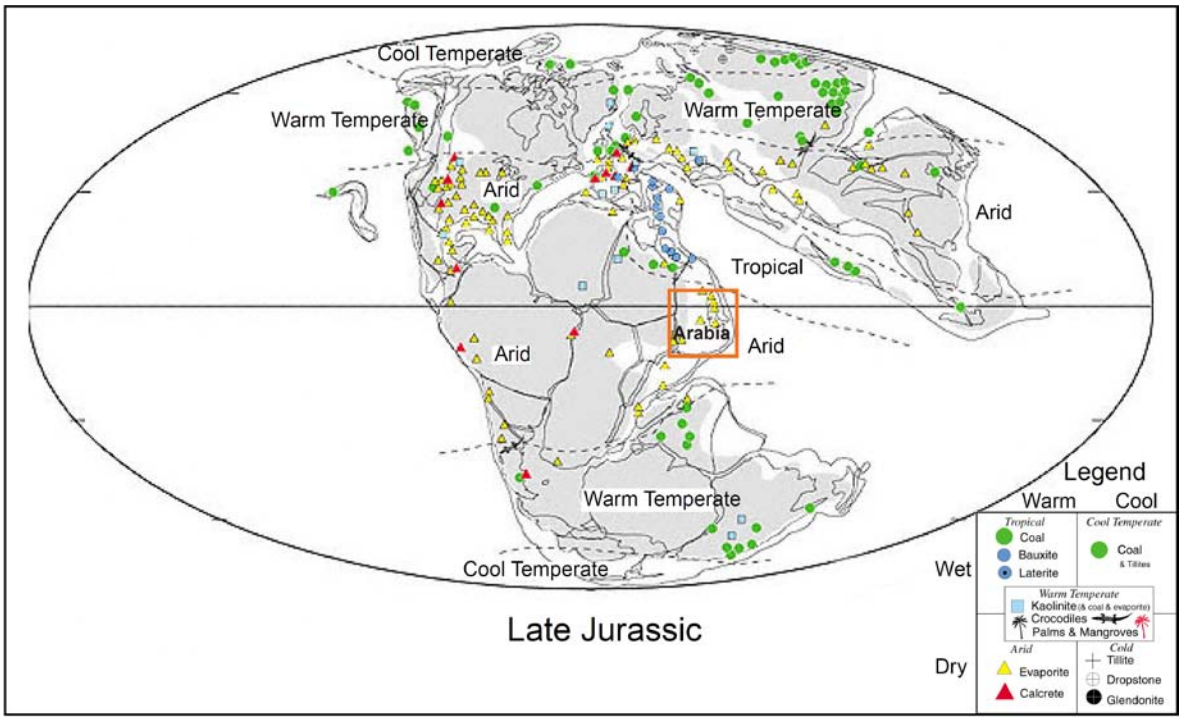

Figure 2. 6: Late Jurassic paleoclimate map showing paleoclimatic zones. Arabia (outlined by orange box) lies in the arid desert belt which forms a broad band throughout the tropics. Modified from Scotese, 2003.

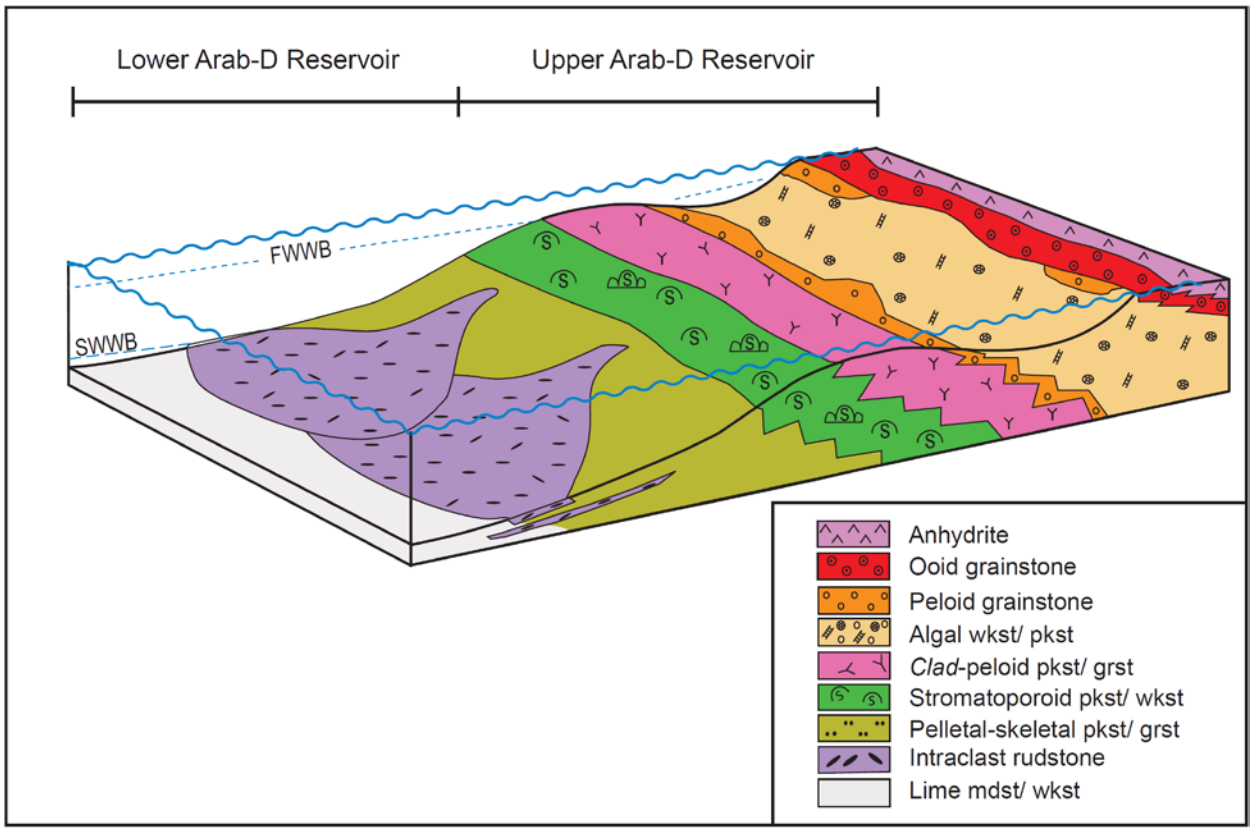

Figure 2.7: Depostional model showing relative position of facies in terms of relative water depths. At no time did the deeper water facies coexist with the shallow water facies on the diagram. Deeper water facies on the left hand side of the diagram dominate in the lower Arab-D reservoir, while the intermediate and shallow water facies on the right hand side make up the upper Arab D reservoir and anhydrite. However, facies mapping does show that interfingering between stromatoporoid facies and deeper water facies occurs in the study area.

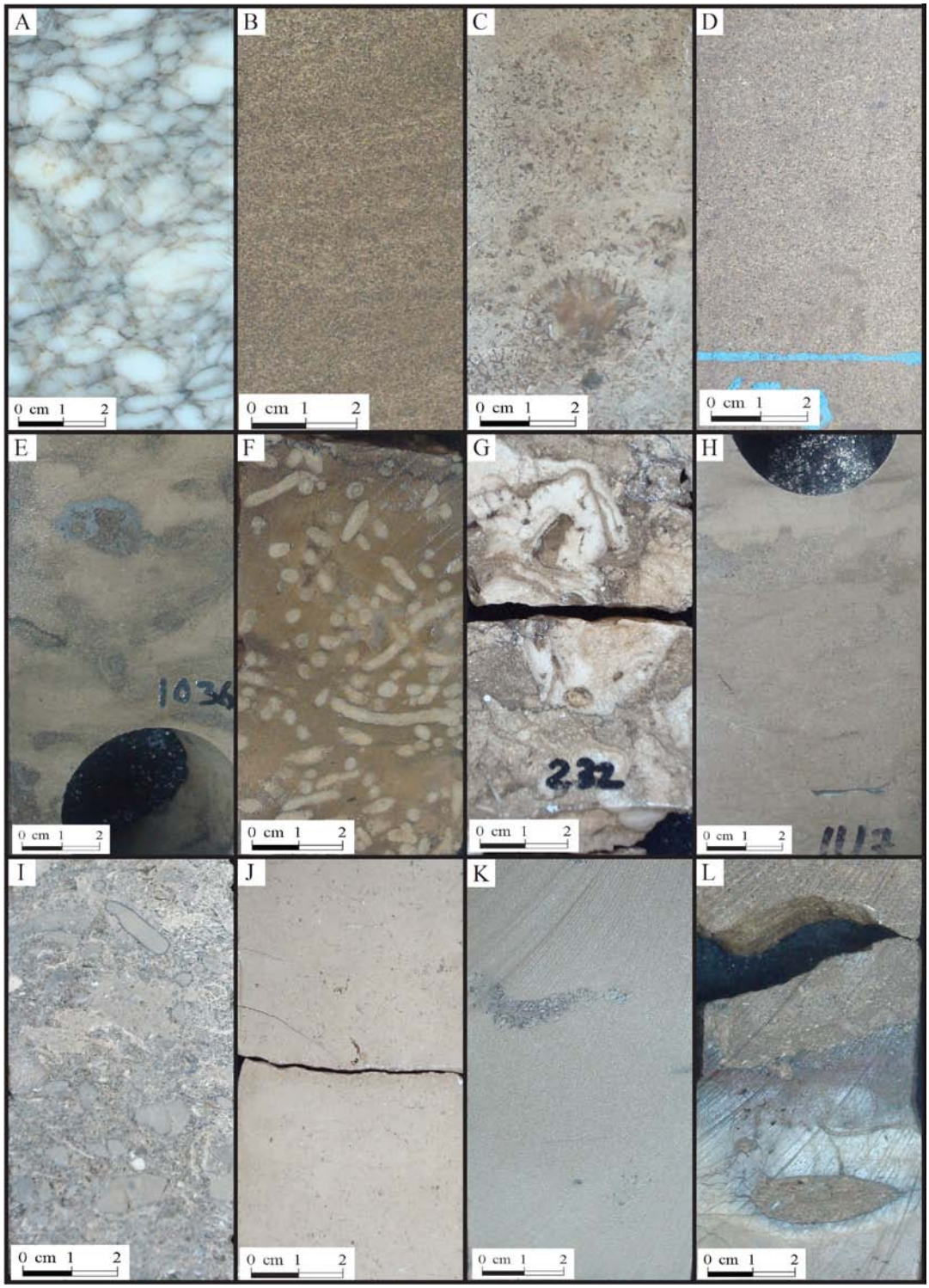

Figure 2.8: Slab photos of major facies in the study interval arranged from shallow to deep. A. Anhydrite, B. Ooid grainstone, C. Gastropod ooid grainstone, D. Peloid, skeletal-fragment grainstone-packstone, E. Algal wackestone, F. Peloid-Cladocoropsis packstone, G. Stromatoporoid wackestone, H. Fine grained pelletal-skeletal packstone, I. Fine grained pelletal-skeletal packstone, J. Peloid skeletal wackestone, K. Lime mudstone, L. Hardground.

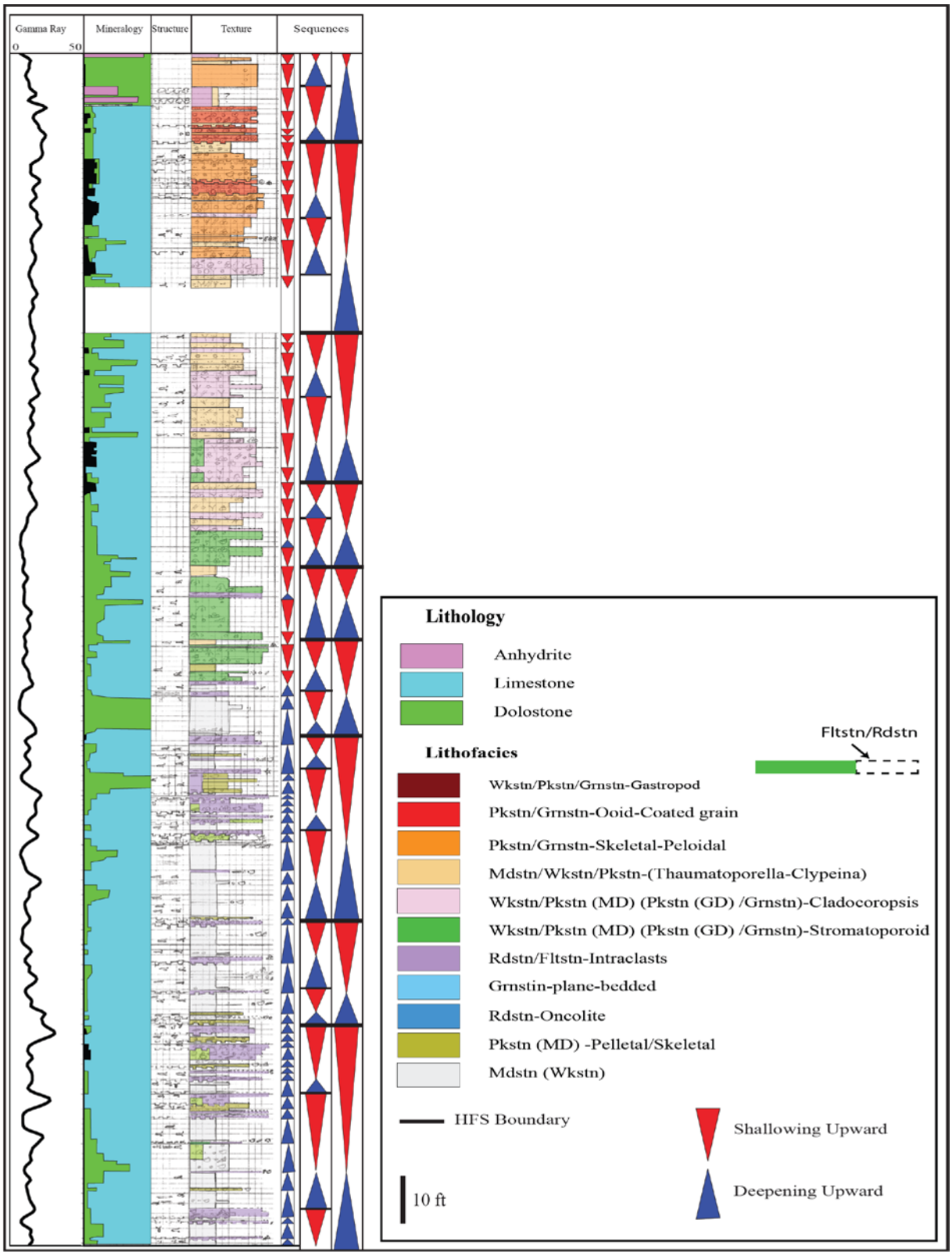

Figure 2.9: Selected stratigraphic column from Harmaliyah showing the facies stacking and the sequences.

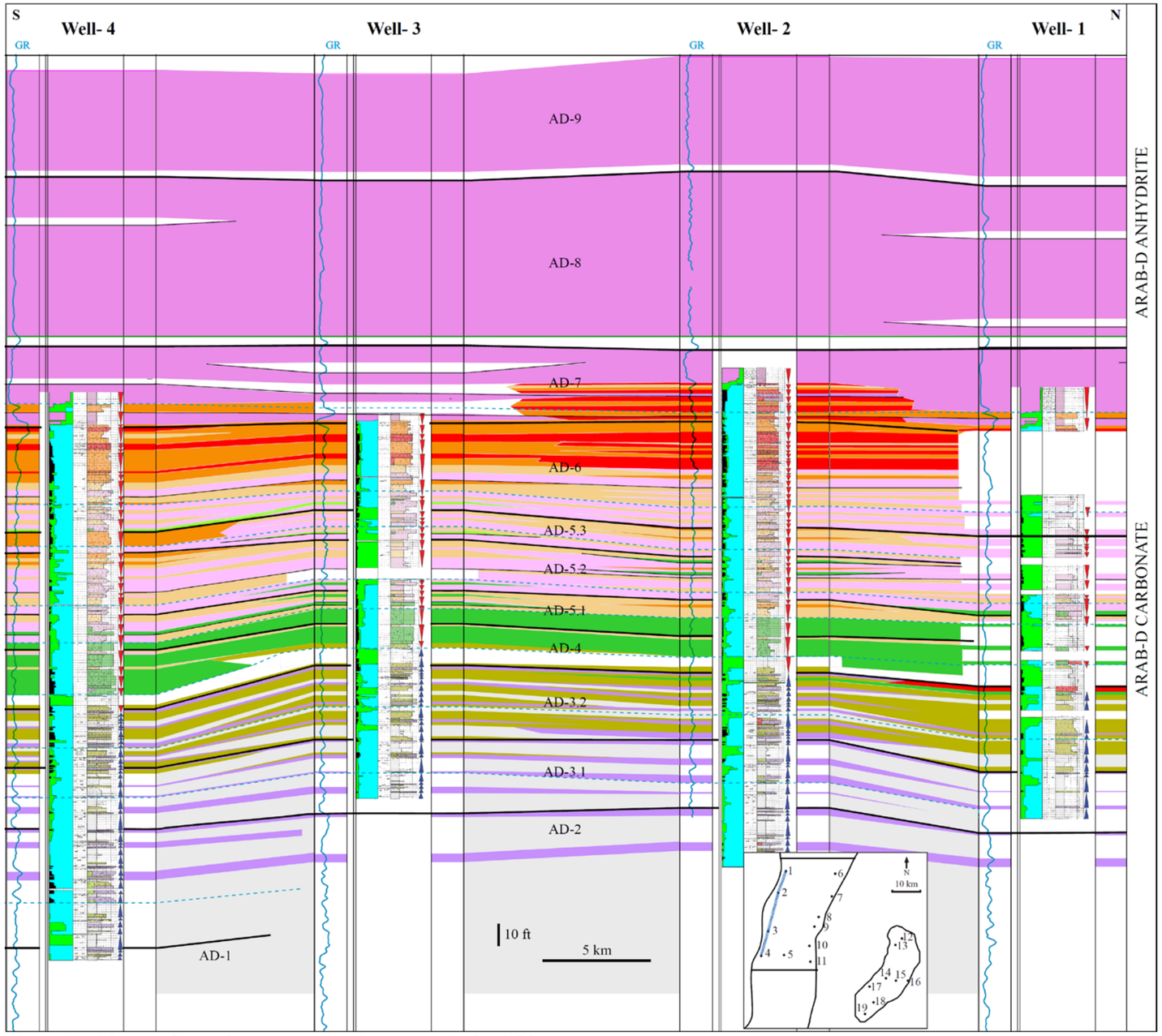

Figure 2.10A: North-south cross section from Hawiyah Field.

Figure 2.10B: North-south cross section from Harmaliyah Field.

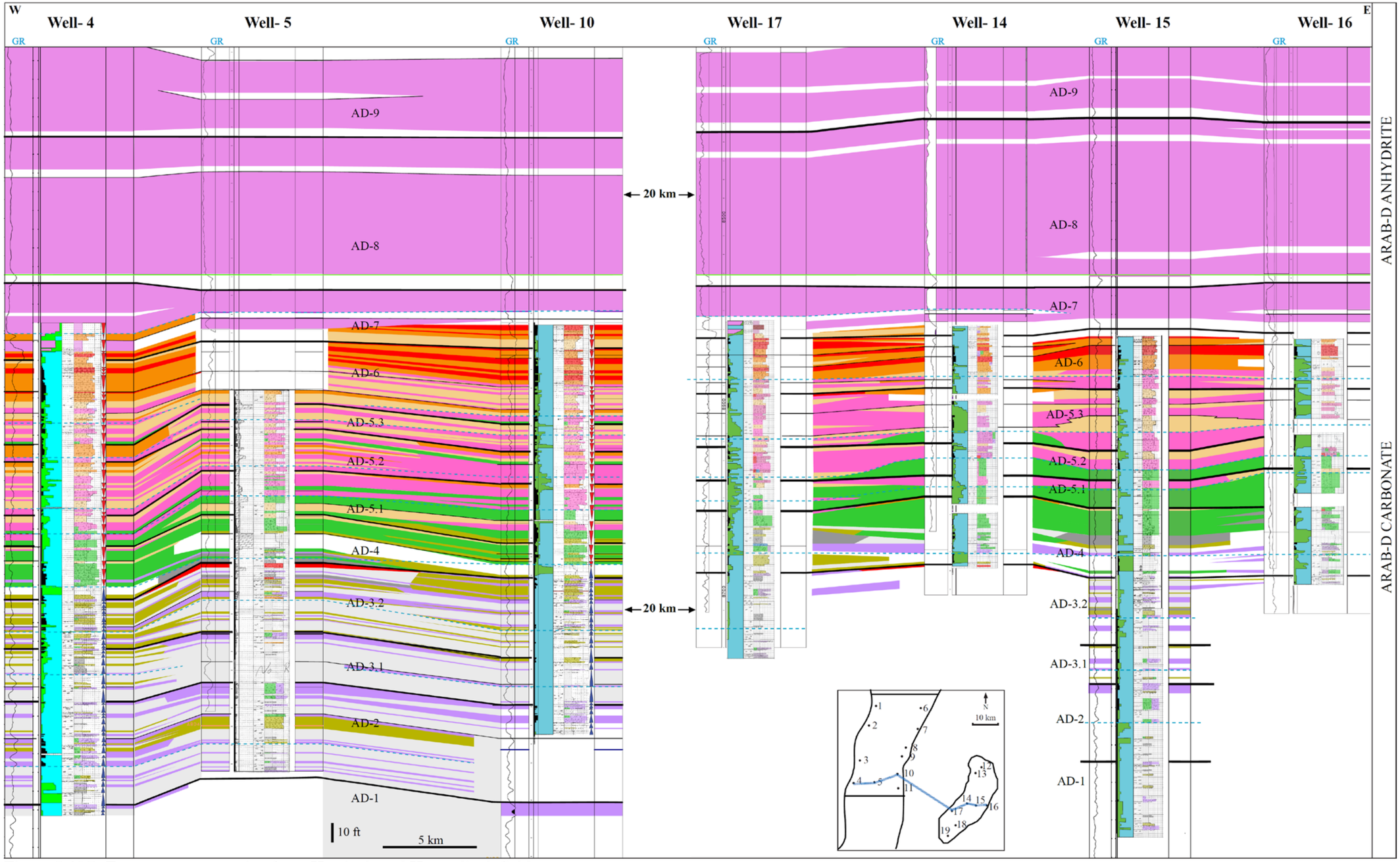

Figure 2.10C: East-west cross section from Hawiyah and Harmaliyah fields.

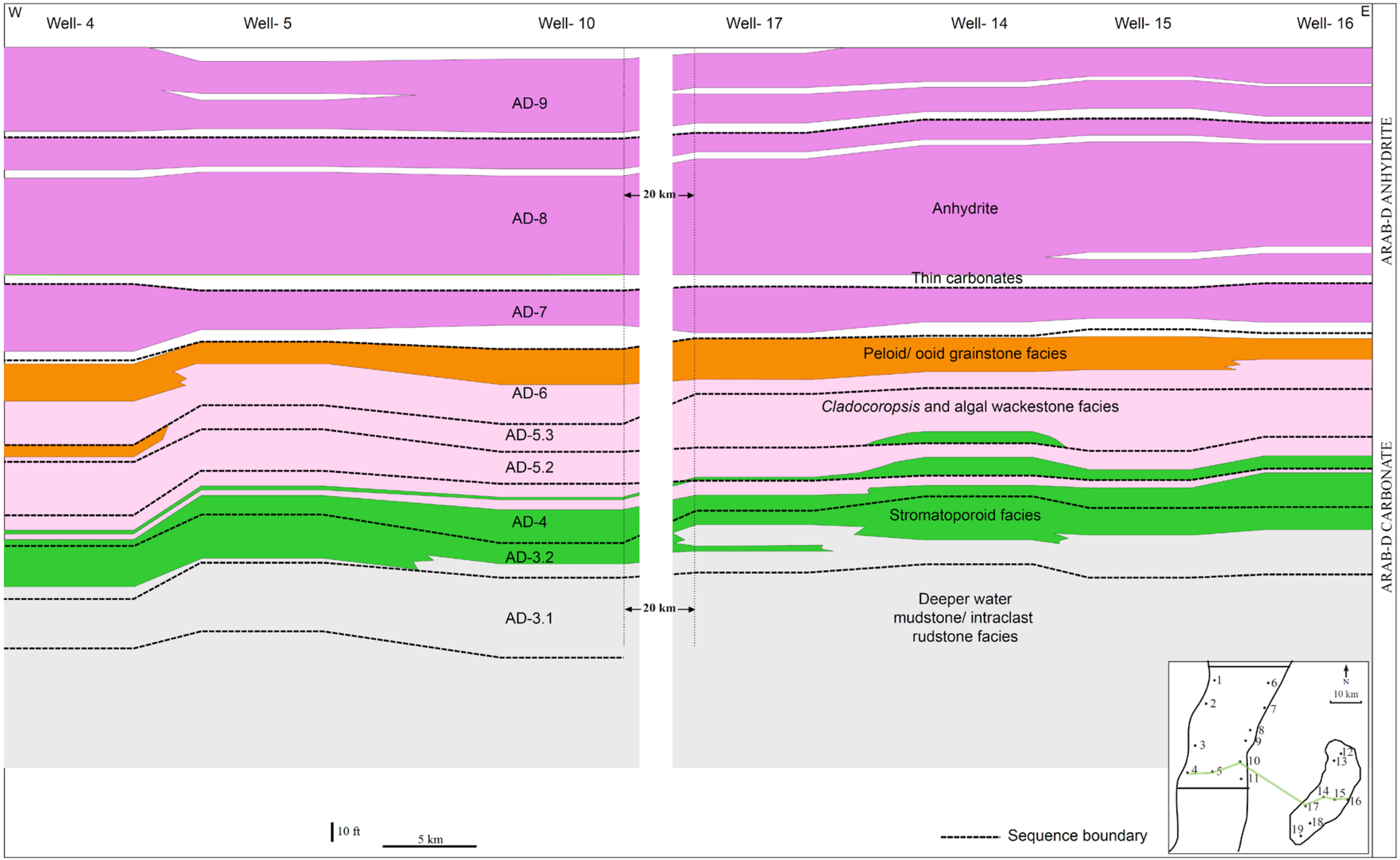

Figure 2.10D: Simplified schematic W-E cross section to illustrate progradation direction. Stromatoporoid facies of AD-4 show eastward progradation over deeper ramp facies below. Stromatoporoids remain locally developed in east, within prograding Cladocoropsis facies. Peloid-ooid grainstone facies show progradation to the east in AD-6. Within AD-8, a thin carbonate tongue extends from the east into the anhydrite, again indicating more open marine conditions to the east, as does the local pinchout of the carbonate to the west, within the AD-9 anhydrite.

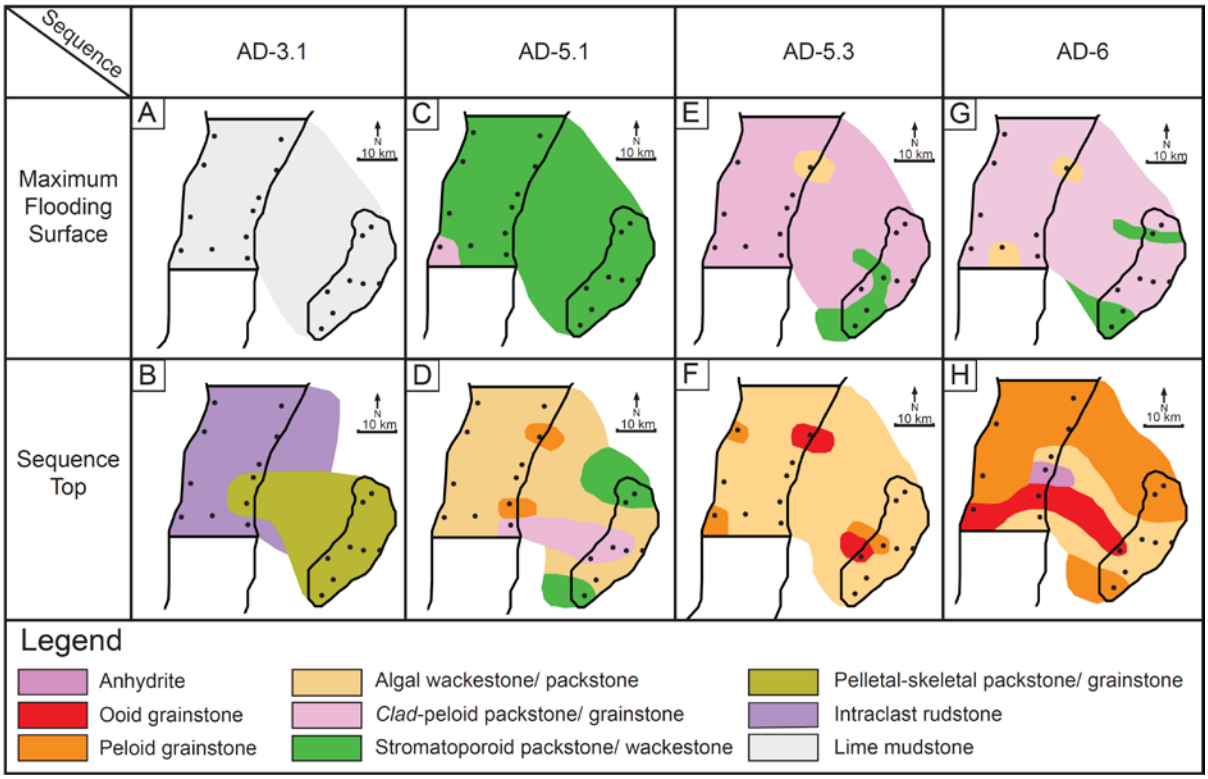

Figure 2.11: Selected facies maps spanning Hawiyah and Harmaliyah fields showing the distribution of rock types at the MFS and at the top of the sequence (late HST) for sequences AD-3.1, AD-5.1, AD-5.3, and AD-6.

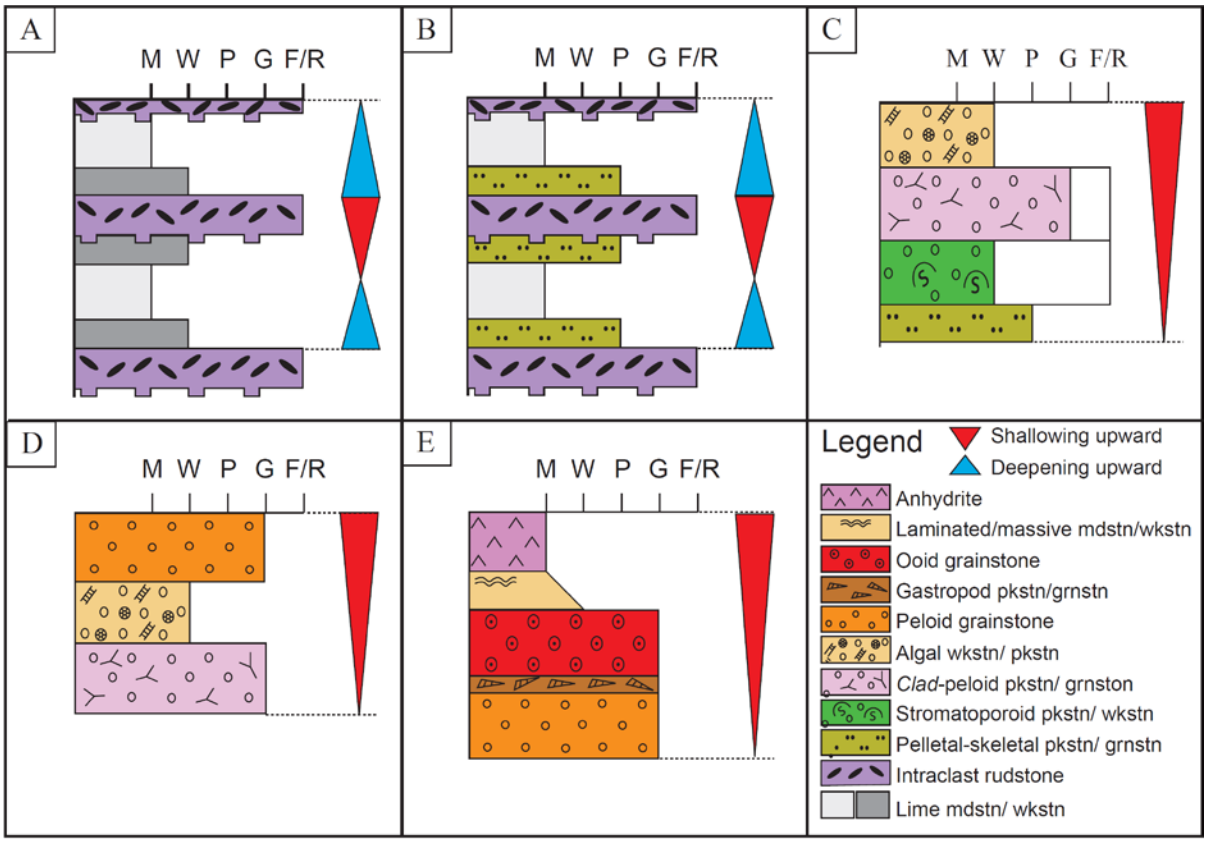

Figure 2.12: Diagram illustrating the different types of idealized parasequences in Arab-D reservoir. A, B. Symmetrical and asymmetrical Intraclast rudstone-lime mudstone (lower Arab-D). C. Stromatoporoid parasequence . D. Cladocoropsis parasequences. E. Ooid grainstone-dominated parasequence.

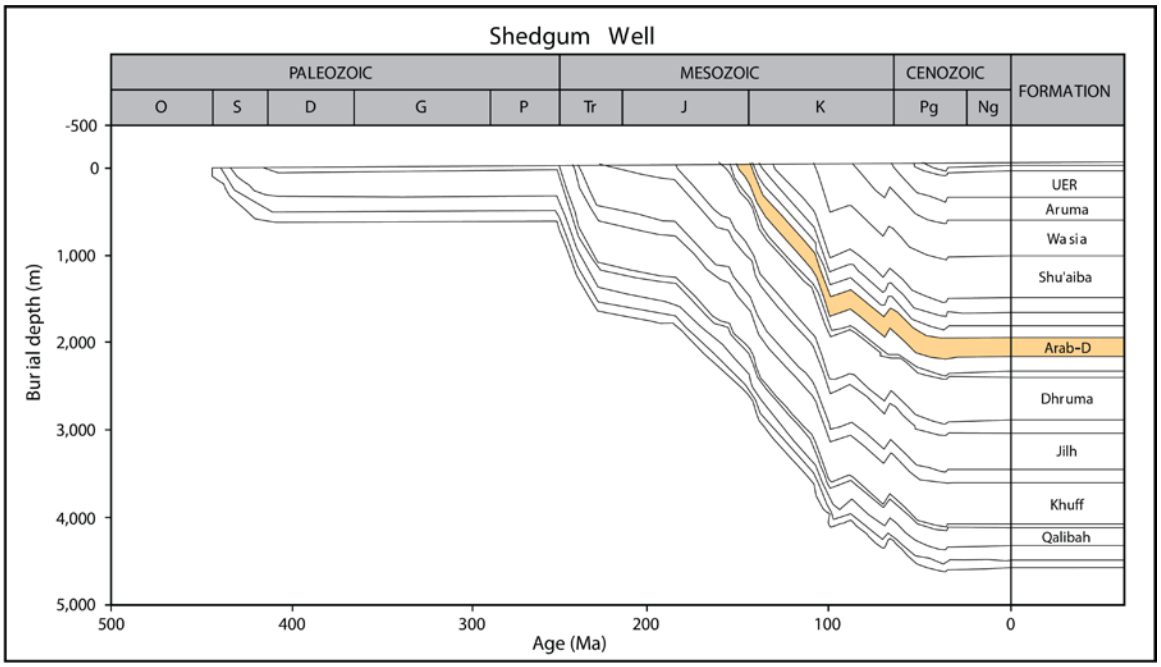

Figure 2.13: Subsidence history plot from Ghawar (modified after Abu Ali and Littke, 2005). The Arab-D study interval is shaded orange. There is relatively rapid subsidence in the Late Jurassic during Arab-D deposition, which was initiated in the middle Jurassic and slows into the Cretaceous.

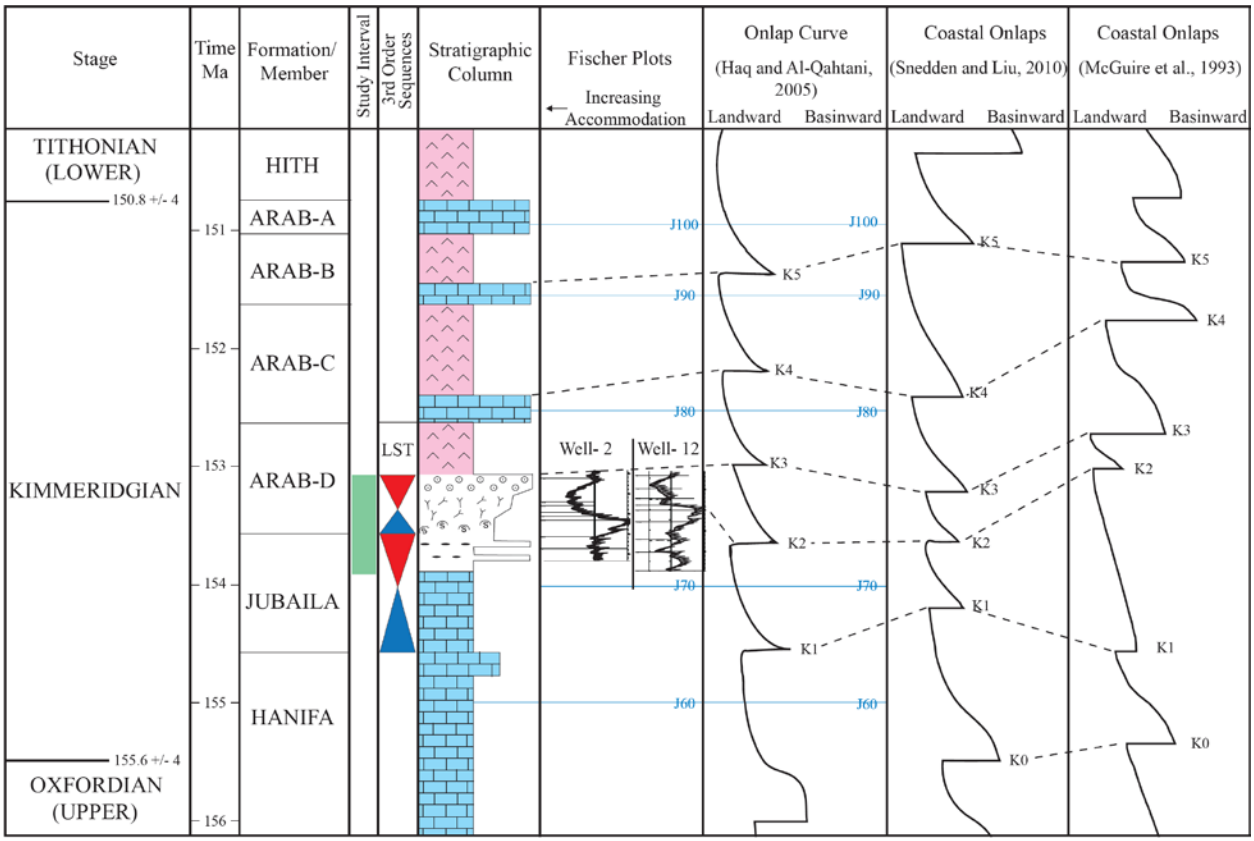

Figure 2.14: Chronostratigraphic chart of the Late Jurassic Hanifa-Jubaila-Arab-Hith interval along with published sea level and the curve for Arabian Plate. Fischer plots of the study interval are shown along side stratigraphic column (see Fig. 2.15 for enlarged plots of the study interval are shown along side stratigraphic column (see Fig. 2.15 for enlarged plots). Dashed correlation lines linking sea level events are tentative, given the poor biostratigraphic control on the interval.

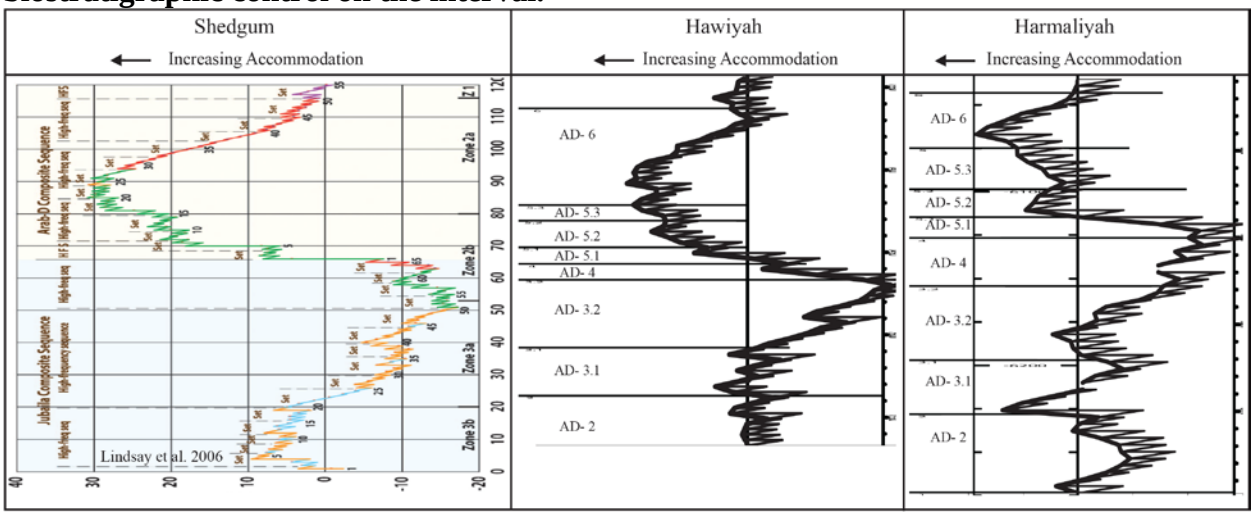

Figure 2.15: Fischer plots of cyclic successions of two wells from Hawiyah and Harmaliyah fields (this study) compared with Shedgum well from Lindsay et al. (2006). The Fischer plots graph cumulative departure from average cycle thickness against cycle number up the section.

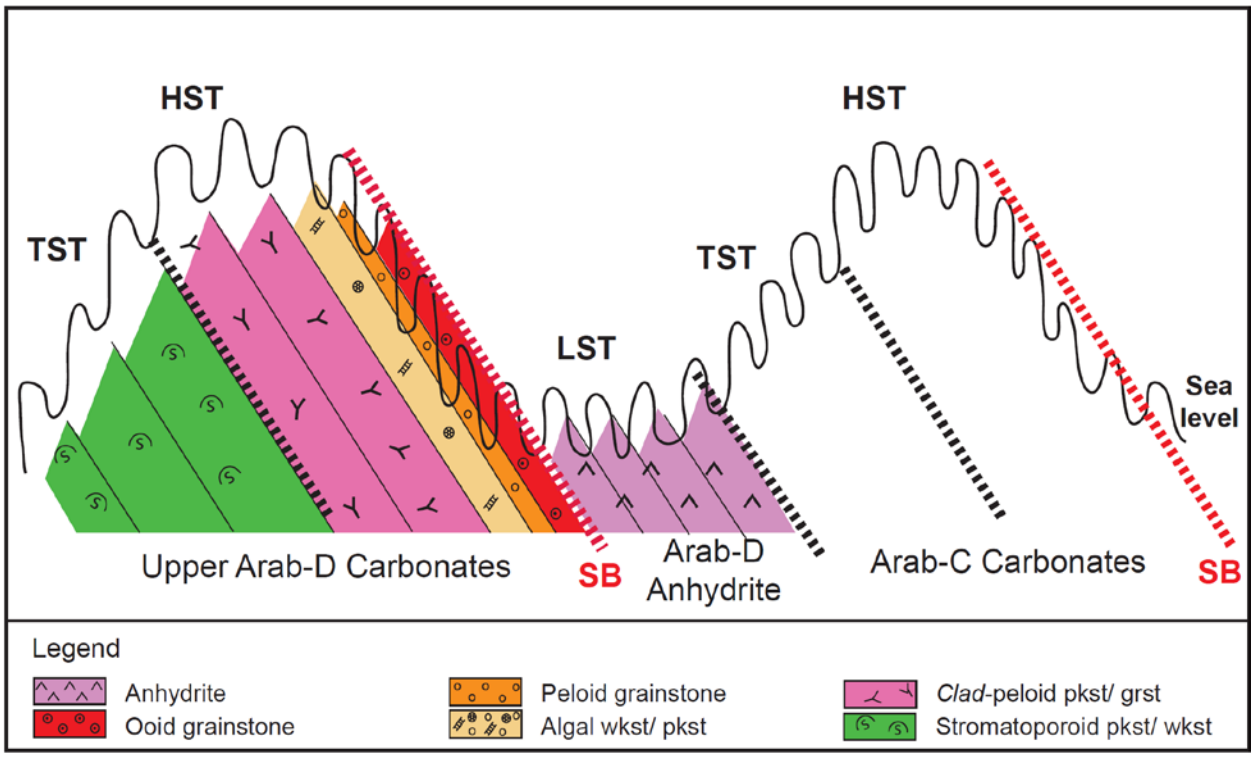

Figure 2.16: Formation of the overall shallowing upward succession of the upper subsequence of the Arab-D. Horizontal axis is time and vertical axis is distance. Deposition of stromatoporoid parasequences during 3rd order sea level rise. *Cladocoropsis* parasequences developed following 3rd order maximum flooding, as sea level rise slowed. This was followed by deposition of peritidal parasequences during initial 3rd order fall. Sequence boundary developed during zero accommodation, followed by deposition of anhydrites during lowstand.

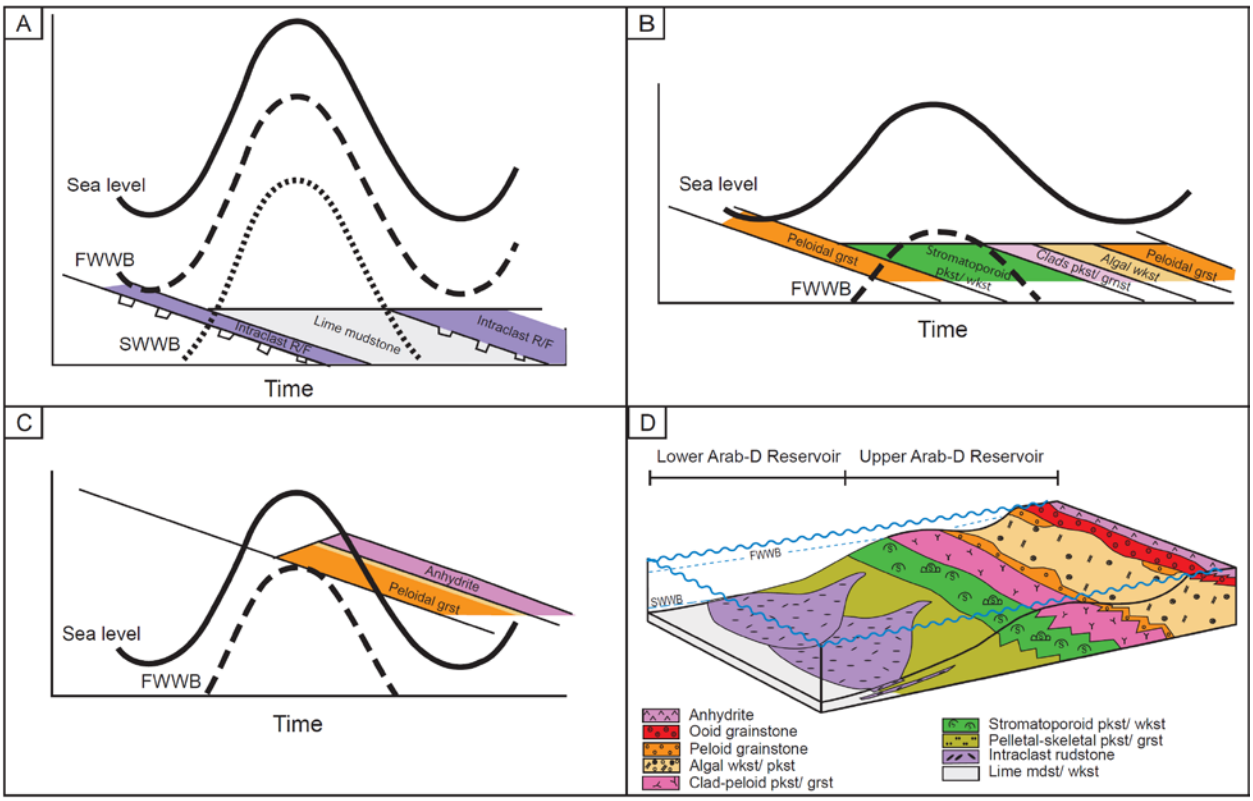

Figure 2.17: Schematic plots with time (horizontal axis) and distance or depth (vertical axis), showing how the parasequences formed with respect to subsidence and a single precessional sea level cycle. SWWB: storm weather wave base, FWWB: fair weather wave base. A. Formation of deeper ramp parasequences: Hardgrounds may have formed either during peak water depths (by sediment starvation) or during falling sea level due to sediment bypass. Intraclastic storm beds were deposited between SWWB and FWWB during base level lowering. Lime mudstones were formed below SWWB during sea level rise and highstand. B. Formation of stromatoporoid parasequences: Sea level rise flooded grainstones, which following a lag time, were overlain by stromatoporoid facies (water depths up to 10 m). With shallowing due to sea level fall, a regressive succession of Cladocoropsis and algal carbonates, capped by grainstone were deposited. Sea level fall may or may not expose tops of parasequences. C. Formation of peritidal grainstone-evaporite cycles: Sea level rise floods platform, and grainstones are deposited above FWWB following a short lag time. With shallowing and energy decrease tidal flat carbonates and evaporites are deposited. Sea level fall results in emergence and disconformity on paraquence. D. Inset sows depostional model and legend.

TABLES

Table 2. 1: Description of main Arab-D facies

Facies	Anhydrite, minor dolomite	Microbial laminae	Ooid grainstone to packstone	Gastropod grainstone to packstone	Peloid- skeletal fragments grainstone to packstone	Algal wackestone to packstone	*Cladocoropsis*, peloidal grainstone to wackestone	Stromatoporoid packstone to wackestone	Fine pelletal-skeletal packstone	Intraclast rudstone to floatstone and pellet packstone/ grainstone	Peloidal, Skeletal wackestone	Lime mudstone
Occurance and Thickness	Upper Arab-D 40 m	Upper Arab-D 60 cm- 80 cm	Upper Arab-D 20 cm- 1m	Upper Arab-D 30 cm- 1 m	Upper Arab-D 30 cm- 1.2 m	Upper Arab-D 20 cm- 1.2 m	Upper and middle Arab-D 30 cm- 2.13 m	Middle Arab-D 30 cm- 3 m	Middle Arab-D few cm- 1.1 m	Middle and lower Arab-D few cm- 1.1 m	Lower Arab-D few cm- 1 m	Lower Arab-D few cm- 2.13 m
Mineralogy	Anhydrite	Calcite and Dolomite	Calcite	Dolomite	Calcite	Calcite	Calcite and dolomite	Calcite and dolomite	Calcite	Calcite	Calcite	Calcite
Color	White	Brown	Light to medium brown stain	Light gray to white	Light to medium brown stained	Light to medium brown stained	Brown stained	Brown stained	Brown stained	Gray	Gray to dark gray	Gray to dark gray
Sedimentary Structures	Massive to nodular to bedded nodular anhydrite and fine laminated dolomite layers and lenses	Planar, wavy, and crinkly microbial laminae	Cross-bedding and angle horizontal lamination	Coss-bedded to massive	horizontal mechinical laminae, to cross laminae, to massive	Common to abundant subhorizontal to short vertical burrows	Cross-bedding locally in grainy units	Massive	Massive; less commonly laminated above storm beds	Hardgrounds and firm grounds	Hardgrounds and firm grounds capping units, Thallassinoides, rare horizontal and wavy laminae	Hardgrounds and firm grounds capping units, burrows, laminiations
Texture	Mud-support	Dolomudstone, fine Packstone	Grainstone to packstone	Grainstone to packstone	Grainstone to packstone	Wackestone to packstone	Grainstone to wackestone	Packstone to wackestone	Packstone, minor grainstone	Rudstone to floatstone	Wackestone	Mudstone
Grain size, grain Types, fossils, and matrix	Silt to clay size, unfossiliferous	Silt to clay size pellet, lime mudstone and fine dolomite crystals	Fine to medium sand size of ooids, peloids, forams (miliolids), and lime mudstone in packstone	Fine sand to gravel size of ooids, peloids, and whole and fragmented gastropod, forams (miliolids), and minor lime mudstone in packstone	fine sand to granule size of peloids, mollusks, forams (miliolids), rare *Cladocoropsis*	mud-size to very coarse sand size of peloids, calcareous algae (*Thaumatoporella* and Clypeina), and forams (miliolids), with common to abundant lime mud	mud, fine sand to granule size of peloids, *Cladocoropsis*, algae, forams (miliolids), and lime mud	Mud to sand size host of Peloids, forams, and mud with 2-10 cm of encrusting and domal stromatoporoids, *Cladocoropsis*, and rare large gastropods	Dominantly very fine matrix of pellets with very coarse sand size of mollusks, echnoderms, and minor interstitial lime mud	fine to pebble size of peloids, Intraclasts, mollusks, Brachipod, forams (Lenticulina), Stromatoporoids (rare)	Fine to medium size of peloids, sponge spicules, forams (Lenticulina), mollusks, brachiopods	Silt to clay with minor fine to very coarse size of peloids, sponge spicules, mollusks, brachiopods
Diagenesis		partially to completely dolomitized in some areas	-	dolomitized, leached mollusk and grains	--	Some fine to medium dolomite crystals	Partially dolomitized, some leached *Cladocoropsis*	Partially to totally dolomitized in some areas	Rare rim cementing on echidoderms		Partially to totally dolomotized in some areas, or at least dolomitized burrows	
Reservoir Quality	None	None	High interparticle porosity	Low, moldic porosity	High to moderate interparticle porosity	None	Moderate to low intraskeletal and interpaticle porosity	Moderate to low intraskeletal porosity; some interparticle in packstone	None	Fair to high porosity	None	None

Table 2. 2: Brief description of Arab-D sequences.

Sequence	Lithostrat and Sequence thinckness (meters)	Basal Boundary	Lowstand Systen Tract (LST)	Transgressive System Tract (TST)	Maximum Flooding Surface (MFS)	Highstand System Tract (HST)
AD-1 - AD-3.2	Dominantly lower Arab-D, part of **AD-3** is in the middle Arab-D **AD-1**: at least 12 m thick (no base in cores) **AD-2:** 10 m to 16 m thick **AD-3.1 and 3.2:** 17 m to 22.5 m thick	**SB-1:** Not cored **SB-2, 3.1 and 3.2**: conformable on grainy or resedimented carbonates underlain by hardgrounds on lime mudstone or wackestone	May include grainy resedimented carbonates included in top of HST of sequence	TST of AD-2, 3.1 and 3.2 comprised of one and a part of a parasequence, composed of thinning and fining upward packages of grainy (storm) beds up into wackestone and mudstone-dominated units.	Difficult to define as a single surface; above lower 1/3 of of AD-2 and AD-3, beneath lime mudstone units.	Fining upward parasequences of resedimented grainy facies and wackestone- mudstone. Grainy facies increase upward in HST.
AD-4	Middle Arab-D 4 m to 11.5 m thick	Sharp contact, conformable and locally disconformable on thin resedimented carbonates or in situ oolitic grainstone		Fining up, part of lower parasequence with multiple resedimented beds at the base locally, passing up into peloidal wackestone.	Probably within dolomitized muddy facies in lower part of sequence.	HST consists of up to 3 parasequences of muddy carbonates up into stromatoporoid carbonates commonly capped by peloid grainstone
AD-5 (5.1, 5.2, & 5.3)	AD-5.1 and 5.2 are in the middle Arab-D. 5.3 is in the upper part AD-5.1: 1.8 m to 6.7 m thick AD-5.2: 4.5 m to 6 m thick AD-5.3: 8 m to 14.5 m thick	Conformable on thin ooid and peloid grainstone, with sharp to locally gradational contacts.		Lower parasequence dominated by stromatoporoid carbonates	On thickest stromatoporoid carbonates.	Up to 15 parasequences of *Cladocoropsis*carbonates (w/p/g), lagoonal muddy carbonates and thin peloid grainstone caps
				AD- 5.1: Dominated by parasequences of stromatoporoid carbonates up into *Cladocoropsis* carbonates. **AD- 5.2:** Dominated by parasequences of *Cladocoropsis* carbonates, less algal wackestone/ mudstone and peloid grainstone. **AD- 5.3:** Dominated by parasequences of *Cladocoropsis* carbonates, less algal wackestone/ mudstone and peloid grainstone.		
AD-6	In Upper Arab-D; 8 m to 14 m thick	Sharp and conformable with local hardgrounds; on lagoonal mudstone, and less commonly on ooid grainstone		**AD-6**: 4-6 parasequences of *Cladocoropsis* and lagoonal algal wackestone/ mudstone	In the lower 1/3 to 1/2 of the sequence, at top of *Cladocoropsis* carbonates.	HST comprises upper 1/2 to 2/3 of the sequence; composed of up to 8 parasequences of peloid/ ooid grainstone and minor lagoonal algal wackestone/ mudstone
AD-7 - AD-9	In Upper Arab-D AD-7: 7 m to 11.5 m thick AD-8: 19 m to 28 m thick AD-9: 11 m to 18 m thick	**SB-7:** Sharp, dominantly disconformable (hardground surfaces) on peloid and ooid packstone/ grainstone, and locally gradational contacts. **SB-8** and **9**: Locally sharp contact on underlying evaporites		**AD-7:** TST consists two and a part of parasequence, of peloid-ooid grainstone **AD-8:** TST is within lower parasequence dominated by grainstone **AD-9:** TST is thin bed of carbonates within evaporite dominated sequence.	**AD-7:** In middle of sequence on top ooid, peloid grainstone units. **AD-8:** on top of basal thick carbonates within evaporite dominated sequence. **AD-9:** on top of basal carbonates within evaporite dominated sequence.	**AD-7**: evaporites dominated **AD-8**: evaporites dominated with 2 discontinous carbonate units. **AD-9**: evaporite dominated with discontinous carbonate layers.

REFERENCES

Abu-Ali, M., R. Littke, 2005. Paleozoic petroleum systems of Saudi Arabia: a basin modeling approach. GeoArabia 10 (3), p. 131–168.

Al-Husseini, M. I., 1997. Jurassic sequence stratigraphy of the western and southern Arabian Gulf, GeoArabia, v. 2, no. 4, p. 361- 382.

Al-Husseini, M. I., 2000. Origin of the Arabian Plate structures: Amar Collision and Najd Rift, GeoArabia, v. 5, no. 4, p. 527- 542.

Ayres, M. G., M. Bilal, R. W. Jones, L. W. Slentz, M. Tartir, and A. O. Wilson, 1982. Hydrocarbon habitat in main producing areas, Saudi Arabia: AAPG Bulletin, v. 66, p. 1-9.

Bathurst, R. G. C., 1970. Problems of lithification in carbonate muds: Geol. Assoc. London Proc, v. 81, p. 429-440.

Bathurst, R. G. C., 1976. Carbonate sediments and their diagenesis: Amesterdam, Elsevier, Developments in sedimentology 12, 658 p.

Beydoun, Z. R., 1991. Arabian plate hydrocarbon geology and potential- A plate tectonic approach: AAPG Studies in Geology 33, 77 p.

Beydoun, Z. R., 1998. Arabian plate oil and gas: Why so rich and so prolific?: Episodes, v. 21, p. 74–81.

Bott, M. H. P, 1992. Passive margins and their subsidence. Journal of the Geological Society, London, v. 149, p. 805-812.

Boulila, S., L.A. Hinnov, E. Huret, P. Y. Collin, B. Galbrun, D. Fortwengler, D. Marchand, and J. Thierry, 2008. Astronomical calibration of the Early Oxfordian (Vocontian and Paris basins, France): consequences of revising the Late Jurassic time scale. Earth and Planetary Science Letters, 276, p. 40–51.

Boulila, S., B. Galbrun, L. A. Hinnov, and P. Y. Collin, 2008. Orbital calibration of the Early Kimmeridgian (southeastern France): implications for geochronology and sequence stratigraphy. Terra Nova 20, p. 455–462.

Boulila, S., B. Galbrun, L. A. Hinnov, and P. Y. Collin, 2008. High-resolution cyclostratigraphic analysis from magnetic susceptibility in a Lower Kimmeridgian (Upper Jurassic) marl-limestone succession (La Méouge, Vocontian Basin, France). Sedimentary Geology 203, p. 54–63.

Boulila, S., B. Galbrun, K. G. Miller, S. F. Pekar, J. V. Browning, J. Laskar, and J. D. Wright, 2008. On the origin of Cenozoic and Mesozoic “third-order” eustatic sequences: Earth Science reviews, v. 109, p. 94-82.

Brett, C.E., T. A Algeo, and P. I. McLaughlin, 2003. Use of event beds and sedimentary cycles in high-resolution stratigraphic correlation of lithologically repetitive successions: the Upper Ordovician Kope Formation of northern Kentucky and southern Ohio. In: Harries, P., Geary, D. (Eds.), High-Resolution Stratigraphic Approaches to Paleobiology. Kluwer Academic Publishing/Plenum Press, New York, NY, p. 315–350.

Cantrell, D. L., 2006. Cortical fabrics of upper Jurassic ooids, Arab formation, Saudi Arabia: implications for original carbonate mineralogy. Sedimentary Geology, v. 186, 3-4, p. 157-170.

Cantrell, D. L., P. K. Swart, and R. M. Hagerty, 2004. Genesis and characterization of dolomite, Arab-D reservoir, Ghawar field, Saudi Arabia: GeoArabia, v. 9, no. 2, p. 1-26.

Choquette, P.W., N. P. James, 1990. Limestones: The burial diagenetic environment. In: McIlreath, I.A., Morrow, D.W. (Eds.), Diagenesis. Ottawa, Canada. Geosci. Can. Reprint Ser. 4, p. 75-81.

Choquette, F. W., and L. C. Pray, 1970. Geologic nomenclature and classification of porosity in sedimentary carbonates. AAPG, v. 54, p. 207-250.

Dickson, J. A. D., R. A.Wood, H. Bu Al Rougha, and H. Shebl, 2008. Sulphate reduction associated with hardgrounds: lithification afterburn!, Sedimentary Geology, 205(1-2): p. 34-39.

Dunham, R. J., 1962. Classification of carbonate rocks according to depositional texture, in W. E. Ham, ed., Classification of carbonate rocks. AAPG Memoir 1, p. 108–121.

Elrick, M., S. Berkyova, G. Klapper, Z. Sharp, M. Joachimski, and J. Fryda, 2009. Stratigraphic and oxygen isotope evidence for My-scale glaciation driving euastasy in the Early-Middle Devonian greenhouse world. Palageography, Palaeclimatology, Palaecology, v. 276, p. 170-181.

Embry, A. F., and J. E. Klovan, 1971. A Late Devonian reef tract on north-eastern Banks Island, N.W.T.. Bulletin of Canadian Petroleum Geology, v. 19, p. 730–781.

Evans, G., 1975. Intertidal flat deposits of the wash, Western Margin of the North Sea. In: R.M. Ginsburg (Editor), Tidal Deposits. Springer, New York, N.Y., p. 13-20.

Fischer, A.G., 1964. The Lofer cyclothems of the Alpine Triassic. Geol. Surv. Kansas Bull., 169, p. 107–149.

Frakes, L. A., J. E. Francis, and J. I. Syktus, 1992. Climate Modes of the Phanerozoic. The History of the Earth's Climate over the Past 600 Million Years. Cambridge University Press, Cambridge, 274 p.

Goldhammer, R. K., 1987. Platform carbonate cycles Middle Triassic of northern Italy: The interplay of local tectonics and global eustasy: [Ph.D. thesis]: Baltimore, Maryland, John Hopkins University, 468 p.

Gradstein, F. M., J. G. Ogg, and A. G. Smith, 2004. A Geologic Time Scale 2004. Cambridge University Press, Cambridge, 610 p.

Handford, C. R. and R. G. Loucks, 1993. Carbonate depositional sequences and systems tracts-responses of carbonate platforms to relative sea-level changes. In: Carbonate Sequence Stratigraphy: Recent Developments and Applications (Ed. By B. Loucks&R.J. Sarg), AAPG., 57, p. 3-41.

Handford, C. R., D. L. Cantrell, and T. H. Keith, 2002. Regional facies relationships and sequence stratigraphy of a super-giant reservoir (Arab-D Member), Saudi Arabia, in J. M. Armentrout, ed., Sequence stratigraphic models for exploration and production: Evolving methodology, emerging models and application histories, 22nd Annual Bob F. Perkins Research Conference: Gulf Coast Section SEPM, p. 539–564.

Haq, B. U., and A. M. Al-Qahtani, 2005. Phanerozoic cycles of sea-level change on the Arabian Platform. GeoArabia, v. 10, p. 127-160.

Haq, B. U., J. Hardenbol, and P. R. Vail, 1987. Chronology of fluctuating sea levels since the Triassic. Science, 235, p. 856– 867.

Hughes, G. W., 2004. Middle to Upper Jurassic Saudi Arabian carbonate petroleum reservoirs: Biostratigraphy, micropaleontology and paleoenvironments. GeoArabia, v. 9, no. 3, p. 79–84.

Husinec, A. and J. F. Read, 2007. The Late Jurassic Tithonian, a greenhouse phase in the Middle Jurassic-Early Cretaceous? cool? mode: evidence from the cyclic Adriatic Platform, Croatia. Sedimentology, 54, p. 317–337.

Koerschner, W.F. and J. F. Read, 1989. Field and modeling studies of Cambrian carbonate cycles, Virginia Appalachians. J. Sed. Petrol., 59, p. 654–687.

Konert, G., A. M. Al-Afifi, S. A. Al-Hajri, and H. J. Droste, 2001. Paleozoic stratigraphy and hydrocarbon habitat of the Arabian plate. GeoArabia, v. 6, p. 407– 442.

Leinfelder, R. R., F. Schlagintweit, W. Werner, O. Ebli, M. Nose, D. U. Schmid, and G. W. Hughes, 2005. Significance of stromatoporoids in Jurassic reefs and carbonate platforms-Concepts and implications:Facies. International Journal of Paleontology, Sedimentology and Geology, v. 51, p. 287–325.

Lindsay, R. F., D. L. Cantrell, G. W. Hughes, T. H. Keith, H. W. Mueller III, and S. D. Russell, 2006. Ghawar Arab-D reservoir: widespread porosity in shoaling-upward carbonate cycles, Saudi Arabia. In P. M. Harris and L. J. Weber, eds., Giant hydrocarbon reservoirs of the world: From rocks to reservoir characterization and modeling. AAPG Memoir 88/ SEPM Special Publication, p. 97-137.

Lucia, F. J., 1995. Rock-fabric/ petrophysical classification of carbonate pore space for reservoir characterization. AAPG Bulletin, v. 79, no. 9, p. 1275–1300.

Markello, J. R., R. B. Koepnick, L. E. Waite and J. F. Collins, 2008. The carbonate analogs through time (CATT) hypothesis and the global atlas of carbonate fields – a systematic and predictive look at Phanerozoic carbonate systems. SEPM Special Publication, v. 89, p. 15-45.

Matthews, R. K. and C.F. Frohlich, 2002. Maximum flooding surface and sequence boundaries: comparisons between observation and orbital forcing in the Cretaceous and Jurassic (65-190 Ma). GeoArabia, v. 7, no. 3, p. 503-538.

McGuire, M. D., G. Kompanik, M. Al-Shammery, M. Al- Amoudi, R. B. Koepnick, J. R. Markello,M. L. Stockton, and L. E. Waite, 1993. Importance of sequence stratigraphic concepts in development of reservoir architecture in upper Jurassic grainstones, Hadriya and Hanifa reservoirs, Saudi Arabia. Proceedings of 8th Middle East Oil Show, Society of Petroleum Engineers Paper 25578, p. 489–499.

McKenzie, J.A, 1981. Holocene dolomitization of calcium carbonate sediments from the coastal sabkas of Abu Dhabi, U.A.E.. Jour. Geology, v. 89, p. 185-198.

McKenzie, J. A., K. J. Hsu, and J. F. Schneider, 1980. Movement of subsurface waters under the sabkha, Abu Dhabi, UAE, and its relationship to evaporitive dolomite genesis. SEPM Spec. Publ. 28, p. 8-38.

Meyer, F. O., and R. C. Price, 1993. A new Arab-D depositional model, Ghawar field, Saudi Arabia. 8th Middle East Oil Show and Conference Proceedings, Bahrain, p. 465–474.

Miall, A. D., 1991. Hierarchies of architectural units in terrigenous clastic rocks, and their relationship to sedimentation rate, in Miall, A. D., and Tyler, N., eds., The three-dimensional facies architecture of terrigenous clastic sediments and its implications for hydrocarbon discovery and recovery: Society of Economic Paleontologists and Mineralogists, Concepts in Sedimentology and Paleontology, v. 3, p. 6-12.

Mitchell, J. C., P. J. Lehmann, D. L. Cantrell, I. A. Al-Jallal, and M. A. Al-Thaghafy, 1988. Lithofacies, diagenesis and depositional sequence; Arab-D member, Ghawar field, Saudi Arabia, in A. J. Lomando and P. M. Harris, eds., Giant oil and gas fields: Society of Economic Paleontologists and Mineralogists Core Workshop 12, v. 1, p. 459-514.

Mitchum, R.M. Jr., P. R. Vail, and S. Thompson, 1977. Seismic stratigraphy and global changes of sea level, part 2: the depositional sequence as a basic unit for stratigraphic analysis. In: C.W. Payton (Editor), Seismic Stratigraphic Applications to Hydrocarbon Exploration. AAPG Memoir, 26: p. 53-62.

Montanez, I. P., and. A. Osleger, 1993. Parasequence stacking patterns, third-order accommodation events, and sequence stratigraphy of Middle to Upper Cambrian platform carbonates, Bonanza King Formation, southern Great Basin. In Loucks, R., and Sarg, R., eds., Recent advances and applications of carbonate sequence stratigraphy: Tulsa, Oklahoma. AAPG Memoir 57, p. 305–325.

Murris, R. J., 1980. Middle East: stratigraphic evolution and oil habitat. AAPG Bulletin, v. 64, p. 597-618.

Nicholson, P. G., 2000. Compressional, fault-related folds and Saudi Arabia's major hydrocarbon fields. GeoArabia, v. 5, p. 152–153.

Nicholson, P. G., 2002, A 700 million year tectonic framework for hydrocarbon exploration and production in Saudi Arabia. GeoArabia, v. 7, p. 284.

Oterdoom, W. H., M. Worthington, and M. Partington, 1999. Petrological and tectonostratigraphic evidence for a Mid-Ordovician rift pulse on the Arabian Peninsula. GeoArabia, v. 4, no. 4, p. 467-500.

Parrish, J. T.,1993. Climate of the supercontinent Pangea. Journal of Geology, v. 101, p. 215–233.

Patterson, R. J., and D. J. J. Kinsman, 1982. Formation of diagenetic dolomite in coastal sabkha along Arabian (Persian) Gulf. AAPG Bull., v. 66, p. 28-43.

Pemberton, S. G., M. K. Gingras, 2005. Classification and characterizations of biogenically enhanced permeability. AAPG Bulletin 89, p. 1493–1517.

Powers, R. W., 1962. Arabian Upper Jurassic carbonate reservoir rocks, in W. E. Ham, ed., Classification of carbonate rocks-a symposium. AAPG Memoir 1, p. 122-192.

Powers, R. W., 1968. Saudi Arabia: Lexique Stratigraphique International, 3: Paris, Centre National de la Recherche Scientifique, 171 p.

Powers, R. W., L. R. Ramirez, C. D. Redmond, and E. L. Elberg, 1966. Sedimentary geology of Saudi Arabia: Geology of the Arabian Peninsula. U.S. Geological Survey Professional Paper 560-D, 150 p.

Price, G.D., 1999. The evidence and implications of polar ice during the Mesozoic. Earth-Science Reviews, v. 48, p. 183–210.

Purser, B. H., 1973. The Persian gulf. Holocene carbonate sedimentation and diagenesis on shallow epicontinental sea. Springer, Berlin.

Read, J. F., 1989. Controls on evolution of Cambrian-Ordovician passive margin, U.S. Appalachians. In Crevello, P.D., Wilson, J.L., Sarg, J.F., and Read, J.F., eds., Controls on Carbonate Platform and Basin Development. Society for Sedimentary Geology Special Publication 44, p. 147–166.

Read, J. F., 1998. Phanerozoic carbonate ramps from greenhouse, transitional and ice-house worlds: clues from field and modelling studies. In Wright, V.P. and Burchette, T. P., eds., Carbonate Ramps. Geological Society of London, Special Publications, v. 149, p. 107-135.

Read, J. F. and R. K. Goldhammer, 1988. Use of Fischer plots to define third-order sea-level curves in Ordovician peritidal cyclic carbonates. Appalachians Geology, 16, p. 895–899.

Reid, R. P., I. G. Macintyre, 1998. Carbonate recrystallization in shallow marine environments: a widespread diagenetic process forming micritized grains. J. Sediment. Res. 68, p. 928–946.

Riding, R., 2000. Microbial carbonates: the geological record of calcified bacterial-algal mats and biofilms. Sedimentology, 47 (Supplement 1), p. 179-214.

Riding, R., 2005. Phanerozoic reefal microbial carbonate abundance: comparisons with metazoan diversity, Mass Extinction events, and seawater saturation state. Rev. Esp. Micropal. 37, p. 23– 39.

Riding, R., 2006. Microbial carbonate abundance compared with fluctuations in metazoan diversity over geological time. Sedimentary Geology, 185, p. 229–238.

Riding, R. and L. Liang, 2005. Geobiology of microbial carbonates: metazon and seawater saturation state influences on secular trends during the Phanerozoic. Palaeogeography, Palaeoclimatology, Palaeoecology, 219, p. 101-85.

Royer, D. L., R. A. Berner, I. P. Montanez, N. J. Tabor, and D. J. Beerling, 2004. CO_2 as primary driver of Phanerozoic climate. GSA Today, 14, p. 4–10.

Sadler, P. M., D. A. Osleger, and I. P. Montanez, 1993. On the labeling, length and objective basis of Fischer plots. Journal of Sedimentary Petrology, v. 63, p. 360–368.

Schlager, W., 1989. Drowning unconformities in carbonate platforms. In: Controls on carbonate platform and basin development. Soc. Econ. Paleontol. Mineral. Spec. Publ., 44: p. 15-25.

Scotese, C. R., A. J. Boucot and W. S. McKerrow, 1999. Gondwanan palaeogeography and palaeoclimatology. Journal of African Earth Sciences, v. 28, no. 1, p. 99-84.

Scotese, C. R., 2003. Paleomap project, Earth History and Climate History, Late Jurassic. Paleomap, URL HTTP://WWW.SCOTESE.COM.

Sellwood, B. W., P. Valdes, and G. D. Price, 2000. Geological evaluation of multiple general circulation model simulations of Late Jurassic palaeoclimate. Palaeogeography. Palaeoclimatology, Palaeoecology, 156, p. 147-160.

Sharland, P. R., R. Archer, D. M. Casey, R. B. Davies, S. H. Hall, A.P. Heward, A. D. Horbury and M. D. Simmons, 2001. Arabian Plate sequence stratigraphy. GeoArabia Special Publication 2, 371 p.

Snedden, J. W., and C. Liu, 2010, A compiliation of Phanerozoic sea level change, coastal onlaps, and recommended sequence designations. AAPG Search and Discovery article 40594, HTTP://WWW.SEARCHANDDISCOVERY.NET documents/2010/40594snedden/ndx_snedden.pdf.

Stanley, S.M. and L. A. Hardie, 1998. Secular oscillations in the carbonate mineralogy of reef-building and sedimentproducing organisms driven by tectonically forced shifts in seawater chemistry. Palaeogeogr. Palaeoclimatol. Palaeoecol., 144, p. 3-19.

Steckler, M.S. and A.B. Watts, 1982. Subsidence history and tectonic evolution of Atlantic-type continental margins, Amer. Geophys. Union, Geodynamics Series 8, p. 184-196

Steineke, M., R. A. Bramkamp, and N. J. Sander, 1958. Stratigraphic relations of Arabian Jurassic oil, in Habitat of oil. AAPG, p. 1294-1329.

Swart, P.K., D. L. Cantrell, H. Westphal, C. R. Handford, and C. G. Kendall, 2005. Origin of dolomite in the Arab-D reservoir from the Ghawar Field, Saudi Arabia: evidence from petrographic and geochemical constraints. J. Sed. Res., 75, p. 476–491.

Van Wagoner, J.C., H. W. Posamentier, R. M. Mitchum, P. R. Vail, J. F. Sarg, T. S. Loutit, and J. Hardenbol, 1988. An overview of the fundamentals of sequence stratigraphy and key definitions. In: C.K. Wilgus, B.J. Hastings, H. Posamentier, J.C. Van Wagoner, C.A. Ross and C.G.St.C. Kendall (Editors), Sea-Level Change: An Integrated Approach. Soc. Econ. Paleontol. Mineral. Spec. Publ., 42: p. 39-46.

Warren, J.K., C. G. St. C Kendall, 1985. Comparison of sequences formed in marine sabkha (subaerial) and salina (subaqueous) settings- modern and ancient. AAPG, 69, p 1013–1023.

Warren, J. K., 2006. Evaporites. New York, NY: Spring Berlin Heidelberg, 1035 p.

Weedon, G. P., A. L. Coe, J. G. Ogg, R. W. Gallois, 2004. Cyclostratigraphy, orbital tuning and inferred productivity for the type Kimmeridge Clay (Late Jurassic), southern England. Journal- Geological Society London 161, p. 655–666.

Wilson, J. L., 1975. Carbonate Facies in Geologic History. New York, Springer-Verlag, 471 p.

Ziegler, M. A., 2001. Late Permian to Holocene paleofacies evolution of the Arabian Plate and its hydrocarbon occurrences. GeoArabia, v. 6, p. 445-504.

CHAPTER 3

LATE JURASSIC ARAB-D DOLOMITES, HARMALIYAH AND HAWIYAH FIELDS, SAUDI ARABIA: DOLOMITE RE-EQUILIBRATION AND OVERGROWTH IN ISOTOPICALLY HEAVY BRINES DURING BURIAL

ABSTRACT

Dolomites from the Late Jurassic (Kimmeridgian) Arab-D reservoir zones 1 to 4, in Hawiyah field (in Ghawar field) and Harmaliyah field to the east, were studied to better understand their origin. The dolomites are dominantly fabric destructive medium to coarse grained types, and much less common fabric retentive finer grained dolomites just beneath the anhydrite. They are nonluminescent, near stoichiometric (averaging 51-52 mole% Ca), and lack Ca-zoning even with back-scattered electron (BSE) imaging. They have low Mn (10-35 ppm) and Fe (12-1800 ppm), low Sr (15-225). Ca shows no correlation with Sr, and the $^{87/86}Sr$ tends to increase slightly with core depth. The $\delta^{13}C$ values are rock buffered while the $\delta^{18}O$ values have been greatly shifted toward negative values relative to unaltered early dolomite, and dolomite crystal rims generally have lighter $\delta^{18}O$ values than cores (from less than 1 per mil to 9 per mil).

The dolomites were initiated at different times during shallowing phases on the Arab-D platform, with the bulk of the fabric destructive dolomites initially nucleating under near normal salinities from calcitic sediments, while the fabric preserving dolomites higher in the section were from dolomitized aragonitic sediments from progressively more evaporated waters. During deposition of the overlying evaporites, saline brines several times seawater salinities and with $\delta^{18}O$ values of from +4 to +8 per mil_{SMOW} percolated down into the reservoir dolomites. The early dolomites continued to grow at these near surface temperatures. However, with increasing burial and increasing temperature, the early dolomites re-equilibrated with the increasingly warm basinal brines resulting in replacement of cores, and dolomite cementation by rim overgrowth. Progressive plugging of higher dolomites earlier, caused some of these to retain slightly heavier

$\delta^{18}O$ values (suggestive of 60 to 80 ^{o}C temperatures) and marine seawater Sr isotope values while those that remained permeable developed very light $\delta^{18}O$ values (80 to over 120 deg C) and more radiogenic Sr values, shifting them toward the field of late stage baroque dolomite.

INTRODUCTION

Differentiation between early dolomite and later burial dolomite has been greatly aided by use of cathodoluminescence (CL) which provides a framework for sampling trace element and stable isotopes (Cander, 1994; Kupecz and Land, 1994; Vahrenkamp and Swart, 1994; Barnaby and Read, 1992; Montanez and Read, 1992; Choquette and Hiatt, 2008). This CL zonation from much early dolomite forming in oxidizing environments, so that they are nonluminescent, while later dolomites are luminescent because the formative waters have become reducing.

However, the dolomites of the Late Jurassic Arab-D reservoir, Arab Formation, Ghawar field, Saudi Arabia (Figs. 3.1, 3.2) are uniformly nonluminescent, and form tight to highly porous zones within the largest oil reservoir in the world (Cantrell et al., 2001, 2004; Swart et al., 2005). They consist of simple planar faced crystals, and show little major and trace element (Ca, Mg, Fe, Mn) variation, suggesting that at least in terms of elemental chemistry they are a single phase. The dolomites also lack any Ca-zoning from cores to rims of crystals (Wheeler et al., 1999; Suzuki et al., 2006) thus back scattered electron (BSE) images also show no zonation. These dolomites were considered to have formed as peritidal and reflux dolomites during development of the overlying evaporites (Cantrell et al., 2004; Swart et al., 2005), and are post-dated by later saddle (baroque) dolomite in some cores in Ghawar.

The present study of dolomite in the Arab-D reservoir from two wells in Hawiyah and Harmaliyah fields (Figs. 3.1, 3.2) builds on the work of Cantrell et al. (2001; 2004) and Swart et

al. (2005). The stratiform horizons of petrographically and chemically uniform, non-luminescent pre-baroque dolomite generation, formed as early syndepositional to early postdepositional reflux dolomite, during several dolomitizing phases prior to evaporite deposition. Utilizing microanalysis of dolomite zones within crystals, we document that the dolomite has been highly modified in terms of trace element and stable isotope compositions during burial to present reservoir depths and temperatures while continuing to undergo dolomite cementation with burial. That the CL, BSE images and trace element data do not differentiate between any early and late dolomites is surprising, although the oxygen isotopes within the dolomite crystals do reflect increasing temperatures. We suggest that the chemical uniformity of the dolomites relates to the distinctive evolving chemistry and heavy oxygen isotope values of the formation waters and to the long residence time the porous reservoir dolomites remained within the oil window, allowing re-equilibration of dolomite compositions to prevailing conditions.

REGIONAL AND STRATIGRAPHIC SETTING

The Jubaila-Arab-Hith carbonates and evaporites formed on the wide Arabian Platform (Fig. 3.1) during the Late Jurassic Kimmeridgian to Early Tithonian and was bounded to the southwest by land and to the northeast by a passive margin bordering Neo-Tethys (Al-Husseini, 1997; Ziegler, 2001; Sharland et al., 2001). The stratigraphic subdivisions of the Juabaila-Arab-Hith succession are shown on Figure 3.2. The Jubaila Formation consists of slightly deeper water carbonates. The Arab Formation consists of Arab-D carbonates (averaging more than 60 m thick) consisting of deeper to shallower water carbonates (mainly limestone with some continuous and discontinuous dolomites), the D Anhydrite, the C Carbonate and C Anhydrite, the B Carbonate and B Anhydrite and the A Carbonate. The Hith Anhydrite (more than 170 m thick) overlies the Arab-A carbonate and provides the major seal.

Dolomites within the Arab-D reservoir, which are the topic of this paper, occur in several continuous to discontinuous horizons, that have been related to the reservoir zones 1 to 4 defined on porosity (Figs. 3.3, 3.4; Cantrell et al., 2004; Swart et al., 2005). The burial history of the succession in Ghawar has been documented by Abu-Ali and Littke (2005), who show relatively rapid burial in the late Jurassic, decreasing slightly into the Cretaceous, followed by relatively little subsidence in the region during much of the Cenozoic.

METHODS

The percent dolomite, calcite, anhydrite and porosity was estimated visually during logging of the Arab-D cores. Grain sizes of the dolomite were classified according to Lucia (1995) into fine (less than 20 micron), medium (20-100 micron), large (greater than 100 micron) as these ranges govern the petrophysical properties. The dolomites and limestones were sampled at a spacing of 0.6 meters for C and O analysis for chemostratigraphy by drilling butts of cores to obtain powdered samples. The C-O isotope analyses were done by Saudi Aramco and are expressed relative to VPDB, with an error +/- 0.2 per mil. For the dolomite study, samples of dolomites and dolomite-calcite mixtures were obtained from plugs from selected horizons. The calcite was leached from the mixtures using 15% acetic acid for 2 hours, stirring frequently. It is possible that leaching selectively dissolves the less stoichiometric phases, but the analyses of the pure dolomite generations and the leached fraction had similar isotopic composition, suggesting that this was not a major problem. Thin sections of plugs were examined using plane light, and using cathodoluminescence. The major elements were determined using a Cameca SX50 Electron Microprobe by traverses across crystals (error: +/- 0.4 wt. percent). Major and trace element maps also were obtained using the microprobe to determine any zoning in crystals. Traverses for trace elements across crystals were done using the Laser Ablation ICP-MS; limits

of detection for the trace elements were all well below 1 ppm. Crystals were also examined under Camscan Series II Scanning Electron Microscope for zoning. Determination of any stable isotope variation across crystals was done using SIMS (Cameca IMS 7f GEO) housed in ICTAS, Virginia Tech; analyses are +/-0.7 per mil. $^{87/86}$Sr was determined from pure dolomites by Kreuger Geochron Laboratories (error: +/- 0.000008). Fluid inclusions were examined but were too small to be used with a heating and cooling stage as they were under 2 microns. As they were oil filled, the oil fluorescence prevented use of the Raman spectrometer for determining compositions of fluids.

RESULTS

The vertical and lateral distribution of the dolomites in Hawiyah and Harmaliyah Fields is shown in Figures 3.3 and 3.4 which also shows the reservoir zones (labeled Zones 1 to 4) and the sequence stratigraphic framework. Dolomitized units vary in terms of porosity from tight to very porous (Fig. 3.5). The generalized paragenetic sequence of the Arab-D member has been described by Mitchell et al. (1988), Cantrell and Hagerty (1999), Cantrell et al. (2001, 2004) and Swart et al. (2005), and summarized in Table 3.1. The characteristics of the dolomites from the various reservoir zones are summarized in Table 3.2.

Dolomite Petrography and CL:

The petrography of the Arab-D dolomites of this study, from Hawiyah in Ghawar and Harmaliyah, is similar to that outlined in and Cantrell et al. (2004) and Swart et al. (2005). *Fabric Preserving Dolomite*: These typically are fine- to medium grained dolomites that preserve the depositional fabric of rock (Fig. 3.6D), which include ooid and gastropod grainstones, and rare microbial laminites. Ooids and mollusk fragments commonly are leached to

form moldic pores lined by dolomitized cement linings bordering interparticle pores. They are relatively rare, ocurring in reservoir zone 1, close to the overlying anhydrites.

Fabric Destructive Dolomite: These dolomites (Figs. 3.6B, C) typically are medium (20 to 100 microns) to coarse grained (over 100 microns), typically with a turbid cores containing numerous calcite inclusions (several to 10 microns in size, and staining pink with Alizarin Red S) surrounded by a clear dolomite rim. Cores and rims are nonluminescent although spots of orange luminescence appear in pits. Rarely, the dolomites show dedolomitized cores with replacement by calcite. These fabric destructive dolomites are the dominant type in the Arab-D occurring in Zones 2 and 3.

Baroque Dolomite: Baroque or saddle dolomite has been documented from the Arab-D as a late stage dolomite (Cantrell et al., 2004). However it was not encountered in the present two well study from Harmaliyah and Hawiyah fields.

For this study, the dolomites were grouped according to which of the four reservoir zones they came from:

Reservoir Zone 4 Dolomites: These occur in Sequences AD-1 and lower part of sequence AD-2 (Fig. 3.3). These dolomites consist of fabric desctructive, fine to coarse crystals (less than 20 to 100 micron) occurring as scattered disseminated rhombs in the muddy limestones of the Upper Jubaila and basal Arab-D (Fig. 3.6A).

Reservoir Zone 3 Dolomites: These occur in the upper part of sequence AD-2 to lower AD-4 where they typically form relatively discontinuous dolomitic limestone and limy dolomite zones (Figs. 3.3, 3.4). These dolomites become more continuous and dolomitic at the top of zone 3 where they are 1 m to 4 m thick. The dolomites are fabric destructive, and range from fine to

coarse grained (less than 20 to over 100 microns; Figs. 3.6B, C). Dolomites near the top of Zone 3 commonly are porous, sucrosic dolomites.

Reservoir Zone 2 Dolomites: These occur in the upper part of sequence AD-4 to lower AD-7 (Fig. 3.3). These dolomites generally form continuous to discontinuous units that can be over 10 m thick. They mainly are medium to coarse size grained (20 to over 100 microns; Fig. 3.6C), fabric destructive types. They range from tight interlocking mosaics to porous sucrosic types, and may contain leached carbonate grains and leached *Cladocoropsis* leaving moldic and vuggy porosity (Figs. 3.5A, 3.6C).

Zone 1 Dolomites: These are confined to the lower part of sequence AD-7 (Fig. 3.3). These dolomites commonly are fabric retentive, very fine to fine- to medium grained and range from non-porous to less common porous types (Fig. 3.6A). Zone 1 is highly dolomitized in all the wells and the dolomites, are relatively continuous across the fields.

Cathodoluminescence, Major and Trace Element Geochemistry

Calcium and Magnesium:

Most of the dolomites have from 51 to 52 mole % Ca with a few samples ranging down to 48 mole %, and up to 66 mole % (Figs. 3.7A, B). Traverses across dolomite crystals from clear rims into the turbid cores show that they have almost the same Ca (and Mg) compositions. This also is confirmed by scanning electron microscope (SEM) back-scattered electron images and electron microprobe major element maps of the dolomites (Figs. 3.8A, B, and C) which do not show any zoning. Some dolomite crystal cores are dedolomitized and replaced by patches of calcite, with an associated increase in Ca mole % depending on the amount of calcitization of the core.

Iron and Manganese:

Iron values in the dolomites range from 12 ppm to higher that 1800 ppm with most between 22 and 1000 ppm (Fig. 3.9). In general zone 3 and 4 dolomites have relatively low iron (less than 800 ppm), whereas zones 1 and 2 dolomites may range from below 100 ppm to relatively elevated iron values up to 1400 with rare values up to 1800 ppm. There is no clear trend for iron values within individual dolomite crystals, as determined by Laser Ablation ICP-MS. In some traverses from rim into the core, the Fe values are similar, while others have higher Fe values in the cores, and still others have higher values in the rim. The variation of Fe values within single crystals may be just a few tens of ppm or up to several hundred ppm.

Mn values in the dolomites are low (from ~10 ppm to 35 ppm) without significant change in Mn concentration from rim to core. There is a little variation of the Mn values in dolomites from different reservoir zones with respect to change in $\delta^{18}O$ (Fig. 3.10).

Strontium and Uranium:

Sr values in the dolomites range from 15 to 255 ppm with most being between 50 and 100 ppm with little difference between the dolomites from different reservoir zones. There is only a weak correlation between increasing Ca and increasing Sr (Fig. 3.11) unlike many unaltered Cenozoic dolomites (Vahrenkamp and Swart, 1994; Budd, 1997). Also, there is no obvious correlation between Sr and $\delta^{18}O$ values of the dolomites from different reservoir zones, as the dolomites from the different reservoir zones have similar range of Sr values (Fig. 3.12).

The bulk U values for the dolomites range from 0.1 to 3 ppm which is within the typical range of U in sedimentary carbonate rocks (Mielke, 1979).

Carbon and Oxygen Stable Isotopes:

The undolomitized Arab-D limestones in the study area have $\delta^{13}C$ values of +1.6 to +2.4 per mil_{PDB} and $\delta^{18}O$ values of -3.2 to -4.5 per mil_{PDB}. These values are considerably lighter than coeval Kimmeridgian marine calcites from Croatia, which have $\delta^{13}C$ ranges from +1 to +3.7 and $\delta^{18}O$ ranges from +0.5 to -2.5 per mil_{PDB} (Read, personel communication, 2012; cf. Veizer et al., 1999).

The $\delta^{13}C$ values of the dolomites in this study (Fig. 3.13) range from +2.9 to +4 per mil_{PDB} for reservoir zone 1 and 2 dolomites; +2.3 to +3.4 per mil_{PDB} for reservoir zone 3 dolomites; and +2.8 for the single sample of reservoir zone 4 dolomite. Overall, although the dolomites from the various reservoir zones have overlapping values, they tend to shift toward slightly lighter O values going from reservoir zones 1 and 2, through 3 to 4. The $\delta^{13}C$ values of the Arab-D dolomites tend to be heavier than Late Jurassic-Early Cretaceous Croatian dolomites that have been little altered (Cangialosi et al., in prep.).

The $\delta^{18}O$ values of reservoir zone 1 and 2 dolomites range from -0.7 to -4.8 per mil_{PDB}; for zone 3 the $\delta^{18}O$ values overlap zones 1 and 2 dolomites, ranging from -1.6 to -4 per mil_{PDB} with the values of upper zone 3 dolomites being generally lighter (-3.5 to below -6 per mil_{PDB}). Zone 4 dolomite has a single sample -6.8 per mil_{PDB} that is the most negative of all the dolomites (Fig. 3.13). These $\delta^{18}O$ values are significantly lighter (-2 to -8 per mil_{PDB}) than little altered early dolomites from Croatia (Fig. 3.13). The $\delta^{18}O$ values of late stage baroque dolomite from elsewhere in Ghawar are -6 to -9 per mil_{PDB}, which are the lightest values of any of the dolomites observed (Fig. 3.13). Overall, the $\delta^{18}O$ values in Arab-D reservoir dolomites tend to show a very weak decrease with increasing depth (from reservoir zone 1 to reservoir zone 4; Fig. 3.14).

The SIMS data shows that the rims of dolomite crystals generally have more negative $\delta^{18}O$ values than the cores (Fig. 3.15). The average difference between $\delta^{18}O$ values of the cystal cores and the rims from the reservoir zones 2, 3 and the top of zone 3 range from 1 to 6.5 per mil_{PDB}.

Strontium Isotopes:

The $^{87/86}Sr$ values of the Arab-D dolomites in this study range from 0.706915 to 0.707012, spanning the sea water values for the Kimmeridgian, which are 0.7069 to just below 0.7070 (Fig. 3.16; Price and Grocke, 2002). The $^{87/86}Sr$ values show a monotonic increase with stratigraphic depth in the core (Fig. 3.17). These $^{87/86}Sr$ values are slightly more enriched than those given for similar Arab-D dolomites elsewhere in Ghawar by Cantrell et al. (2004).The $^{87/86}Sr$ values of the dolomites in this study are all below the values of late stage baroque dolomite sampled from Ghawar (0.70712+/-0.00006; Cantrell et al., 2004). Given that total Sr of the dolomites from all the reservoir zones is low, 1/total Sr versus $^{87/86}Sr$ shows little variation of Sr with increase in $^{87/86}Sr$ toward the deeper reservoir zones (Fig. 3.18).

Fluid Inclusions:

Although Cantrell et al. (2004) obtained fluid inclusion data from the saddle or baroque dolomites, the fluid inclusions in the non-baroque dolomites of their study and the present study were micron-sized, contaminated with hydrocarbon, and were too small to obtain freezing and melting temperatures. An attempt was made to obtain water salinities using the Laser Raman spectrometer but this was unsuccessful because of the intense fluorescence from the oil within the fluid inclusions which masked any other signal. Two phase fluid inclusions found by Cantrell et al. (2004) in the non-baroque dolomites are secondary, and have similar melting and

homogenization temperatures as the baroque dolomite inclusions which are more likely to be primary. Homogenization temperatures (uncorrected for pressure for the given depth) reported by Cantrell et al. (2004) are minumum temperatures and were generally in the range of 85 to 115 ^{o}C (similar to bottom hole temperatures today), and salinities were 190 to 240 parts per thousand (or 6 to 7Xseawater).

DISCUSSION

Given the arid climate during deposition of the Arab-D carbonates and evaporites, models proposed for the origins of the dolomites including those outlined by Cantrell et al. (2001; 2004) and Swart et al. (2005) include:

1. Marine dolomitization by shallow marine waters acting on the deeper seafloor during shallowing phases that culminated in non-depositional hiatuses (Swart et al., 2005)
2. Dolomitization of near surface sediments by brines sourced from salinas directly overlying the carbonates (fabric preserving dolomite; Cantrell et al., 2004),
3. Deep penetration or reflux of evaporitic of brines into the Arab-D carbonates during deposition of the Arab-D anhydrite (Adams and Rhodes, 1960; Cantrell et al., 2004), and
4. Dolomitization by warm burial fluids ascending up through the section along fractures and faults (Cantrell et al., 2004; Davies and Smith, 2006).

Implications of Petrography:

The relatively fine grained fabric preserving dolomites of the Arab-D formed by replacement of aragonite precursors, which were ooid/mollusk grainstones (Cantrell, 2005; Lindsay et al., 2010). These aragonite-rich sediments developed only with hypersaline conditions and high calcium carbonate supersaturation in the evaporated marine waters, prior to

or in front of the evaporites. Thus they are confined to the top of the Arab-D reservoir. The coarser grained, fabric destructive dolomites formed by replacement of calcite precursors more typical of the Late Jurassic calcite seas (Stanley and Hardie, 1998), and thus make up the bulk of the dolomites in the Arab-D reservoir.

The plane light petrography of the coarser grained, fabric destructive dolomites suggests two generations of dolomite, an earlier one making up the turbid cores with numerous calcite inclusions remaining from incomplete dolomitization of the host limestone, and a later, clear limpid dolomite that forms clear dolomite rims of crystals. The cathodoluminescence (CL) suggests that the cores and the overgrowths belong to a single nonluminescent CL generation.

The origin of the pore space in the dolomites is complex, as many of the dolomites appear to have formed from muds, while some have formed from grainy facies (indicated by mechanical sedimentary structures). Porosity development in some of the muddy facies could relate to leaching of limestone as acidic burial fluids undersaturated with respect to calcite moved through the sediments in front of the hydrocarbon charge (Hanor, 1994; Cantrell et al., 2004).

The minor dedolomite observed may relate to development of Ca-rich brines during burial from evaporite dissolution or it could reflect cooling from previously higher temperatures pushing the stability field from dolomite into the calcite field (Rosenberg and Holland 1964). Long term cooling of the passive margin following breakup, and decreased heat flow might result in some cooling from peak temperatures (Bott, 1992). Also, Abu-Ali and Littke (2005) show three periods of uplift in Shedgum field, Ghawar, in the Cretaceous through Paleogene which might have been associated with short periods of cooling.

Significance of Major and Trace Element Data:

Ca, Mg, Fe and Mn: The lack of Ca zoning within the dolomite crystals of the Arab-D, evidenced by BSE images and major element maps, suggests that the dolomite cores and rims have similar major (and minor) element chemistry. Locally high values of Ca in the cores of dolomite crystals may be due to calcite inclusions in the cores, which are absent in the rims or they could be due to patchy dedolomitization.

The lack of any difference in the Mn and Fe contents of dolomite cores and rims supports the idea of a chemically homogeneous dolomite. The relatively low Mn values (below 35 ppm) in the cores and rims of the dolomites are compatible with the dolomites being nonluminescent under the operating conditions used (Gillhaus et al., 2001). Dolomites precipitated from oxidizing surface seawater (0.0003 ppm Mn) using K_{Mn} of between 6 and 36 (Veizer, 1983; Donat and Bruland, 1995) and present day Ca concentrations would yield a dolomite with 1 to 6 ppm Mn, and less than this if higher Ca concentrations of Jurassic seawater were used. Thus although the Mn values are low and lack any change from cores to rims, the slightly elevated values suggest that the pore water brines either had slightly elevated Mn/Ca ratios perhaps because the waters had started to become slightly reducing rather than being as oxidizing as surface marine waters invoked by Swart et al. (2005), or it could relate to precipitation rate effects on the partition coefficient of Mn in dolomite. The documented increase in Mn in the late stage baroque dolomites suggests that supply of Mn within the sediments was not limited, at least for late stage hydrothermal fluids.

With regard to Fe, a few of the laser ICP-MS traverses showed an increase in Fe in the rim relative to the core of the dolomite, suggesting that for these samples there was a slight decrease in redox during dolomization. The scattered high Fe values in some cores may be

caused by microscale replacement of the early dolomite core by a later Fe-rich dolomite (not able to be discriminated using CL or BSE images).

The normal redox response of ground waters to bacterially mediated oxidation of organics which controls reduction of Mn and Fe species, is first removal of oxygen, then denitrification of nitrate, then sulfate reduction (Champ et al., 1979). As the overlying evaporites developed, pore fluids would be expected to maintain high sulfate concentrations from 1300 to 3500 mg/l as well as high alkalinities (Collins, 1970; Holser, 1979; D. Rimstidt, personal communication, 2012) which limited reduction of Mn and Fe species. However, with increasing burial, increasingly reducing conditions initially favored incorporation of Mn and then Fe into the dolomites. However, with migration of hydrocarbons into the reservoir, sulfate in subsurface brines could have gone from seawater or calcium sulphate brine values to markedly reduced sulfate concentrations where they underwent sulfate reduction after reacting with organics (Hanor, 1988). The Mn and Fe values of the non-baroque Arab-D dolomites are very low compared to the burial modified dolomites from the Cambrian and Ordovician of the US Appalachians (Barnaby and Read, 1992; Montanez and Read, 1992). This suggests that prior to late stage baroque dolomitization, the pore waters remained relatively oxidizing, and only the late stage brines had high Mn^{2+} and Fe^{2+} compositions able to form the baroque dolomites (Cantrell et al., 2004).

Sr contents of the dolomites: The low Sr content of the Arab-D dolomites (typically 50-100 ppm) imply that the dolomite formed in a water-buffered diagenetic system in which the amount of Sr in the host rock was low compared to the amount of Sr in the water (Banner, 1995; Budd, 1997) as might be expected with the calcite seas of the Late Jurassic-Early Cretaceous (Stanley and

Hardie, 1999). Strontium-rich dolomites form from aragonite precursors due to buffering of the marine pore fluids by Sr released during aragonite dissolution (Banner, 1995; Budd, 1997).

Using $(Sr/Ca)_{dol} = D_{Sr}^{dol} X (Sr/Ca)_{fluid}$

and D_{Sr}^{dol} of 0.015 to 0.25 (Vahrenkamp and Swart, 1994; Banner, 1995; Budd, 1997) and Sr/Ca ratios for Jurassic and Early Cretaceous seawater of 3 to $5x10^{-3}$ mmoles/mole (Holmden and Hudson, 2003; Coggon et al., 2010), gives stoichiometric dolomites with ~20 to 54 ppm Sr. These low values reflect the Ca-rich composition of Jurassic-Cretaceous seawater. These values are less than the 50 to 100 ppm range of the Arab-D dolomites, which are near stoichiometric, so that Ca excess has not strongly influenced Sr incorporation in dolomite.

The Arab-D dolomites show little relation between increasing Sr with increasing Ca in the dolomites (Fig. 3.11). This differs from Neogene dolomites whose Sr content is strongly correlated with Ca excess in the dolomites (20 ppm Sr per mole of Ca excess) with stoichiometric dolomite having ~50 ppm Sr (Vahrenkamp and Swart, 1994). Late Cenozoic non-fabric preserving coarse dolomites (CNM dolomites) show little relation between Sr and Ca-composition and also formed from calcite precursors (resulting from stabilization of aragonite and Mg-calcite; Wheeler et al., 1999), supporting the calcite precursor origin of the Arab-D fabric destructive dolomites. Also, the Arab-D dolomites appear to have been reset or overgrown during burial, thus Sr incorporation into the dolomites would be related to Sr/Ca ratios in the burial brines rather than the initial seawater. Sr/Ca ratios in the evaporite brines likely would be higher (perhaps double) the initial seawater ratios, and in the basinal brines at depth they could be treble the original seawater values, although uncertainty about the change in $K_D Sr$ in dolomite with increasing temperature makes prediction of the Sr content of the burial dolomite difficult (Holser, 1979; Collins, 1970; Heydari, 1997; Mirnejad et al., 2011). Nonetheless, having such a

wide range of Sr/Ca ratios in the waters coupled with potential changes in distribution coefficients, and the change toward more stoichiometric dolomites with burial could account for the slightly elevated Sr contents of the dolomites compared to the low Sr contents of stoichiometric dolomites precipitated from Late Jurassic seawater.

Significance of C, O and Sr Isotope Data:

Carbon and Oxygen Isotopes, Coeval Marine Calcites: The shallow platform waters of the Arabian Platform in the Late Jurassic would have had higher $\delta^{18}O$ and $\delta^{13}C$ values than the open ocean, using the modern Arabian Gulf analog (Gischler and Lomando, 2005). In the modern Gulf, $\delta^{18}O$ and $\delta^{13}C$ values increase toward the shore. Given the much larger areal extent of the Arabian platform compared to the modern gulf, its relatively shallow water, and the inferred arid climate based on the extent of the Late Jurassic evaporites, it is likely that C and O isotope values of the Arab-D platform waters were even higher than in the present gulf.

Little-altered Croatian early dolomites of Late Jurassic (Tithonian age), now exposed at the surface, were used to assess original reflux dolomite compositions, as these show heavy oxygen isotope values, and little deep burial modification (Cangialosi et al. in prep.). This appears to have been due to the dolomites having lost porosity prior to deep burial, and their relatively short residence time in the burial environment prior to renewed uplift. Assuming that the Arab-D marine calcites originally had similar $\delta^{18}O$ values to little altered Croatian marine calcites (0 to -2 per mil_{VPDB}), and assuming water temperatures of 25 to 35 ^{o}C, would give restricted platform seawater $\delta^{18}O$ values of around 0 to over +4 per mil_{SMOW}. The lack of associated evaporites on the Croatian platform, would suggest that the evaporative Arab-D platform waters had similar to higher $\delta^{18}O$ values than the Croatian waters. These 0 to +4 per mil_{SMOW} values span the estimated water $\delta^{18}O$ values of +1 to +2 per mil_{SMOW} inferred by

Cantrell et al. (2004) using a Trucial Coast analog adjusted for an assumed lighter Late Jurassic ocean water, but are some 2 per mil heavier at the more evaporated end of the spectrum.

The $\delta^{18}O$ values of the Arab-D marine calcites (which formed from more evaporitic platform conditions than the Croatian ones) must have been shifted by burial diagenesis to lighter values by some -3 per mil relative to the little altered Croatian marine calcites (Fig. 3.13). This diagenetic shift reflects the very large oxygen isotope reservoir in the diagenetic pore waters relative to the rock (Lohmann, 1985). If the shift is related to burial diagenesis of the Arab-D calcites with no change in isotopic composition of the water, then the 50^{o} C change from 30 to 80^{o}C would result in a -7 per mil shift in the oxygen isotope values. The actual -3 per mil oxygen isotope shift observed is compatible with burial diagenesis of the Arab-D marine calcites at peak reservoir temperatures and highly saline brines with $\delta^{18}O$ of over +7 per mil_{SMOW} similar to those documented from Cenozoic carbonate-evaporite successions at similar depths in Iran (Mirnejad et al, 2011). The bottom line is that the oxygen isotopic composition of the marine calcites in the Arab-D have been reset due to burial diagenesis and cannot be used as a baseline marine calcite value.

The marine calcite $\delta^{13}C$ values of the Kimmeridgian Arab-D overlap the middle range of coeval marine calcites from Croatia, and globally (Veizer et al., 1999). This suggests that the C-isotopes in the Arab-D marine calcites buffered the system during burial diagenesis, preserving the orginal marine C isotope value.

Carbon and Oxygen Isotopes, Dolomites: The $\delta^{13}C$ values of the Arab-D dolomites commonly are heavier than most of the Arab-D marine calcites, but overlap the upper part of the range of Croatian marine calcites (Fig. 3.13). This could be due to the Δdolomite-calcite, in which $\delta^{13}C$ values of coeval dolomite may be enriched by up to 2 per mil relative to calcite (Ohmoto and

Rye, 1979). Also, since nearshore more saline waters (involved in the dolomitization) may have elevated carbon values relative to open marine seawater in the present day Gulf (Gischler and Lomando, 2005), also could account for the slightly heavier C-isotope values of some of the Late Jurassic dolomites relative to the calcites.

In terms of oxygen isotopes, assuming that the dolomitization of reservoir zones 1 to 3 was initiated in the near-surface or even at the seafloor, then the dolomites *initially* would have had oxygen isotopic compositions similar to the Croatian early dolomites (at least +1 to +3 per mil_{VPDB} or even heavier; Fig. 3.13). These values are compatible with early dolomite compositions suggested for zone 3 dolomites (Swart et al., 2005), and are heavier than the -1 to -2 per milV_{PDB}values used as Zone 2B early dolomites on Figure 3.14 of Swart et al. (2005). A pristine early dolomite from Jurassic seawater should have $\delta^{18}O$ values about 3 per mil heavier than a Jurassic marine calcite (Fig. 3.13). The plot of $\delta^{18}O_{dolomite}$ vs. temperature, with $\delta^{18}O_{water}$ contours (Fig. 3.19) was constructed using the equation of Vasconcelos et al. (2005), based on low temperature microbially induced precipitation experiments, which give similar results for dolomite-water fractionation as the equation of Fritz and Smith (1970). Plotting the field for a Late Jurassic early dolomite at 25 to 35 ^{o}C would suggest waters of +1 to over +5 per mil_{SMOW}, which are compatible with or slightly more evolved than the waters forming the marine calcites, as expected. These values are far heavier than the 0 to -3 per mil_{SMOW} waters postulated by Swart et al. (2005, their Fig. 3.14) that were assumed to have formed the isotopically heaviest Arab-D dolomites.

Given the field for early dolomite with $\delta^{18}O$ values of between +1 to +3 per mil_{PDB} (based on the little altered Croatian dolomite, and which may have originally been between +2 and +4 per mil_{PDB} (Read, pers. comm. 2012), suggests that the $\delta^{18}O$ compositions of all the

Arab-D dolomites have been considerably reset. Reservoir zone 1 and 2 dolomites have undergone burial resetting of the oxygen isotopes by as much as -3 to -7 per mil_{PDB} and zone 3 by even more.

Assuming that resetting would depend on the dolomites being permeable to fluids, then the final temperature of resetting of the various dolomites likely depended on when permeability was lost. During deposition of the overlying evaporites, heavy brines would have seeped down into the Arab-D reservoir (Cantrell et al., 2004), while the Jubaila carbonates acted as a basal seal. Using the Cenozoic carbonate-evaporite successions of Iran as an analog, which have $\delta^{18}O$ values in the reservoir fluids of +8 or +9 per mil_{SMOW} (Mirnejad et al., 2011) suggests that Arab-D reservoir fluids during burial likely were up to +7 or +8 per mil_{SMOW}. This value is adjusted for the oxygen isotope composition of Jurassic ocean water, which was perhaps -1 per mil lighter than today (Viezer et al., 1999). These values are compatible with present formation waters in north Ghawar which are about +6 to +8 per mil_{SMOW} (Stenger et al. 2003). If we assume then that the later dolomitizing pore fluids ranged from +4 to +8 per mil_{SMOW}, these would be higher than the previous estimates of +2 to +4 mil_{SMOW} (Cantrell et al., 2004). These dolomitizing fluids could have been generated as refluxing brines during deposition of the overlying evaporites, modified by subsequent reaction with the limestones. The range of $\delta^{18}O$ values of the dolomitizing brines is compatible with the experimental data of Lloyd (1966) who evaporated sea water under various relative humidity settings to define their oxygen isotopic composition. The high salinities of Arab-D formation waters of 6 to 7 times seawater based on fluid inclusion data (Cantrell et al. 2004) , although compatible with a brine originating in the gypsum or anhydrite precipitation field) probably had their salinities increased relative to the original brines, by reaction with calcite and evaporites in the section during burial.

Estimates of peak burial temperatures within the Arab-D used by Cantrell et al. (2004) were based on homogenization temperatures (T_h) of primary fluid inclusions from the late stage baroque dolomites (and secondary inclusions in the other dolomites), but these are minimum peak temperatures. If corrected for pressures at 2 km depth (present reservoir depth) and salinities of 20 wt. % would give values that might be up to 50 ^{o}C higher (Goldstein and Reynolds, 1994).

If initial resetting took place at between 60 to 80 ^{o}C, then the range of zone 1 and 2 dolomites would require water $\delta^{18}O$ values of up to +8 to form the heaviest zone 1 and 2 dolomites observed, and waters down to +4 per mil_{SMOW} to make the bulk of the lighter zone 1 to 3 dolomites (Fig. 3.19). However, permeability is still present in the some of the dolomite reservoir rocks, suggesting that dolomite resetting of present day reservoir rocks occurred at peak reservoir temperatures of 80 to over 100 ^{o}C. At these minimum temperatures, it would require +8 per mil_{SMOW} waters to make a relatively heavy -2.5 per mil_{PDB} dolomite typical of zone 2 or 3 while the lighter dolomites (to -7 per mil_{PDB} of zones 2 and 3) could have formed from waters as light as +4 per mil_{SMOW}. However, if pore waters locally were hotter (150 ^{o}C for relatively short periods (based on fluid inclusion homogenization temperatures corrected for pressures at 2 km depth pressure and salinity 6 X seawater; Goldstein and Reynolds, 1994) then +8 per mil_{SMOW} waters at these higher temperatures could generate the lightest zone 3 and 4 dolomites observed. Given that these rocks are in the top of the oil window, it is unlikely that the fluid inclusions were methane rich.

Warm hydrothermal fluids have been implicated in the deposition of the relatively rare, late-stage Fe-rich, baroque dolomites that cross-cut the Arab-D stratigraphy elsewhere, are associated in small amounts with fabric-destructive dolomites and have the lightest $\delta^{18}O$ of all

the dolomites (Fig. 3.13; Cantrell et al., 2004). The fact that the present day Arab-D carbonates in Ghawar are at the top of the oil window (Abu-Ali and Littke, 2005) would require these pulses of peak temperature fluids involved in dolomite resetting to be of relatively short duration. The burial history plots show that there was little Cenozoic deposition over Ghawar during the Cenozoic (Abu-Ali and Littke, 2005) and that oil migration into the Arab-D in Ghawar probably occurred in the early Tertiary from Jurassic Oxfordian-Callovian sources (Ayres, 1982). Oil migration would have terminated dolomitization in those rocks saturated with oil.

Using the SIMS data, which shows that most cores typically have heavier $\delta^{18}O$ values than the rims (Fig. 3.15), suggests that for reservoir zone 2 dolomites, the cores were reset at temperatures some 10 to 20 degrees lower than the rim overgrowths. Reservoir zone 3 dolomites also show a similar situation, but some of the cores have from 1 to 9 per mil shifts, these larger shifts would suggest that the rims formed at temperatures some 40 to 90 ^{o}C hotter than the reset cores, supporting the premise that warmer fluids affected the lower zones more than the upper reservoir zones.

There is little correlation of $\delta^{18}O$ with porosity in the Arab-D (except in present day highly permeable so-called “super-k zones”; Cantrell et al. 2001). The presence of flow baffles partitioning the different reservoir zones (and subzones at the sequence scale) would have limited upward migration of pulsed warm brines into the reservoir and subsequent mixing with Kimmeridgian brines in the reservoir. Thus porous units lower in the Arab-D tended to be reset more than those higher in the reservoir, accounting for the relatively heavy oxygen isotopic compositions of some of the higher, zone 1 and 2 dolomites, compared to the lower zones. However, in units that retained high permeabilities (such as the so-called “super-k zones” of Cantrell et al., 2001), there was considerable resetting of dolomites, with hot waters moving up

faults and fractures into the more permeable units, thus accounting for the light $\delta^{18}O$ values of some of the higher dolomites, and the bulk of the lower dolomites (Swart et al., 2005).

$^{87/86}$Sr isotopes in the dolomites:

The $^{87/86}$Sr data of this study, which tends to plot across the range of Kimmeridgian seawater (Fig. 3.16; Price and Grocke, 2002)), strongly suggests that the seawater involved in dolomitization and dolomite resetting was dominantly Kimmeridgian seawater. The mean $^{87/86}$Sr values reported for the non-baroque Arab-D dolomites by Cantrell et al. (2004) generally lie below the values reported in this study, which is puzzling, although they still lie within the range of Oxfordian-Kimmeridgian seawater. The $^{87/86}$Sr vs 1/Sr and the $^{87/86}$Sr vs. depth in the reservoir all suggest that the lowest dolomites in this study are more radiogenic, with the $^{87/86}$Sr decreasing slightly upsection into zone 1 dolomites (Fig. 3.17). It is unlikely that more radiogeneic Tithonian or younger seawater was involved in the diagenetic resetting, because the Hith Anhydrite forms a thick impermeable seal above the Arab Formation. The overall depth increase in $^{87/86}$Sr implies that there was considerable partitioning of the Arab-D reservoir units, which limited mixing of more radiogenic basinal brines from below with the Kimmeridgian seawater in the reservoir zones, the lower zones being affected more than the uppermost zones. Also, some of the dolomites in the upper zones 1 and 2 tended to be "overdolomitized" (in the sense of Choquette and Hiatt, 2008) thus losing porosity earlier than those lower in the section. This also might have protected some these upper dolomites from resetting by the more radiogenic later hydrothermal fluids that formed the fracture-filling baroque dolomites of Cantrell et al. (2004).

Paragenetic Model

The paragenesis of the Arab-D dolomites (Table 3.1; Fig. 3.20) is as follows:

1. Deposition of Arab-D carbonates of low Mg calcite- and lesser high Mg calcite and aragonite sediments from the Late Jurassic calcite seas (Stanley and Hardie, 1998), which become more saline during Arab-D deposition culminating in deposition of aragonite-rich sediments below the D-anhydrite; minor overgrowth by marine fibrous to bladed cements on grainstones (Cantrell and Hagerty, 1999; Cantrell, 2005).

2. Multiple phases of early dolomite nucleation as high-Ca dolomites, as stratiform units within Arab-D member; these likely developed during shallowing phases on the platform associated with hiatal surfaces, when marine waters were pumped downward into the sediments due to density, tidal or pressure head (Fig. 3.20A). The $\delta^{18}O$ values of waters +1 +5 per mil_{SMOW} reflect meso- to hypersaline waters on the restricted platform. Fabric destructive dolomites formed where calcite sediments were replaced, whereas the fabric preserving dolomites developed beneath the evaporites, where aragonite rich sediments were replaced (Fig. 3.20B; Cantrell, 2005; Swart et al., 2005; Lindsay et al., 2006)

3. Deposition of bedded anhydrite in Arab-D anhydrite and anhydrite laths promoted continued formation of replacement dolomite and precipitation of dolomite overgrowth in underlying partly dolomitized units, via refluxing brines ($\delta^{18}O$ values above +5 per mil_{SMOW} at near-surface temperatures (Fig. 3.20C). Brines migrated slowly down through flow barriers in Arab-D via cross formation flow, and more rapidly via early joints, fractures and faults (Cantrell et al., 2004; Stenger et al., 2003). The tight Jubaila limestones formed a basal seal to downward percolating brines. Resetting of earlier dolomites (and limestones) may have been initiated at this stage below 50 ^{o}C, along with initiation of microporosity formation (Cantrell and Hagerty, 1999).

4. Stylolitization and intergrain penetration starting below 300 m burial depth, and precipitation of minor calcite rim cementation on echinoderm grains, while peloids escape cementation. As sediments become brittle, jointing and fracturing of Arab-D sediments initiated.

5. Increasing burial promotes continued dolomitization, dolomite cementation and continued resetting of earlier limestones and dolomites by warm, saline brines at 60 to over 100 ^{o}C and δ^{18}O values of up to +8 per mil$_{SMOW}$, similar to present day north Ghawar waters (Stenger et al., 2003). Dissolved Mn and Fe in brines kept relatively low due to sulphate concentrations maintaining relatively positive redox. The brines within the Arab-D in Ghawar were continually replenished by convecting Kimmeridgian brines (with Kimmeridgian seawater $^{87/86}$Sr values) from deeper, off-structure Arab-D porous facies to west (and perhaps east) in a manner analogous to the theoretical model proposed for flow in porous folded sandstones (Fig. 3.20D; Wood and Hewitt, 1982). These convecting brines also replaced the small amounts of brines periodically leaking upward into overlying units via fractures cutting the minor seals (D, C and B anhydrites) of the Arab Formation (Stenger et al., 2003). This is the mechanism proposed for thermal anomalies on anticlines in the subsurface (Merriam, 2004). These Arab-D reservoir facies off-structure thus provided a continued, major source of convecting Kimmeridgian brines for dolomitization, with the brines ultimately being replaced by intrusion of meteoric waters far to the west (Stenger et al., 2003). The Kimmeridgian brines were increasingly mixed with upward ascending warm brines deeper in the Arab-D reservoir, so that lower units developed a tendency for more depleted δ^{18}O values and more radiogenic $^{87/86}$Sr values compared to higher Arab D units.

6. Prior to hydrocarbon migration in the early Tertiary (Ayres et al. 1982), the acetic acid front ahead of the migrating hydrocarbons caused leaching of calcite, and formation of sucrosic

dolomites. The calcite leaching may have may have been accompanied by minor dedolomitization and replacement with calcite, and burial anhydrite cements.

7. Precipitation of Fe-rich baroque dolomite (not observed in the studied wells) but seen elsewhere in Ghawar, in fractures and faults from upward ascending brines (Fig. 3.20E). These brines were 6 to 7 times seawater salinity, relatively reducing with high dissolved Fe, and Sr isotopes much more radiogenic than Kimmeridgian seawater. These baroque dolomites probably formed during the Cretaceous when most of the structural relief of Ghawar developed (Cantrell et al., 2004).

8. Hydrocarbon emplacement in the Arab-D reservoir in the Early Tertiary (Ayres et al., 1982) terminated diagenesis within the oil/gas saturated zones, although diagenesis probably continued in off-structure areas that were water-wet.

CONCLUSIONS

The initial dolomites of the Arab-D reservoir zones developed during shallowing phases on the platform, which nucleated the early dolomites. It is likely that fabric destructive dolomites making up the bulk of the succession were initiated from more normal marine waters while the higher fabric preserving dolomites formed from aragonitic sediments and more evolved hypersaline marine waters, prior to and during initial Arab-D anhydrite deposition. Each dolomitizing event at the surface also generated refluxing waters that continued to dolomitize deeper, earlier dolomitized units. Prior to burial resetting, these dolomites probably had $\delta^{18}O$ values perhaps as high as +2 and +4 per mil_{VPDB}. However, with onset of evaporite deposition, isotopically heavy dense brines moved down into the section. Cantrell et al. (2004) suggest that fractures cutting the section may have allowed downward migration of the evaporitic brines into the Arab-D reservoir carbonates, breaching any basal hydroseal underneath the evaporites, thus

allowing continued dolomitization during evaporite deposition while the Jubaila carbonates acted as a basal seal.

With onset of burial, both the original limestones and the dolomites started to be reset to lighter oxygen isotope values by the warm connate Kimmeridgian brines which likely were relatively heavy (+4 to +8 per mil_{SMOW}), while the C isotopic composition was buffered by the rock C. This initiated replacement of dolomite cores by more stoichiometric dolomite, and dolomite overgrowths on the rims of dolomite crystals. The off-structure Arab-D units acted as a reservoir for convecting Kimmeridgian brines within the Arab-D reservoir facies; these brines also gradually replenished those lost by upward leakage along fractures and faults cutting the overlying anhydrites. With increasing burial temperatures in the Cretaceous, the dolomites continued to re-equilibrate with the isotopically heavy connate brines, developing even lighter $\delta^{18}O$ values for the bulk dolomites. The fact that the reservoir was partitioned into porosity zones, and because dolomites higher in the section tended to lose porosity by overdolomization earlier than those lower in the section, they tended to be protected from latest burial resetting and dolomite overgrowth from pulsed hydrothermal brines with more radiogenic $^{87/86}Sr$ that moved upward along faults and fractures, and mixed with the connate Kimmeridgian brines, thus resulting in the slight increase in $^{87/86}Sr$ downsection in the Arab-D, as well as the weak trend in depleted $\delta^{18}O$ values downsection. Oil migration into the reservoir in the Early Tertiary terminated dolomitization.

The model differs from previous models in presenting evidence for heavier oxygen isotopic compositions of the original marine limestones than previous workers, and uses unaltered coeval dolomites from Croatia for the initial early dolomites. It emphasizes that the any original limestones and early dolomites have undergone considerable resetting of oxygen

isotopic compositions during later burial dolomitization. It invokes highly evolved, evaporated platform waters with relatively heavy $\delta^{18}O$ compositions as the major dolomitizing fluids. The model proposes lateral inflow of convecting Kimmeridgian brines from the Arab-D off-structure as a continuing source of fluids with Kimmeridgian seawater $^{87/86}Sr$ values. It also invokes evolved subsurface brines at peak temperatures and $\delta^{18}O$ values of +4 to +8 per mil_{SMOW} as being involved in burial dolomite replacement and overgrowth, based on actualistic models from Iranian oil fields and northern Ghawar brines, which have far heavier oxygen isotope compositions than those suggested previously.

FIGURES

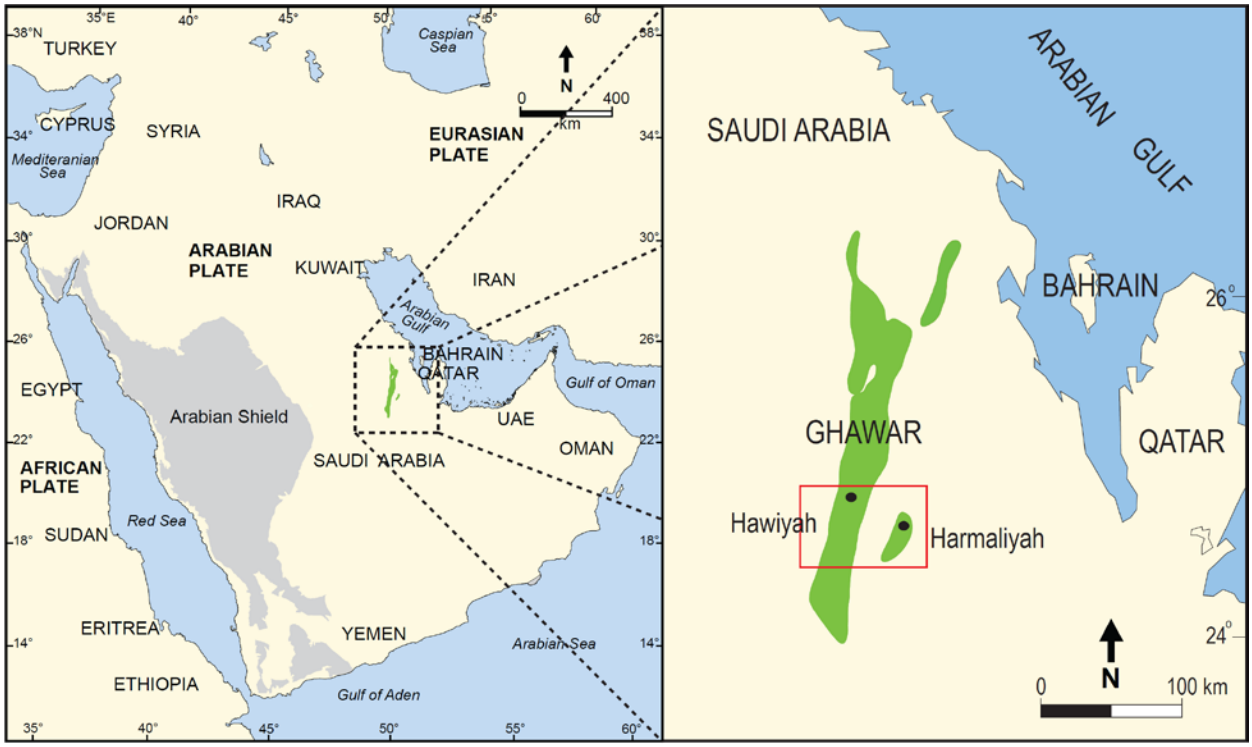

Figure 3.1: Left: Map showing studied area in Saudi Arabia. Right: Locality map showing the location of Hawiyah field in Ghawar, and Harmaliyah field, east of Ghawar, and the location of cores (black) for the dolomite study.

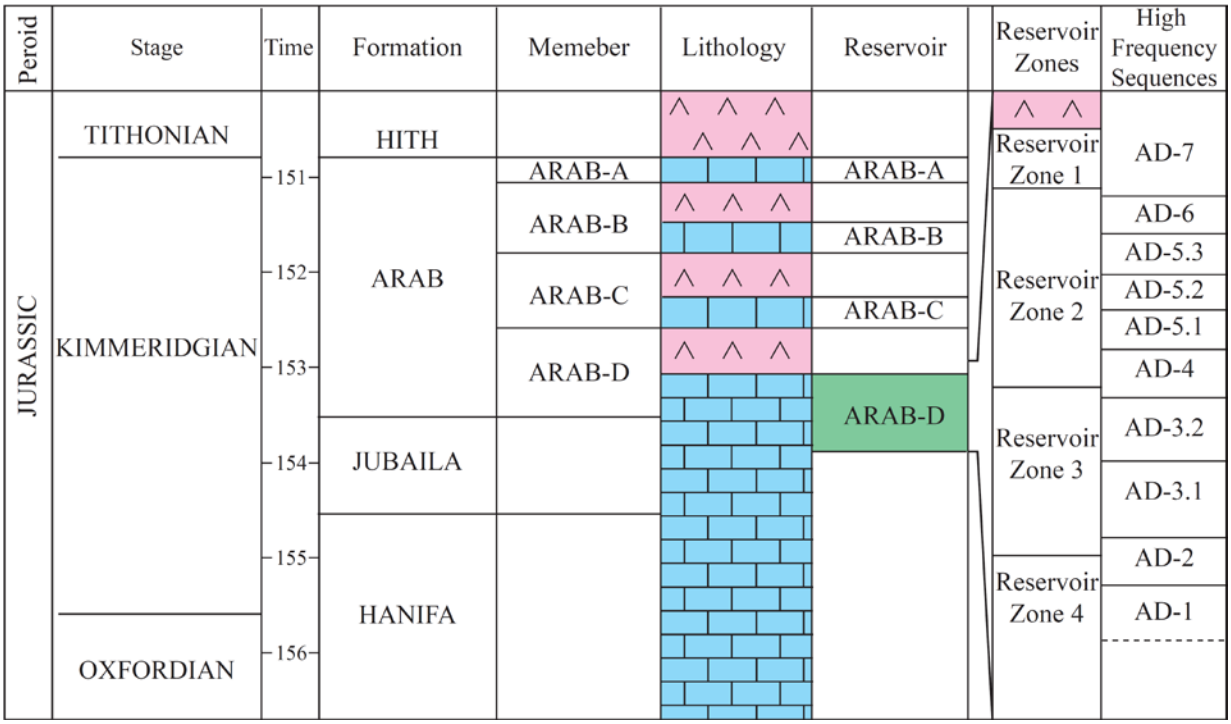

Figure 3.2: Chronostratigraphic chart of Late Jurassic (Kimmeridgian) units. The reservoir zones and sequence stratigraphic subdivisions of the Arab-D used in this paper are shown. The dolomite samples studied are from the Arab-D reservoir (shaded green).

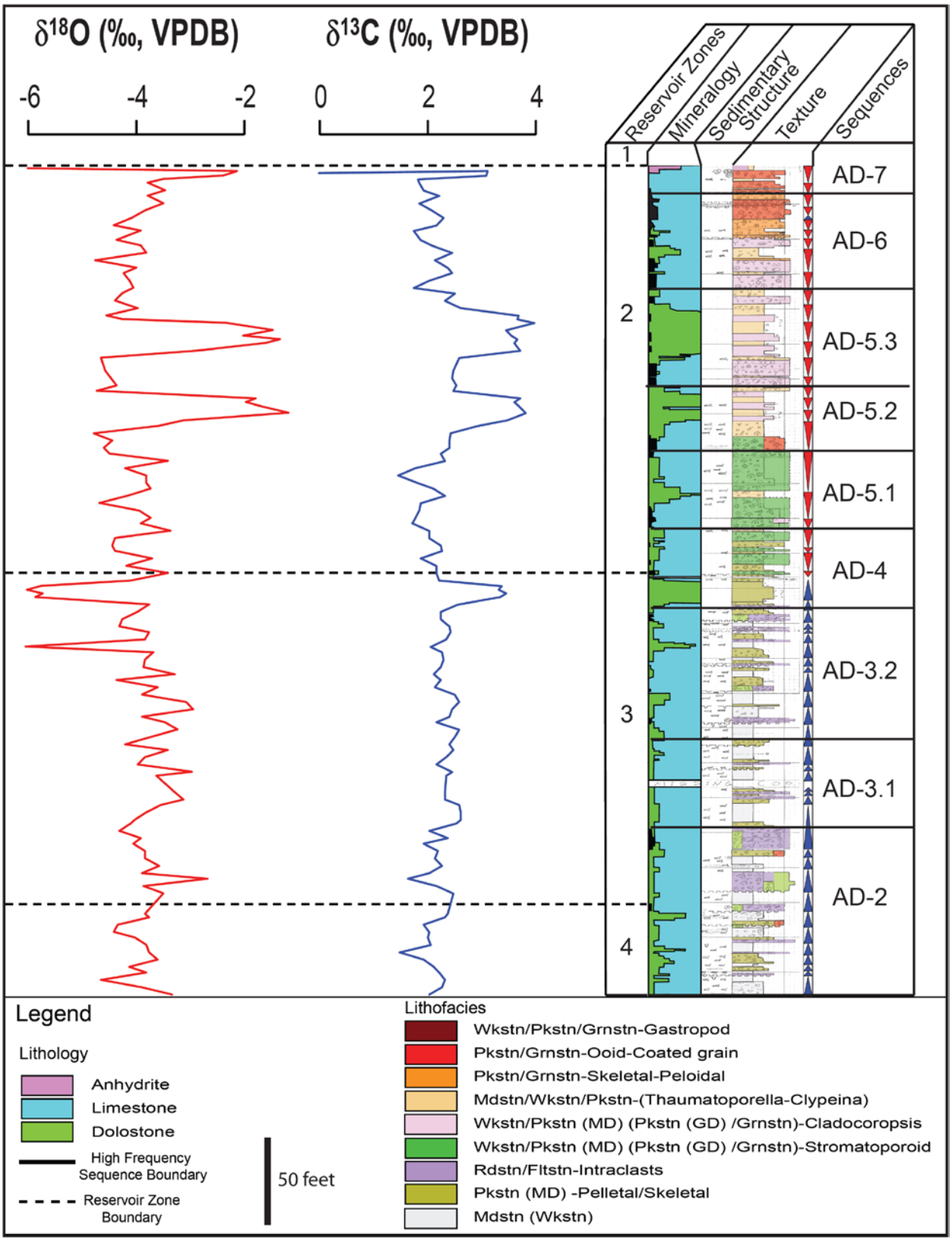

Figure 3.3: Selected core showing stratigraphic position of the Arab-D dolomites (green color in Mineralogy column of corelog) along with Carbon and Oxygen isotope profiles.

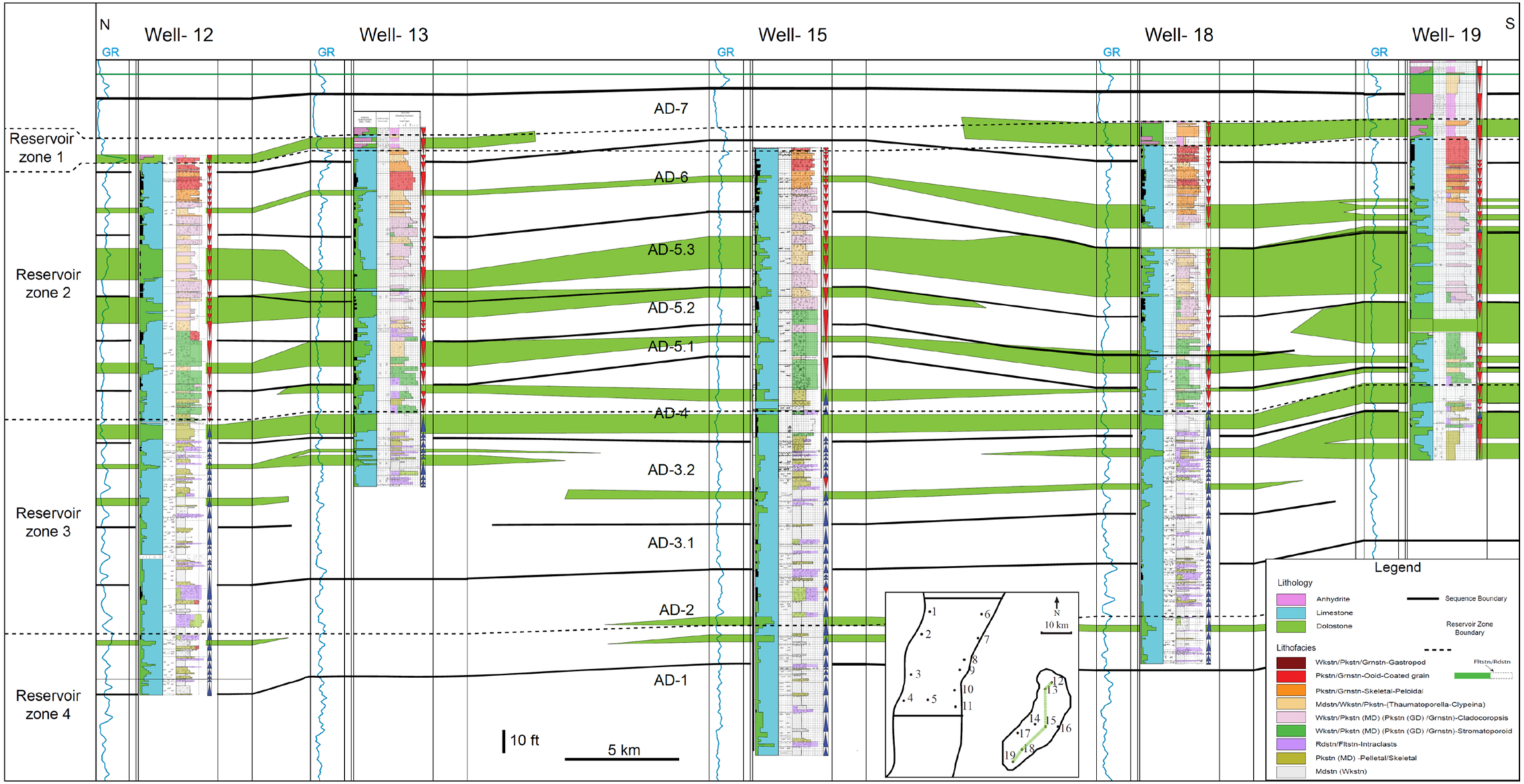

Figure 3. 4: North-south cross section from Harmaliyah Field showing vertical and lateral dolomite distribution across the field. Dashed lines are boundaries of the reservoir zones (Zone 4 to Zone 1). Heavy black lines are the sequence bounaries of the high frequence sequences (AD-1 to AD-7).

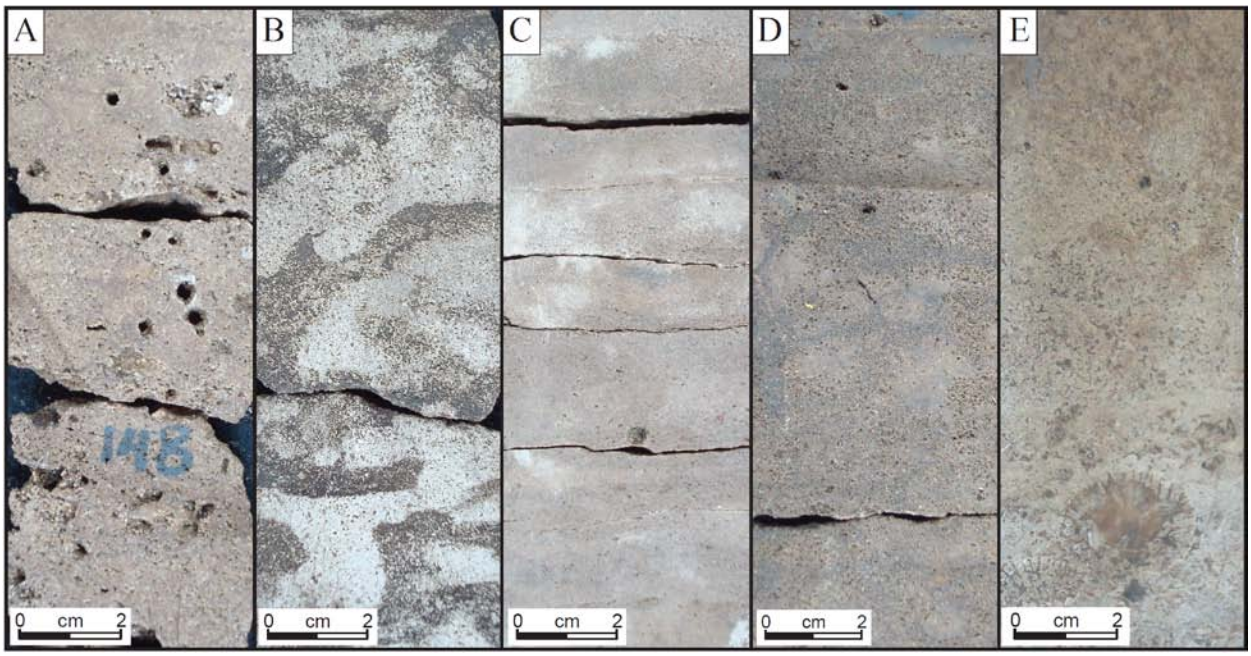

Figure 3.5: Slab photos of cores showing typical Arab-D dolomite fabrics. A. Porous dolomite in the leached Cladocoropsis in reservoir zone 2. B. Dolomitized burrows in lime mudstone. C. Tight fine graind dolomite. D. Medium to coarse grained porous dolomite. E. Fabric preserved dolomite from reservoir zone 1.

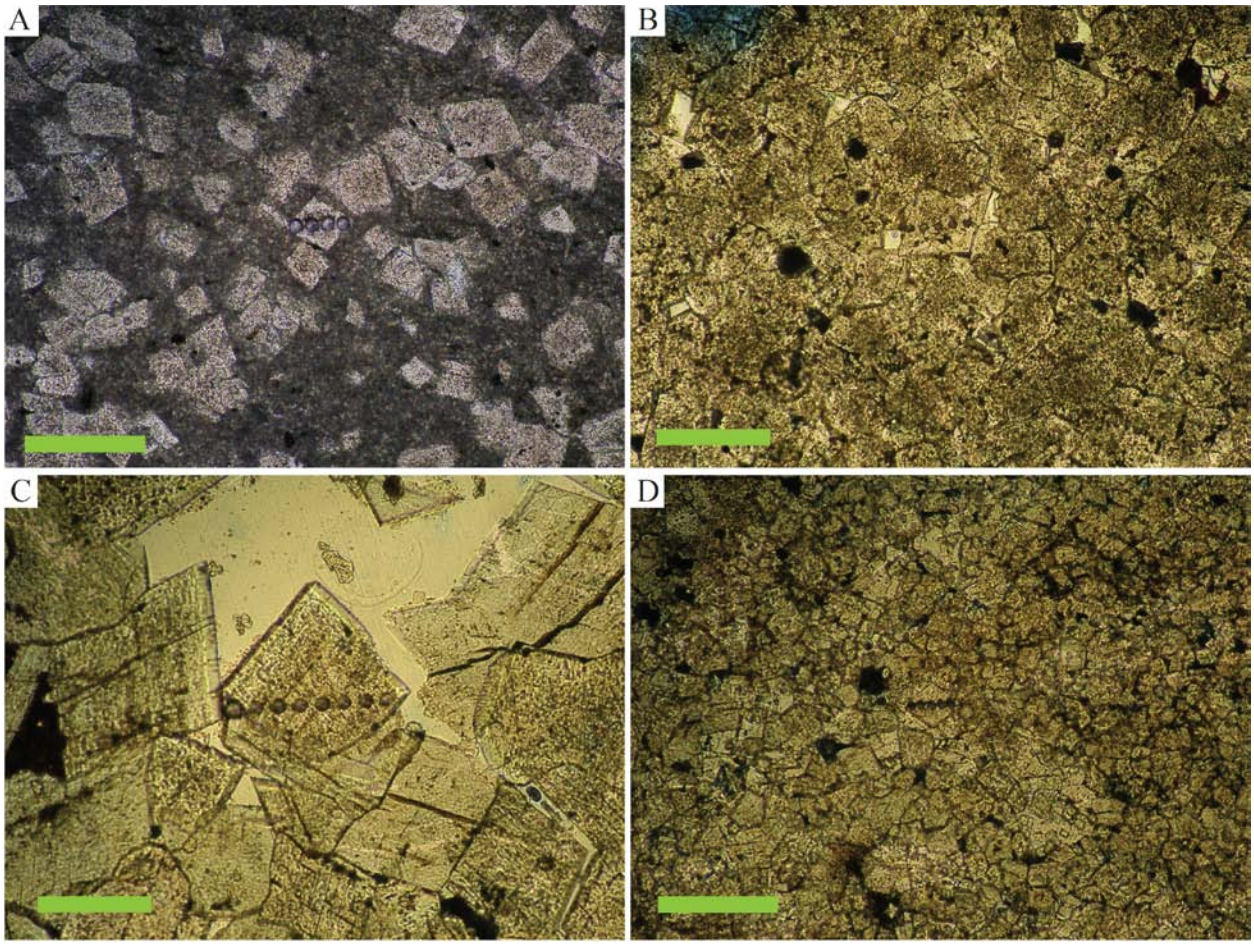

Figure 3.6: Thin section photographs, plane light, showing typical dolomite textures. All the dolomites are nonluminescent under the operating conditions used. The green scale bar is 200 microns. A. Scattered fine grained dolomite rhombs in subwave base lime mudstones typical of reservoir zones 3 and 4 (Sample from zone 3, Harmaliyah well). B. Tight medium- to coarse-grained, fabric-destructive dolomite typical of reservoir zones 3 (sample from Hawiyah well). C. Porous medium- and coarse-grained, fabric-destructive dolomite typical of reservoir zone 2 and upper 3. Turbid cores are inclusion-rich and rims are clear (Sample from zone 2, Harmaliyah well). D. Recrystallized fine-grained weakly fabric preserving dolomite of reservoir zone 1 just beneath the evaporites (sample from Harmaliyah well).

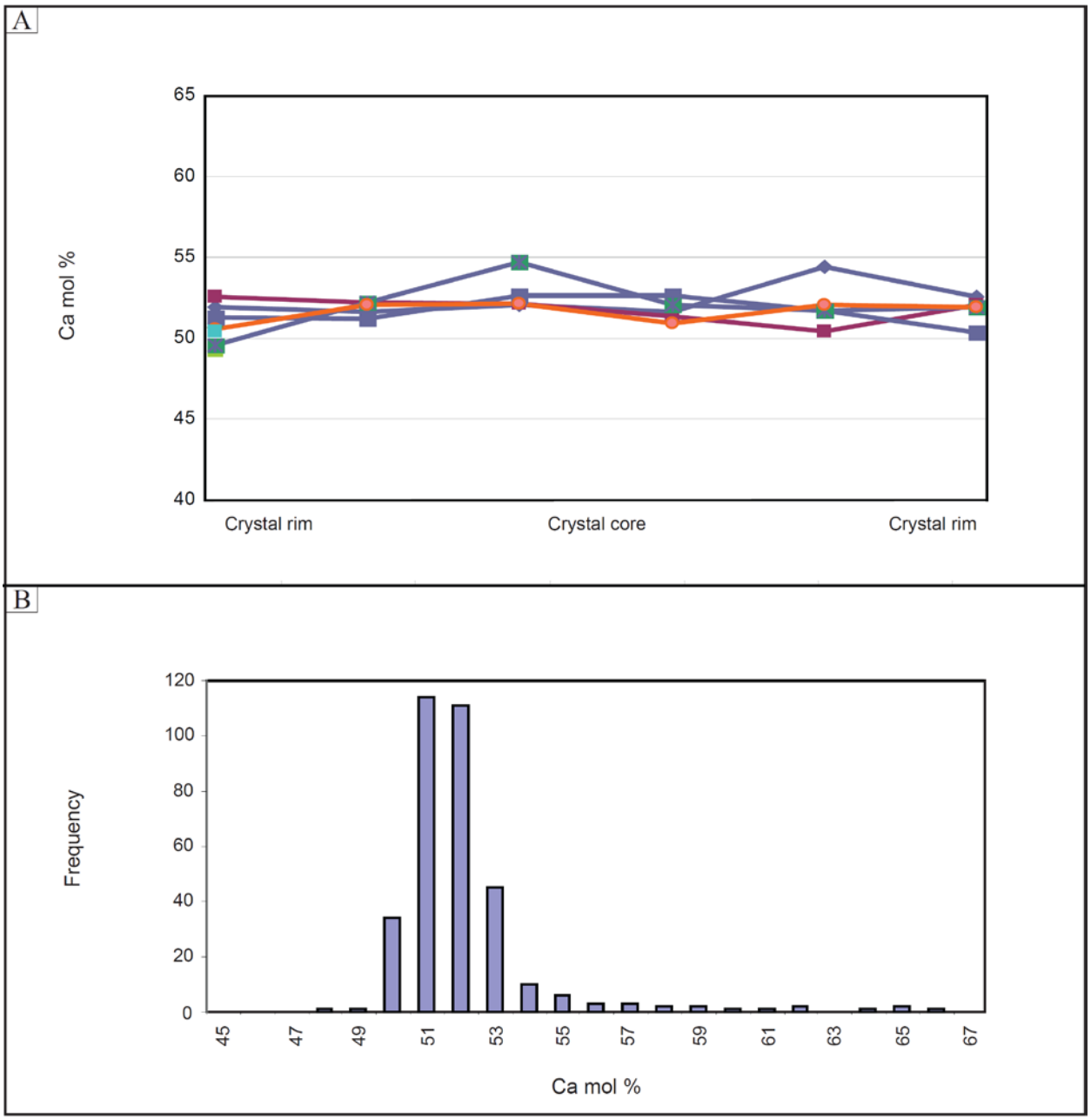

Figure 3.7: A. Electron microprobe traverses of Ca concentration across selected dolomite crystals. B. Histogram of frequency of Ca mol % composition of the dolomites, showing that the dominant composition is between 51 and 52 mol % Ca.

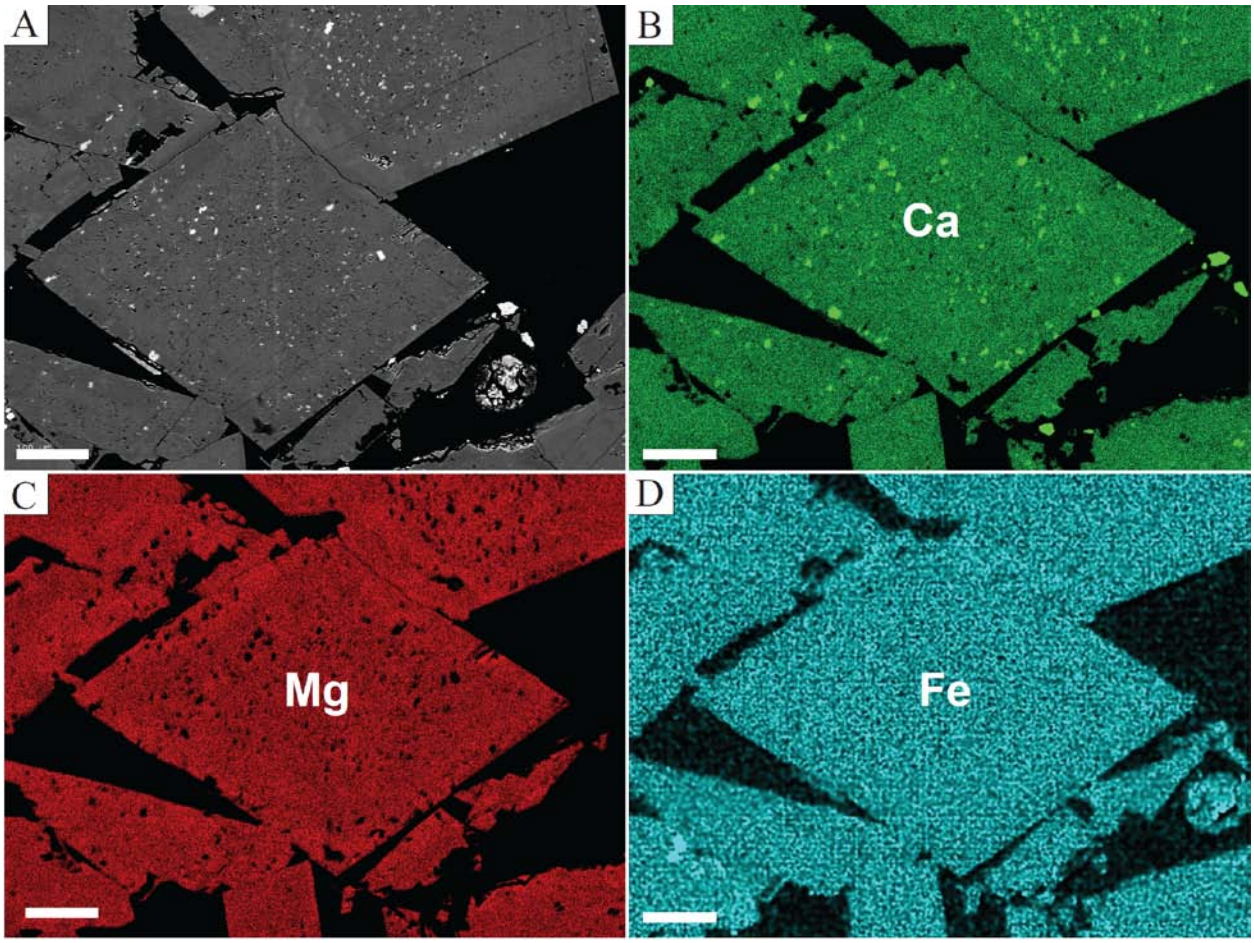

Figure 3.8: Backscattered electron (BSE) images and major element maps of the dolomites. Sample is from reservoir zone 2 in Hawiyah well. Porosity is the black color around dolomite crystals. The white scale bar in the bottom left is 100 microns. All element maps show lack of zonation across dolomite crystals. Mn and Sr were below detection and are not shown. A. BSE image of the dolomite showing lack of chemical zoning in the dolomite. Any Ca-rich, Mg-poor zone would have shown as brighter areas. It indicates a chemically uniform major element (Ca, Mg) composition from core to rim. B. Ca major element map showing uniform distribution of Ca. C. Mg-element map showing uniform distribution of Mg. D. Fe element map showing uniform distribution of Fe.

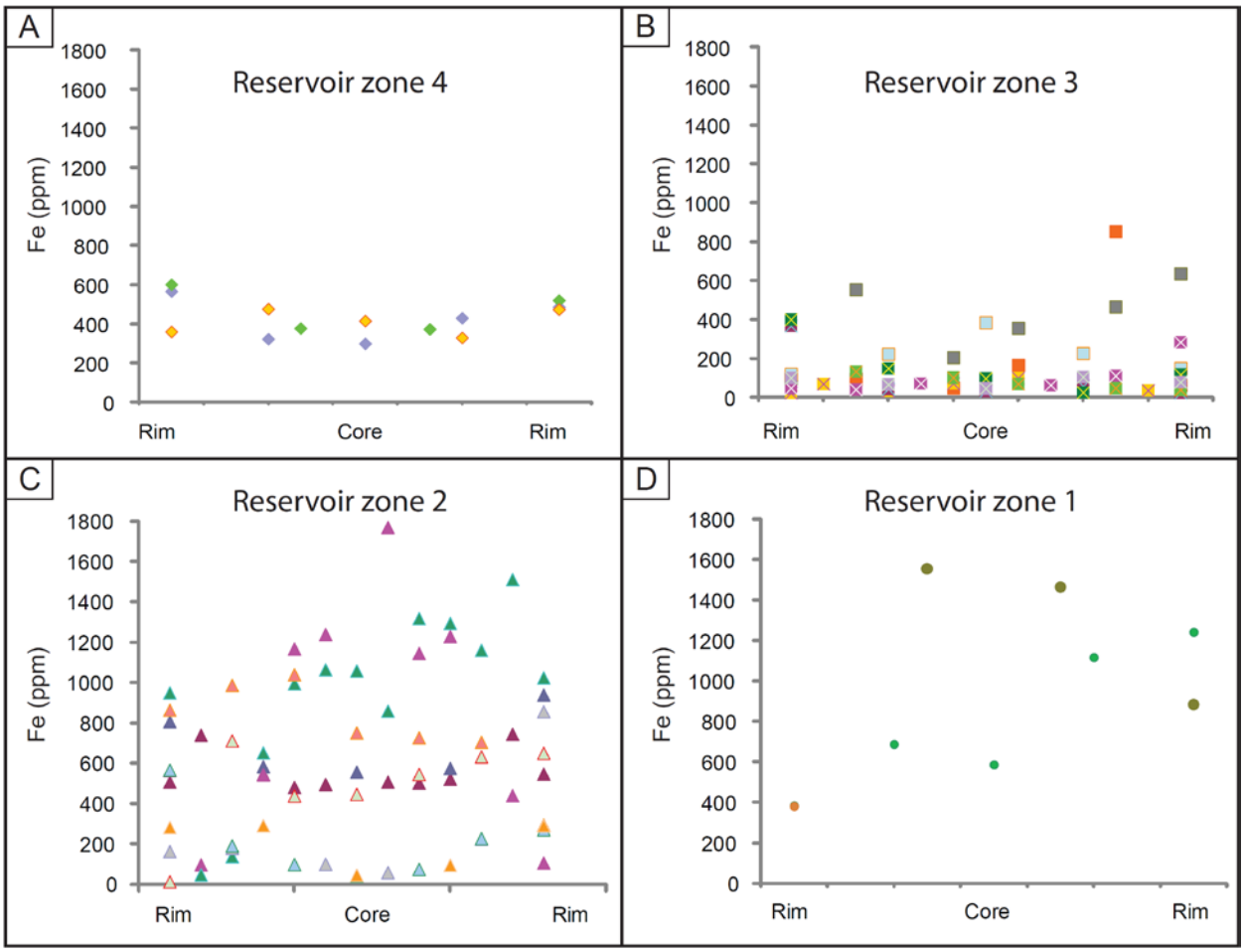

Figure 3.9: Fe values across dolomite crystals, using Laser Ablation ICP-MS, from different reservoir zones. Values of each traverse are color coded. Data shows no clear trend from dolomite crystal rims to cores. A. Fe data from dolomite crystals in reservoir zone 4 showing relarively uniform Fe concentration. B. Fe data from dolomite crystals in reservoir zone 3. C. Fe data from dolomite crystals in reservoir zone 2 showing highly variable concentrations but no clear trends. D. Fe data from dolomite crystals in reservoir zone 1 shwoing higly variable concentration but no clear trends.

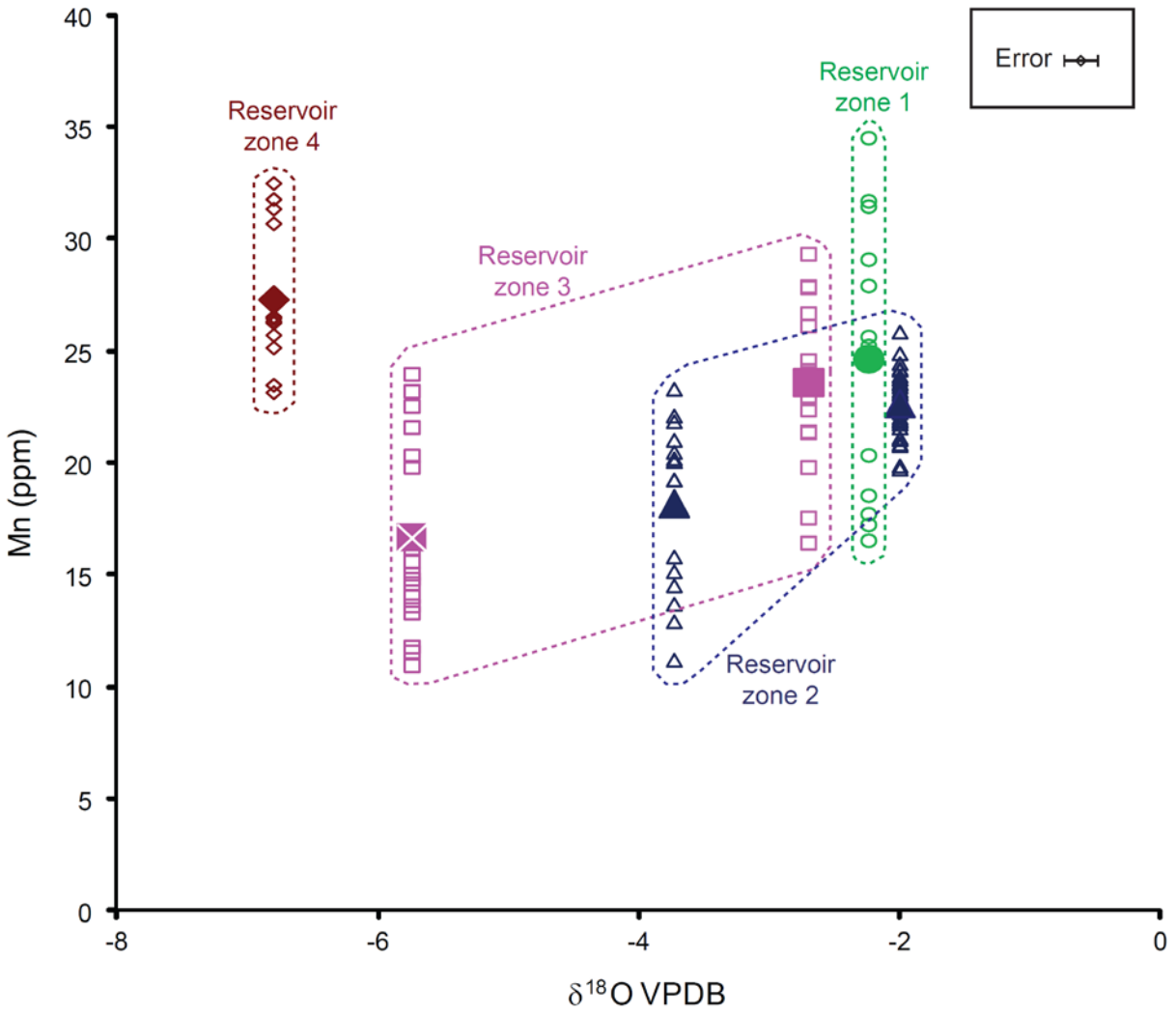

Figure 3.10: Cross plot of Mn (determined by Laser Ablation ICP-MS) vs. $\delta^{18}O$. Mn shows no significat correlation with $\delta^{18}O$. All Mn data is low and has a small variation range between 10 and 35 ppm. Large solid symbols are the mean values for each group.

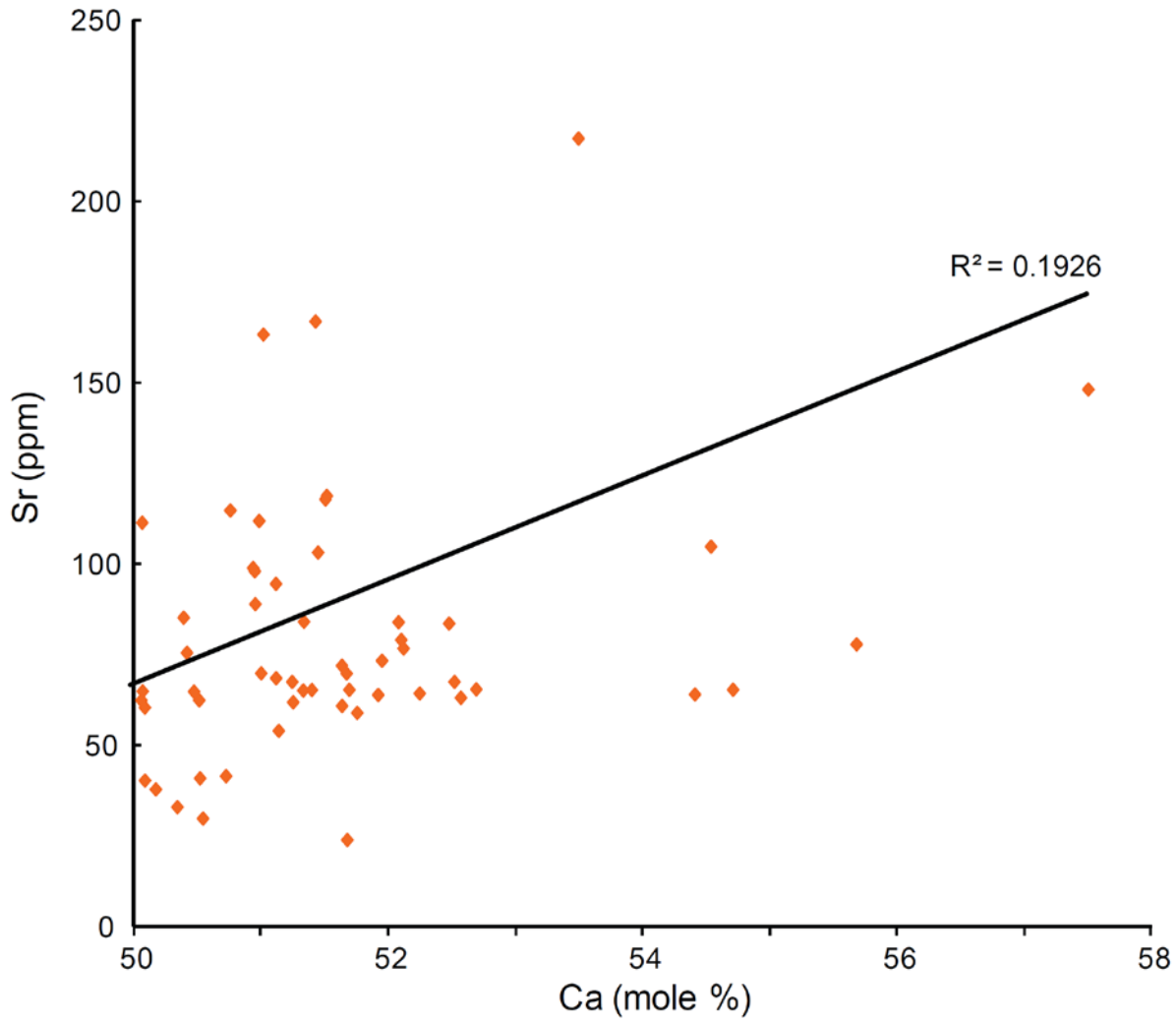

Figure 3.11: Crossplot of Sr (determined by Laser Ablation ICP-MS) with respect to Ca mole % of the dolomites.

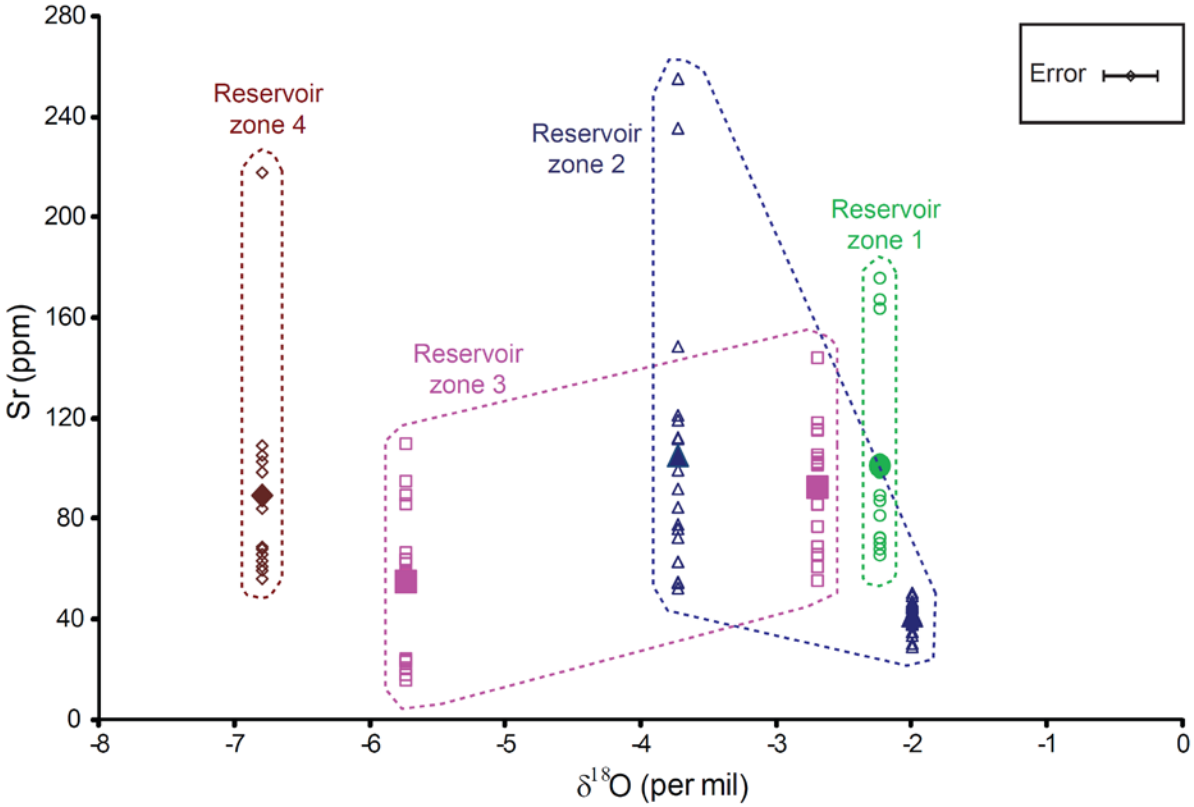

Figure 3.12: Crossplot of total Sr (determined by Laser Ablation ICP-MS) with respect to $\delta^{18}O$. The difference in the data mean values (large solid symbols) has a small range. There is no clear treand between totlal Sr and $\delta^{18}O$.

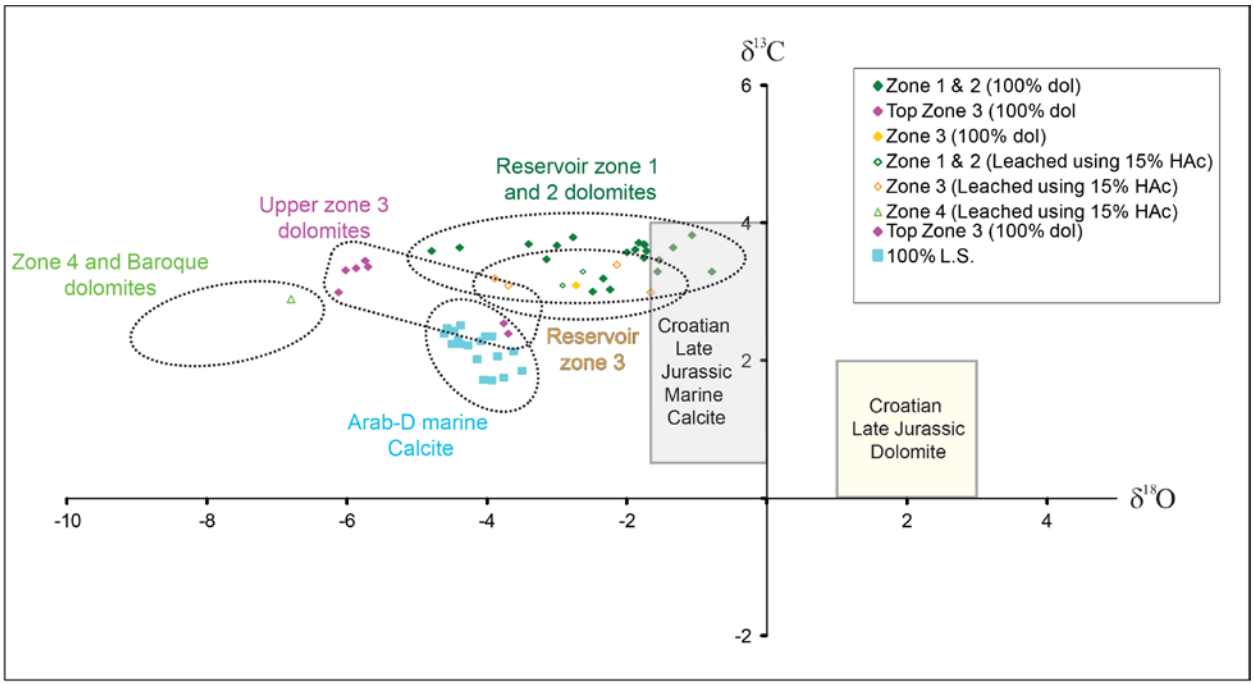

Figure 3.13: Carbon and Oxygen cross-plot of the Arab-D marine limestone, pure dolomite, and from acetic acid leached mixed dolomite-calcite samples, from reservoir zones 1 to 4, compared to Late Jurassic limestone and dolomite from Croatia that has undergone little burial resetting. Baroque dolomite values are taken from Cantrell et al., 2004.

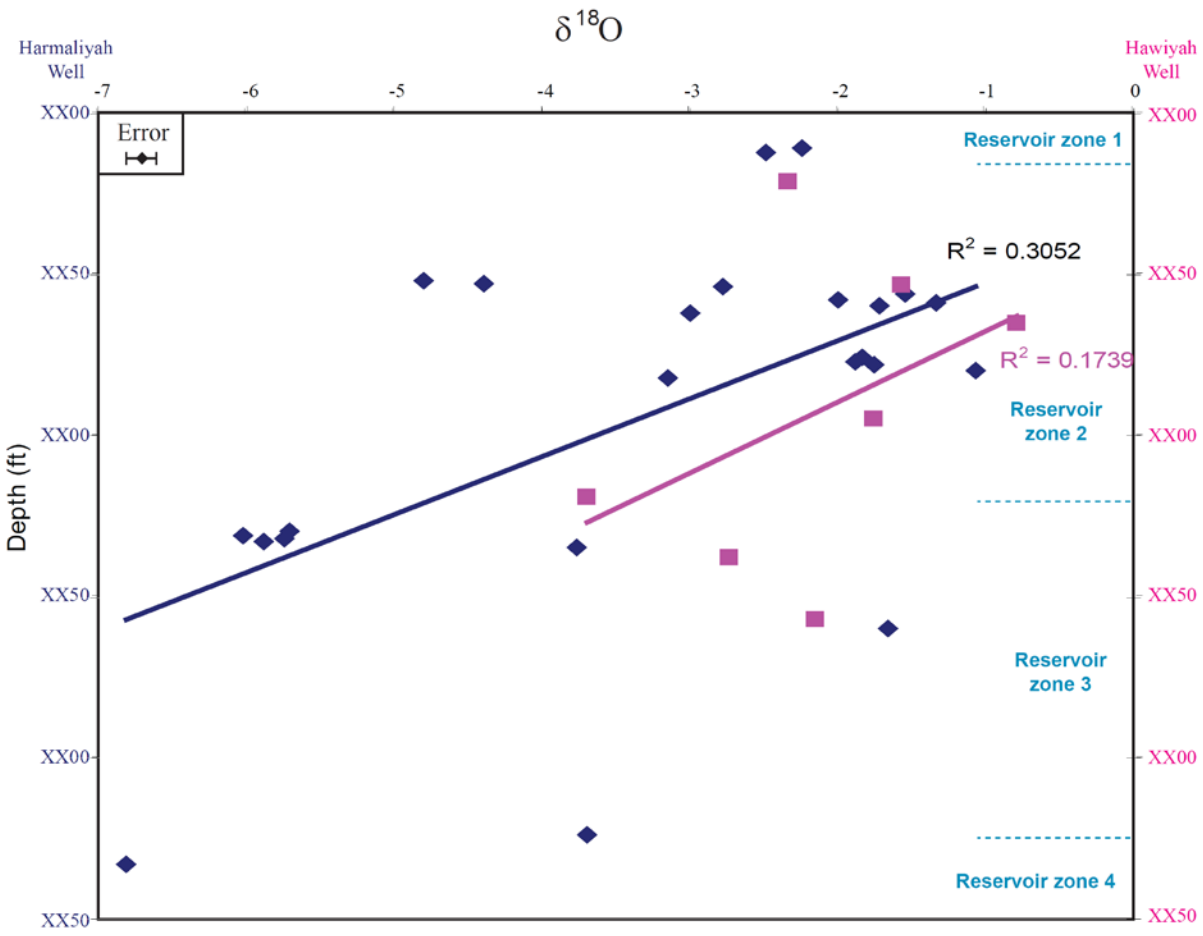

Figure 3.14: $\delta^{18}O$ vs. depth. $\delta^{18}O$ values show an over all depletion with depth. Reservoir zone 2 has the widest range of $\delta^{18}O$.

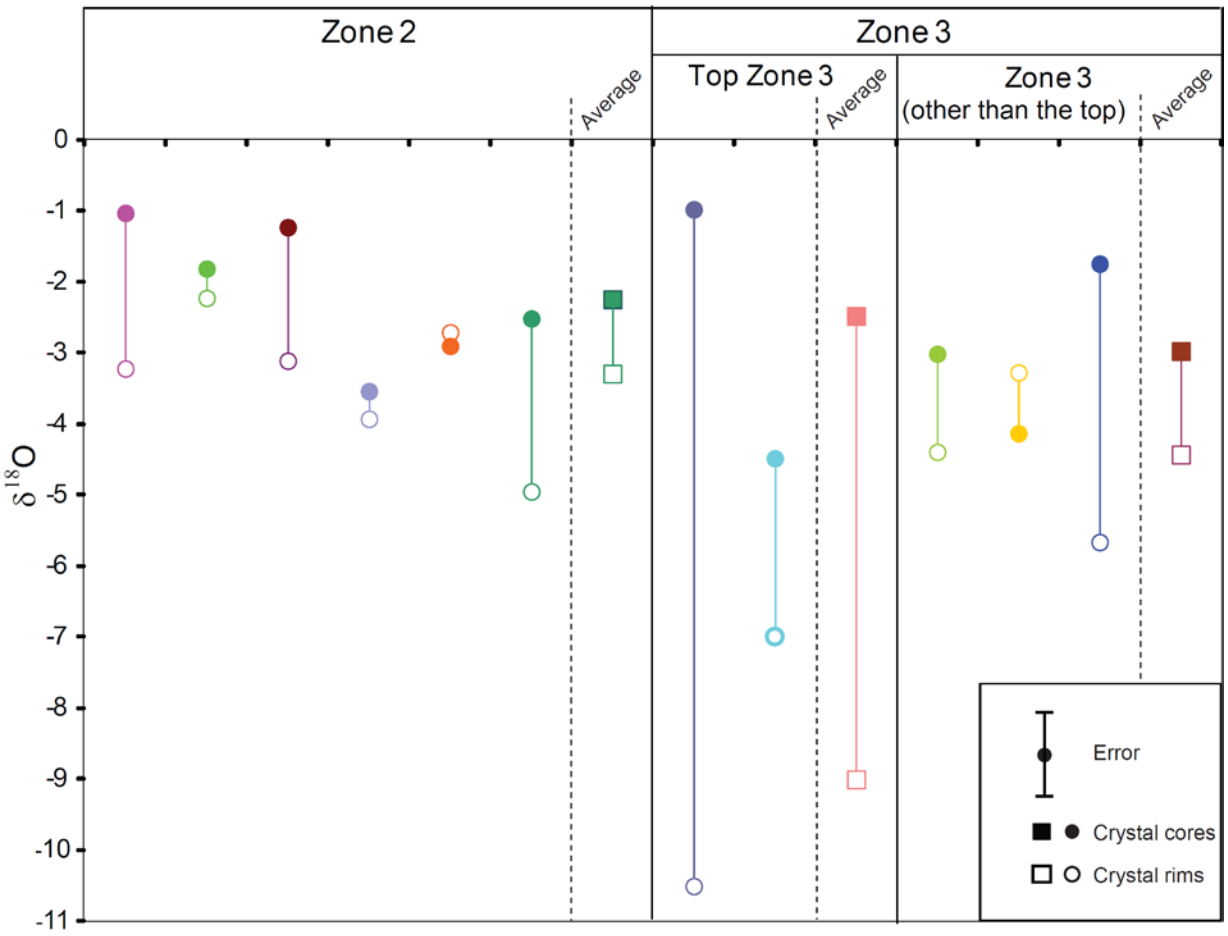

Figure 3.15: SIMS data for $\delta^{18}O$ compositions of cores (solid symbols) versus rims (unfilled symbols) of dolomite crystals. The rims of the dolomite crystals tend to average about 2.5 per mil lighter than the cores, with an average range from 1.0 to 6.5 per mil.

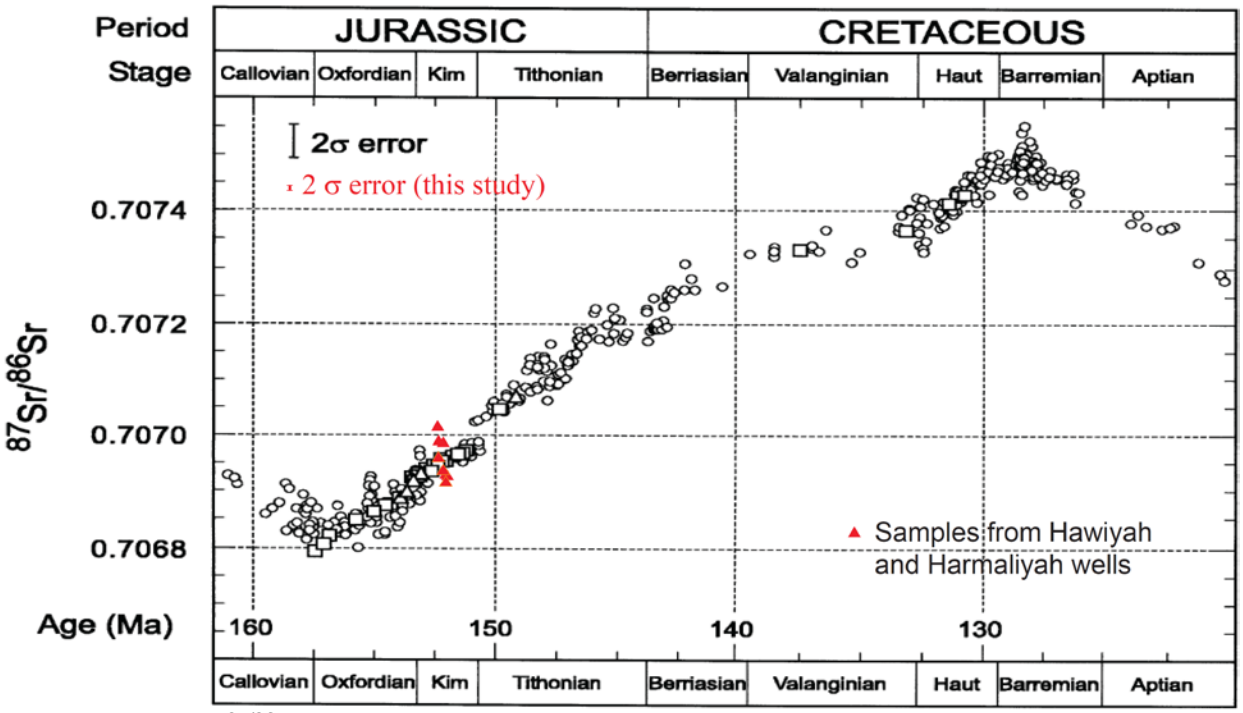

Figure 3.16: The $^{87/86}$Sr values of the dolomites (red solid triangles) plotted on the global strontium isotope curve for the late Jurassic and Early Cretaceous (modified from Price and Grocke, 2002). Arab-D $^{87/86}$Sr values of the Arab-D dolomites are similar to slightly enriched relative to the Kimmeridgian seawater values.

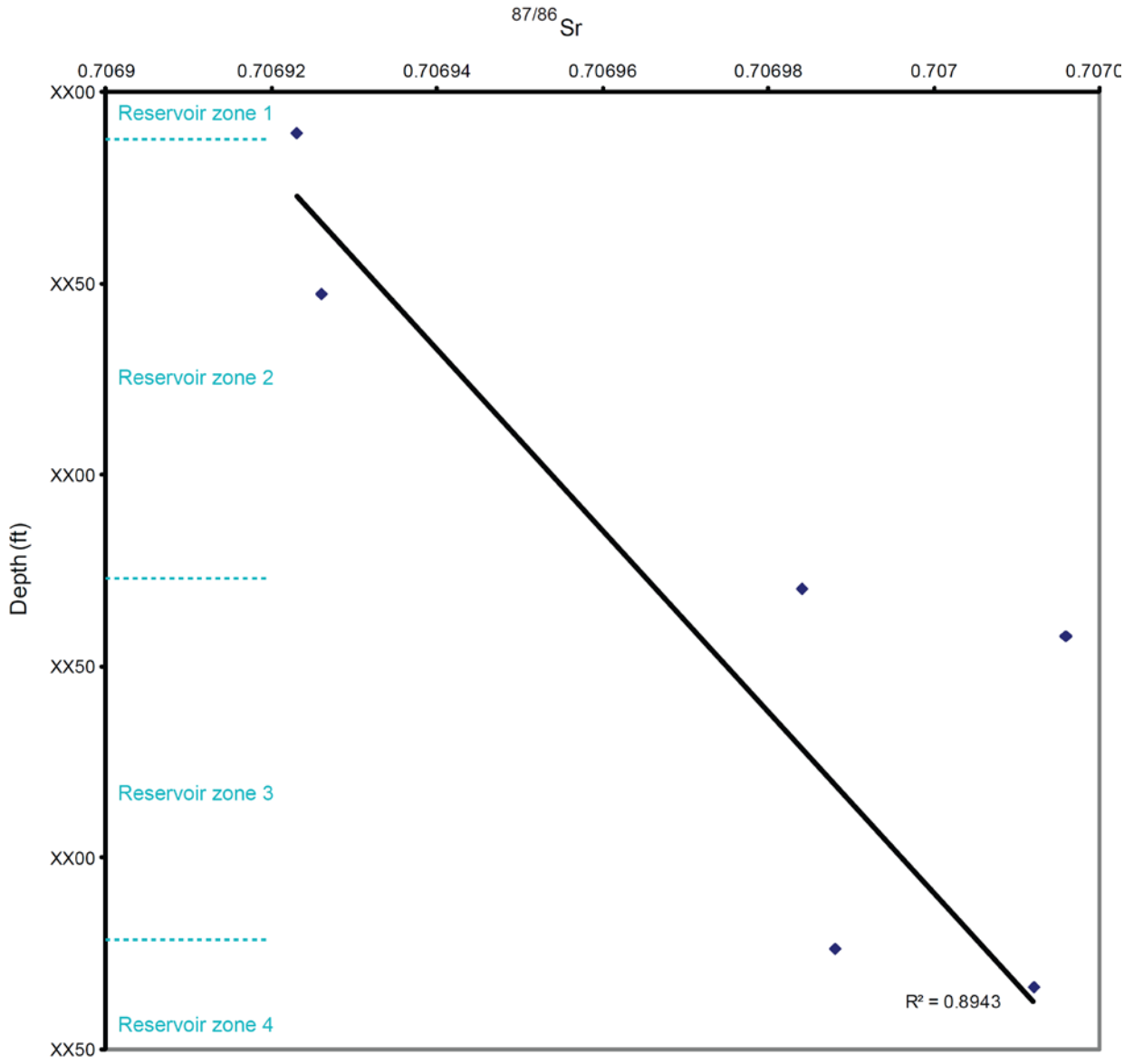

Figure 3.17: Crossplot based on limited data of $^{87/86}$Sr vs. depth, which suggests that $^{87/86}$Sr increases with depth in the reservoir.

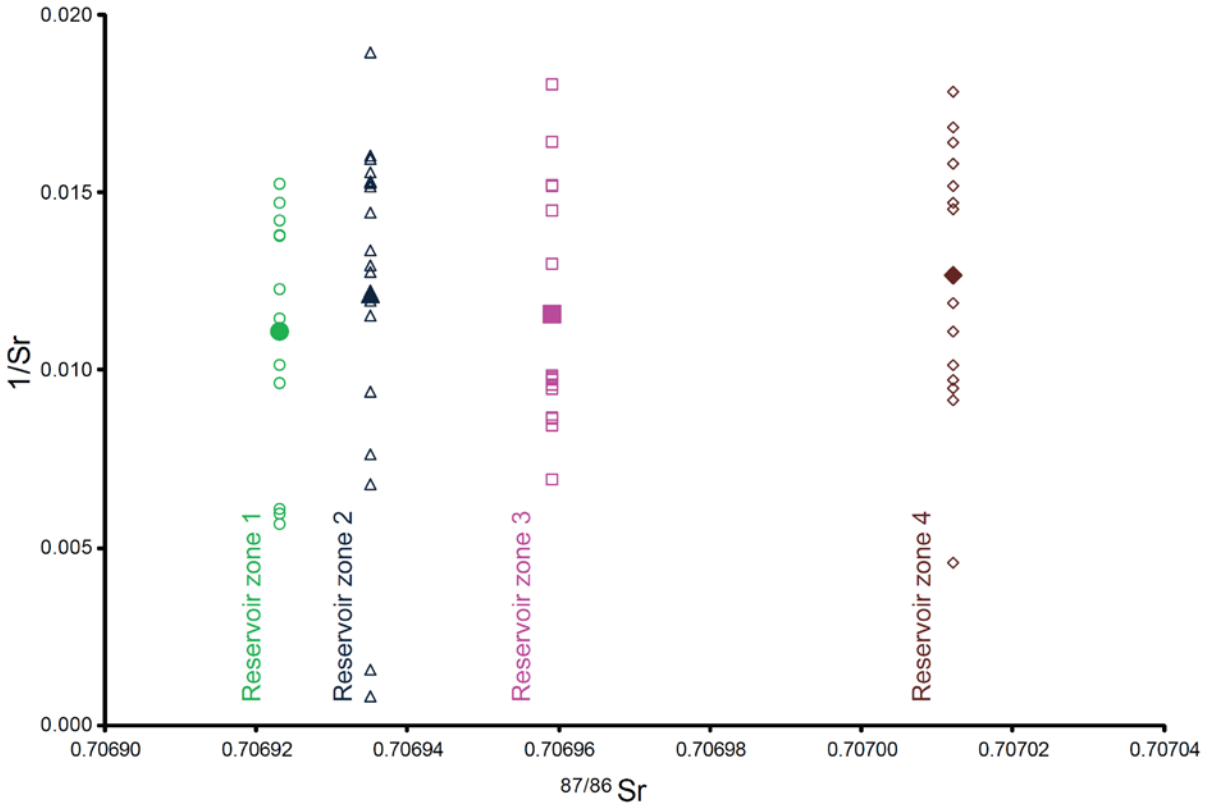

Figure 3.18: Crossplot of 1/Sr (total Sr was determined by Laser Ablation ICP-MS) versus $^{87/86}$Sr. Large symbols are mean values. Mean values of total Sr show slight change. $^{87/86}$Sr becomes more radiogenic from reservoir zone 1 down into reservoir zone 4.

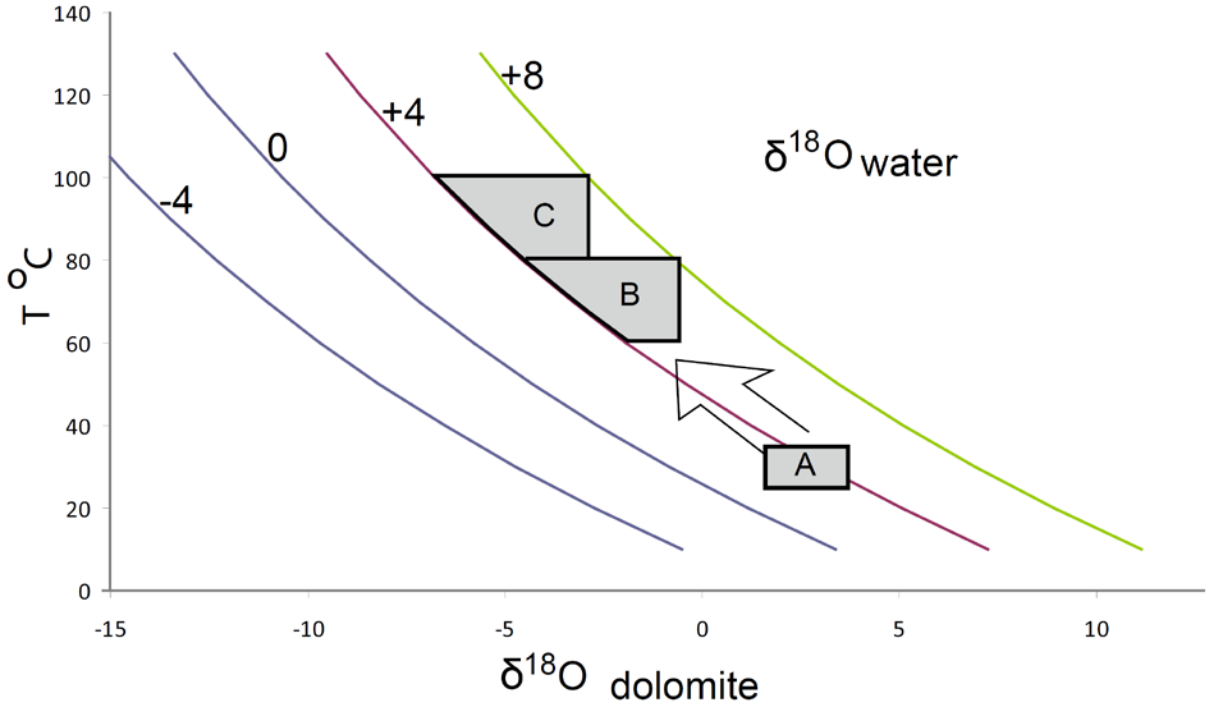

Figure 3.19: Temperature vs. $\delta^{18}O$ dolomite for different $\delta^{18}O$ values of fluid. Area A is the estimated water value in SMOW based on assumed early dolomite $\delta^{18}O$ values and estimated surface temperature. Area B and C show the fileds of $\delta^{18}O$ compositions of +4 to +8 brine at 60-80 C and 80-100 C, that reset and overgrow the earlier dolomites to form the present day dolomite compositions. Curve of $\delta^{18}O$ water was constructed using the equation of Vasconcelos et al. (2005).

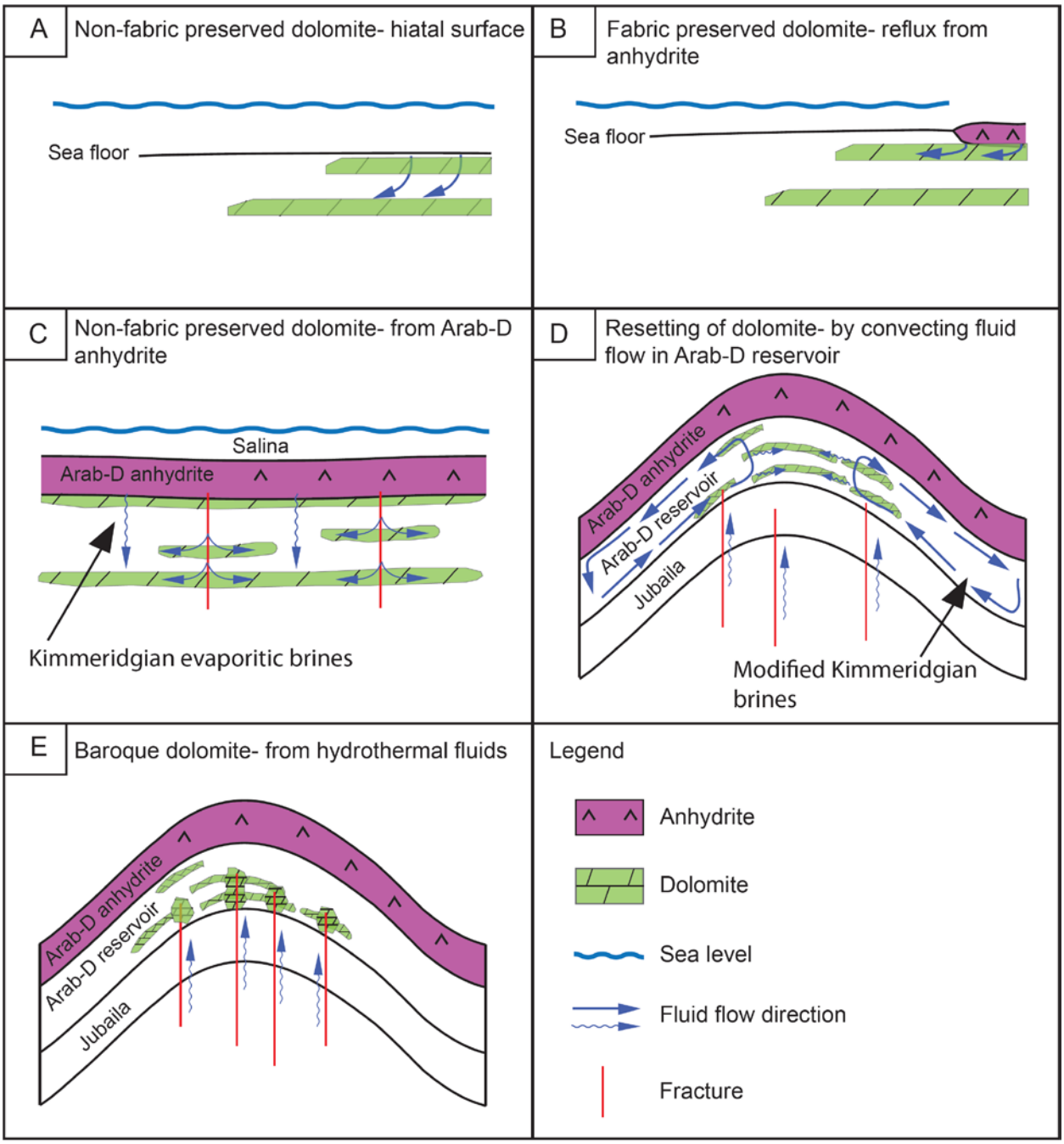

Figure 3.20: Dolomitization model of Arab-D reservoir. A. Non-fabric preserved dolomite forms during hiatal surface. B. Fabric preserved dolomite forms as a result of reflux brines from the above anhydrite. C. Non-fabric preserved dolomite forms from Arab-D anhydrite brines. D. Resetting of dolomite by convecting fluid flow of Kimmeridgian brines in Arab-D reservoir. E. Baroque dolomite forms as a result of hydrothermal fluids.

TABLES

Table 3. 1: Paragenesis in Arab-D reservoir (modified after Mitchell et al., 1988; Cantrell and Hagerty, 1999; Cantrell et al., 2001, 2004; and Swart et al., 2005).

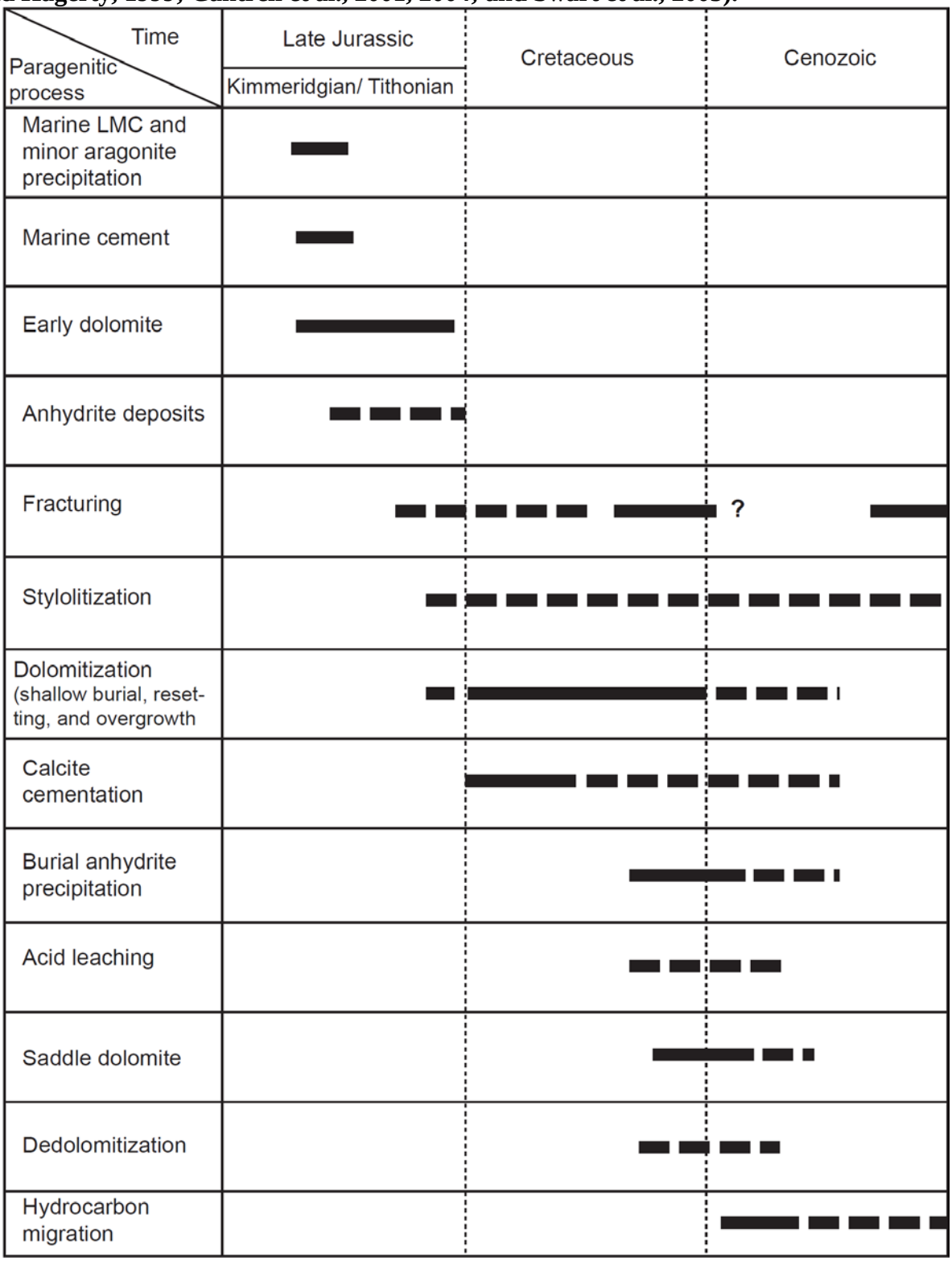

Table 3. 2: Summary of Dolomite types of reservoir zones.

	Reservoir zone 1	Reservoir zone 2	Reservoir zone 3	Reservoir zone 4
Petrography	Fine to medium, Fabric preserving dolmite	Medium to coarse, fabric destructive dolomite	Fine to coarse, fabric destructive dolomite	Fine to coarse, fabric destructive dolomite
$\delta^{18}O_{dol}$(per mil)	-2.40	from -0.8 to -4.80	from -1.70 to -6.10	-6.80
$\delta^{13}C$ (per mil)	3.00	from 3.0 to 3.80	from 2.40 to 3.50	2.90
$^{87/86}Sr$	0.706923	0.706926	0.706984	0.706988 - 0.707012
Fe (ppm)	110 - 2964	13 - 1770	22 - 853	299 - 601
Mn (ppm)	17 - 35	11 -- 26	29-Jul	23 - 33
Sr (ppm)	66 - 176	29 - 255	16 - 1200	56 - 216
U (ppm)	0.70 - 2.48	0.20 - 3.58	0.08 - 2.12	0.19 - 0.35

REFERENCES

Abu-Ali, M., and R. Littke, 2005. Paleozoic petroleum systems of Saudi Arabia: a basin modeling approach. GeoArabia 10 (3), p. 131–168.

Adams, J. E. and M. L. Rhodes, 1960. Dolomitization by seepage refluxion. Bulletin American Association of Petroleum Geologists, vol. 44, p. 1912–1920.

Al-Husseini, M. I., 1997. Jurassic sequence stratigraphy of the western and southern Arabian Gulf, GeoArabia, v. 2, no. 4, p. 361- 382.

Ayres, M. G., M. Bilal, R. W. Jones, L. W. Slentz, M. Tartir, and A. O. Wilson, 1982. Hydrocarbon habitat in main producing areas, Saudi Arabia: AAPG Bulletin, v. 66, p. 1-9.

Banner, J.L., 1995. Applications of the trace element and isotope geochemisty of strontium to studies of carbonate diagenesis. Sedimentology 45 (2), p. 805–824.

Barnaby, R. J., and J. F. Read, 1992. Dolomitization of a carbonate platform during late burial, Lower to Middle Cambrian Shady Dolomite, Virginia Appalachians. Journal of Sedimentary Petrology, v. 62, p. 1023-1043.

Bott, M. H. P, 1992. Passive margins and their subsidence. Journal of the Geological Society, London, v. 149, p. 805-812.

Budd, D. A., 1997. Cenozoic dolomites of carbonate islands; their attributes and origin. Earth Sci. Rev. 42, p. 1-47.

Cander, H., 1994. An example of mixing-zone dolomite, Middle Eocene Avon Park Formation, Floridan Aquifer System. J. Sedimentary Research, v. A64, p. 615-629.

Cantrell, D. L., and R. M. Hagerty, 1999. Microporosity in Arab carbonates, Saudi Arabia: GeoArabia, v. 4, p. 129-154.

Cantrell, D. L., P. K. Swart, R. C. Handford, C.G. Kendall, and H. Westphal 2001. Geology and production significance of dolomite, Arab-D reservoir, Ghawar field, Saudi Arabia. GeoArabia, v. 6, no. 1, p. 45-60.

Cantrell, D. L., P. K. Swart, and R. M. Hagerty, 2004. Genesis and characterization of dolomite, Arab-D reservoir, Ghawar field, Saudi Arabia. GeoArabia, v. 9, no. 2, p. 11-36.

Champ, D. R. , J. Gulens and R. E. Jackson, 1979. Oxidation reduction sequences in ground water flow systems. Can. Jour. Earth Sciences, v.16, p. 12-23.

Choquette, P.W., E. E. Hiatt, 2008. Shallow-burial dolomite cement: a major component of many ancient sucrosic dolomites. Sedimentology 55, p. 423–460.

Coggon R. M., D. A. H. Teagle, C. E. Smith-Duque, J. C. Alt, and M. J. Cooper, 2010. Reconstructing past seawater Mg/Ca and Sr/Ca from mid-ocean ridge flank calcium carbonate veins. Science 327, p. 1114–1117.

Davies, G. R. and L. B. Smith, 2006. Structurally controlled hydrothermal dolomite facies: An overview. Bulletin of the American Association of Petroleum Geologists, v. 90, p. 1641–1690.

Donat J. R., K. W. Bruland, 1995. Trace elements in the ocean. In: Salbu B, Steinnes E, editors. Trace elements in natural waters. Boca Raton: CRC Press: p. 247-281.

Fritz, P. and D. G. Smith, 1970. The isotopic composition of secondary dolomites, Geochim, Consmochim. Acta, 34, p. 1161-1173.

Gillhaus A., D. K. Richter, J. Meijer, R. D. Neuser, A. Stephan, 2001. Quantitative high resolution cathodoluminescence spectroscopy of diagenetic and hydrothermal dolomites. Sedimentary Geology 140, p. 191–199.

Gischler, E., A. J. Lomando, 2005. Offshore sedimentary facies of a modern carbonate ramp, Kuwait, northwestern Arabian–Persian Gulf. Facies 50, p. 443–462.

Goldstein, R. H., T. J. Reynolds, 1994. Systematics of fluid inclusions in diagenetic minerals. SEPM Short Course, v. 31, 198 pp.

Hanor, J.S., 1988. Origin and migration of subsurface sedimentary brines. Soc. Econ, Paleo, Min. Short course, no. 21, 248 pp.

Hanor, J. S., 1994. Origin of saline fluids in sedimentary basins, in J. Parnell, ed., Geofluids: Origin and migration of fluids in sedimentary basins. Geological Society (London) Special Publication 78, p. 151–174.

Heydari, E., 1997. Hydrotectonic models of burial diagenesis in platform carbonates based on formation water geochemistry in North American sedimentary basins. In I.P. Montanez, J.M. Gregg and K.L. Shelton, eds., Basin-Wide Diagenetic Patterns: Integrated Petrologic, Geochemical and Hydrologic Considerations: SEPM Special Publication, no. 57, p. 53-79.

Holmden, C., and J. D. Hudson, 2003. $^{87}Sr/^{86}Sr$ and Sr/Ca investigation of Jurassic mollusks from Scotland: implications for paleosalinities and the Sr/Ca ratio of seawater. Geological Society of America Bulletin 115, p. 1249 – 1264

Holser, W. T., 1979. Mineralogy of evaporites. In: Burns, R.G. (Ed.), Marine Minerals. Reviews in Mineralogy, Chap. 8, vol. 6. Mineralogical society of America, Chelsea, MI, p. 211–235.

Kupecz, J. A., and L. S. Land, 1994. Progressive recrystallization and stabilization of early-stage dolomite: lower Ordovician Ellenburger Group, west Texas. In: Purser, B., Tucker, M., Zenger, D. Eds.., Dolomites - A Volume in Honor of Dolomieu. Special Publication International Association of Sedimentologists, vol. 21. Blackwell Scientific Publications, Cambridge, p. 255–279.

Lloyd R. M., 1966. Oxygen isotope enrichment of sea water by evaporation. Geochim. Cosmochim. Acfa 30, p.801-8 14.

Lindsay, R. F., D. L. Cantrell, G. W. Hughes, T. H. Keith, H. W. Mueller III, and S. D. Russell, 2006. Ghawar Arab-D reservoir: widespread porosity in shoaling-upward carbonate cycles, Saudi Arabia. In P. M. Harris and L. J. Weber, eds., Giant hydrocarbon reservoirs of the world: From rocks to reservoir characterization and modeling. AAPG Memoir 88/ SEPM Special Publication, p. 97-137.

Lucia F. J., 1995. Rock-fabric/petrophysical classification of carbonate pore space for reservoir characterization. AAPG Bull 79 (9): p. 1275–1300.

Mielke, J. E., 1979. Composition of the Earth's crust and distribution of the elements. In: Siegel, F.R. (Ed.), Review of Research on Modern Problems in Geochemistry. UNESCO Report, Paris, p. 13–37.

Mirnejad, H., V. Sisakht, H. Mohammadzadeh, A. H. Amini, B. J. Rostron, and G. Haghparast, 2011. Major, minor element chemistry and oxygen and hydrogen isotopic composition of Marun oil-field brines, SW Iran: Source history and economic potential. Geological Journal, 46, p. 1-9.

Mitchell, J. C., P. J. Lehmann, D. L. Cantrell, I. A. Al-Jallal, and M. A. Al-Thaghafy, 1988. Lithofacies, diagenesis and depositional sequence; Arab-D member, Ghawar field, Saudi Arabia, in A. J. Lomando and P. M. Harris, eds., Giant oil and gas fields: Society of Economic Paleontologists and Mineralogists Core Workshop 12, v. 1, p. 459-514.

Montañez, I., and J. F. Read, 1992. Fluid-rock interaction history during stabilization of early dolomites, Upper Knox Group (Lower Ordovician), U.S. Appalachians. Journal of Sedimentary Petrology, v. 62, p. 753–778.

Ohmoto, H. and R. Rye, 1979. Isotopes of sulfur and carbon. In Geochemistry of Hydrothermal Ore Deposits (ed. H. L. BARNES). p. 509-567.

Price, G. D., D. R. Grocke, 2002. Strontium-isotope stratigraphy and oxygen- and carbon-isotope variation during the Middle Jurassic Early Cretaceous of the Falkland Plateau, South Atlantic. Palaeogeogr. Palaeoclimatol. Palaeoecol. 183, p. 209-222.

Rosenburg, E., and H. Holland, 1964. Calcite-dolomite-magnesite stability relations in solutions at elevated temperature. Science, v. 145, p. 700-701.

Sharland, P. R., R. Archer, D. M. Casey, R. B. Davies, S. H. Hall, A.P. Heward, A. D. Horbury and M. D. Simmons, 2001. Arabian Plate sequence stratigraphy. GeoArabia Special Publication 2, Gulf PetroLink, Bahrain, 371 p.

Stanley, S.M. and L. A. Hardie, 1998. Secular oscillations in the carbonate mineralogy of reef-building and sedimentproducing organisms driven by tectonically forced shifts in seawater chemistry. Palaeogeogr. Palaeoclimatol. Palaeoecol., 144, p. 3–19.

Stenger, B., P. Tony, N. Al-Afaleg, and P. Lawrence, 2003. Tilted original oil/water contact in the Arab-D reservoir, Ghawar field, Saudi Arabia. GeoArabia, v. 8, no. 1, p. 9-42.

Suzuki, Y., Y. Iryu, S. Inagaki, T. Yamada, S. Aizawa, and D. A. Budd, 2006. Origin of atoll dolomites distinguished by geochemistry and crystal chemistry: Kita-daito-jima, northern Philippine Sea. Sedimentary Geology 183, p. 181–202.

Swart, P. K., D. L. Cantrell, H. Westphal, C. R. Handford, and C. G. Kendall, 2005. Origin of dolomite in the Arab-D reservoir from the Ghawar field, Saudi Arabia: Evidence from petrographic and geochemical constraints: Journal of Sedimentary Research, v. 75, p. 480 – 495.

Vahrenkamp, V. C., and P. K. Swart, 1994. Late Cenozoic dolomites of the Bahamas: metastable analogues for the genesis of ancient platform dolomites. In: Purser, B., Tucker, M., Zenger, D. Eds.., Dolomites - A Volume in Honor of Dolomieu. Special Publication International Association of Sedimentologists, vol. 21, p. 133–153.

Vasconcelos, C., J. A. McKenzie, R.Warthmann,and S. M. Bernasconi, 2005. Calibration of the $\delta^{18}O$ paleothermometer for dolomite precipitated in microbial cultures and natural environments. Geol. Soc. Am. 33, p. 317–320.

Veizer, J., 1983. Chemical diagenesis of carbonates: theory and application of trace element technique. In: Arthur, M.A., Anderson, T.F., Kaplan, I.R., Veizer, J., Land, L.S. Eds.., Stable Isotopes in Sedimentary Geology, Vol. 10,. Society of Economic Paleontologists and Mineralogists Short Course Notes, pp. III-1-100.

Veizer, J., D. Ala, K. Azmy, P. Bruckschen, D. Buhl, F. Bruhn, G. A. F. Carden, A. Diener, S. Ebneth, Y. Godde´ris, T. Jasper, C. Korte, F. Pawellek, O. Podlaha, and H. Strauss, 1999. 87Sr/86Sr, d13C and d18O evolution of Phanerozoic seawater. Chemical Geology, 161, p. 59-88.

Wheeler, C. W., P. Aharon, and R. E. Ferrell, 1999. Successions of Late Cenozoic platform dolomites distinguished by texture, geochemistry, and crystal chemistry: Niue, South Pacific. Jour. Sediment. Research, v. 69, p. 239-255.

Wood, J. R., and T. A. Hewitt, 1982. Fluid convection and mass transfer in porous sandstones- a theoretical model: Geochimica et Cosmochimical Acta, v. 46, p. 1707-1713.

Ziegler, M. A., 2001. Late Permian to Holocene paleofacies evolution of the Arabian Plate and its hydrocarbon occurrences. GeoArabia, v. 6, p. 445-504.

CHAPTER 4

CONCLUSIONS

Overall facies and thickness trends across Harmaliyah and Hawiyah fields suggest slight thickening and more open marine conditions toward the east and northeast. The strikingly similar sequence stratigraphic and facies development between the two fields suggests that they were part of a single platform at least during Arab-D deposition with subtle topography developed over the two fields.

The relatively high subsidence rates of ~6 cm/k.y. were suppressing the effects of sea-level fall, thus limiting the development of emergence surfaces. The two 3rd order subsequences (Jubaila and Arab-D formation) have ~ 1 m.y. duration for each one, which may relate to Milankovitch long term obliquity forcing (nodes at 1.2 m.y.). The estimated durations of the 12 high frequency sequences mapped between the two fields likely relate to short term (100 k.y.) orbital eccentricity and the component meter scale parasquences could relate to precessional and sub-precessional forcing and autocyclic processes.

High-frequency sea-level changes in the lower part of Arab-D reservoirs are suggestive of cool- or transitional mode global climates with some buildup of Gondwana ice sheets during cool summers. However, it seems that the bulk of the Arab-D carbonates and evaporates were deposited under greenhouse conditions, with only periodic buildup of small continental ice sheets.

Overall, Arab-D reservoir shows a long term shallowing from the deeper mudstone and intraclast facies in the lower Arab-D to the stromatoporoid and *Cladocoropsis* facies then to

peloid- and ooid grainstone to evaporite facies. The thick Arab-D anhydrite is most likely formed during the 3rd order lowstand system tract.

Early dolomites in the Arab-D reservoir were formed during shallowing phases on the platform. Most of the dolomites within the reservoir are fabric destructive dolomites. The fabric preserved dolomites were formed only in the upper Arab-D reservoir (from aragonitic sediments). However, fractures cutting the section may have allowed downward migration of the evaporitic brines into the Arab-D reservoir carbonates, breaching any basal hydroseal underneath the evaporites, thus allowing continued dolomitization during evaporite deposition while the Jubaila carbonates acted as a basal seal.

With burial and increasing temperature, both the original limestones and the dolomites started to be reset to lighter oxygen isotope values by the warm connate Kimmeridgian brines which likely were relatively heavy (+4 to +8 per mil_{SMOW}), while the C isotopic composition was buffered by the rock C. With increasing burial temperatures in the Cretaceous, the dolomites continued to re-equilibrate with the isotopically heavy connate brines, developing even lighter $\delta^{18}O$ values for the bulk dolomites. Also, hydrothermal brines with more radiogenic $^{87/86}Sr$ that moved upward along faults and fractures, and mixed with the connate Kimmeridgian brines, thus resulting in the slight increase in $^{87/86}Sr$ downsection in the Arab-D, as well as the weak trend in depleted $\delta^{18}O$ values downsection. Oil migration into the reservoir in the Early Tertiary terminated dolomitization.

The model differs from previous models in presenting evidence for heavier oxygen isotopic compositions of the original marine limestones than previous workers, and uses unaltered coeval dolomites from Croatia for the initial early dolomites. Original limestones and early dolomites have undergone considerable resetting of oxygen isotopic compositions during

later burial dolomitization. Based on the Iranian oil fields example and northern Ghawar brines, the subsurface brines are at peak temperatures and $\delta^{18}O$ values of +4 to +8 per mil_{SMOW} as the main source ot resetting dolomite and causing overgrowth and that have much heavier oxygen isotope compositions than those suggested previous studies.